

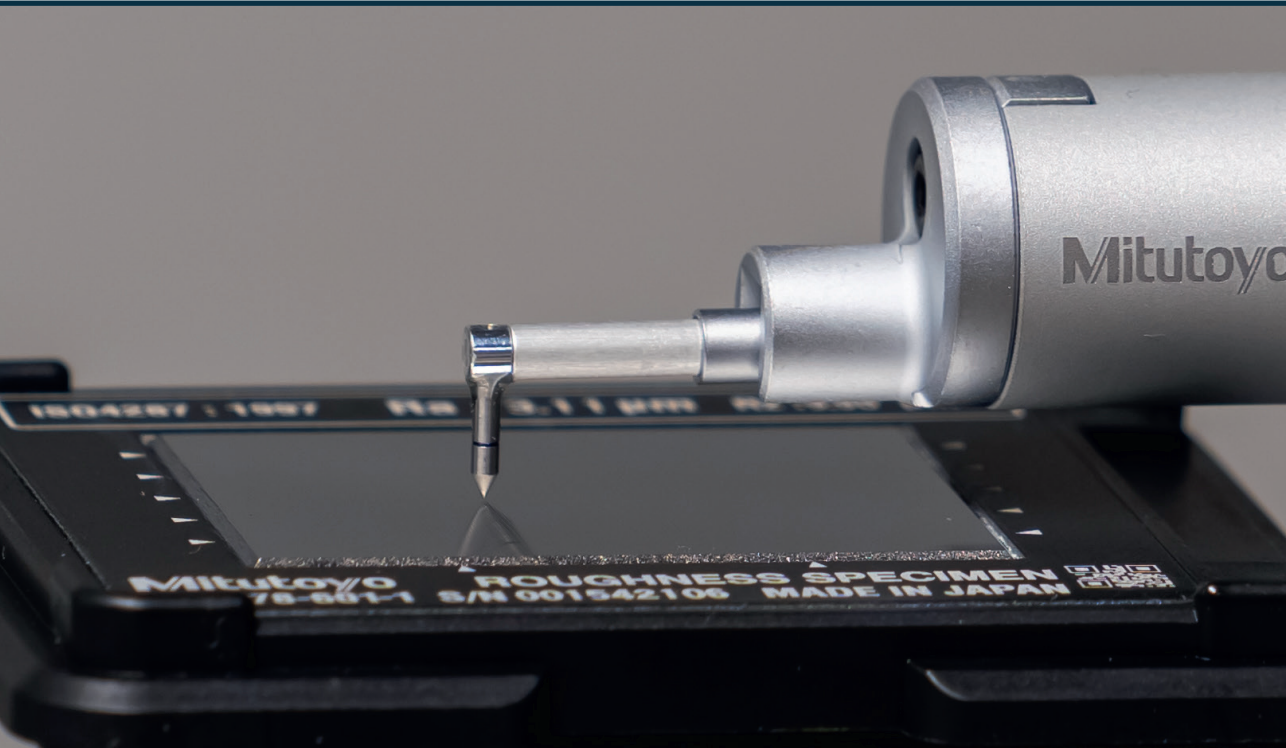
Jānis Lungevičs

**PA LEDU SLĪDOŠĀ NERŪSĒJOŠĀ TĒRAUDA VIRSMAS
MAKROĢEOMETRIJAS UN MIKROĢEOMETRIJAS
IETEKME UZ BERZES KOEFICIENTU**

Promocijas darbs

**EFFECT OF STAINLESS STEEL SURFACE
MACROGEOMETRY AND MICROGEOMETRY
ON THE COEFFICIENT OF SLIDING FRICTION ON ICE**

Doctoral Thesis



RĪGAS TEHNISKĀ UNIVERSITĀTE

Mašīnzinību, transporta un aeronautikas fakultāte
Mehānikas un mašīnbūves institūts

RIGA TECHNICAL UNIVERSITY

Faculty of Mechanical Engineering, Transport and Aeronautics
Institute of Mechanics and Mechanical Engineering

Jānis LUNGEVIČS

Doktora studiju programmas “Mašīnbūve un mehānika” doktorants
Doctoral Student of the Study Programme *Mechanical Engineering and Mechanics*

PA LEDU SLĪDOŠA NERŪSĒJOŠĀ TĒRAUDA VIRSMAS MAKROĢEOMETRIJAS UN MIKROĢEOMETRIJAS IETEKME UZ BERZES KOEFIČIENTU

Promocijas darbs

EFFECT OF STAINLESS STEEL SURFACE MACROGEOMETRY AND MICROGEOMETRY ON THE COEFFICIENT OF SLIDING FRICTION ON ICE

Doctoral Thesis

Zinātniskie vadītāji
Scientific supervisors

Professor *Dr. sc. ing.*
IRĪNA BOIKO

Professor *Ph. D.*
KĀRLIS AGRIS GROSS

Professor *Dr. habil. sc. ing.*
JĀNIS RUDZĪTIS

Rīga 2023/Riga 2023

Lungevičs, J. Pa ledu slīdoša nerūsējošā tērauda virsmas makroģeometrijas un mikroģeometrijas ietekme uz berzes koeficientu. Promocijas darbs. Rīga: RTU, 2023. 127 lpp.

Lungevičs, J. Effect of Stainless Steel Surface Macrogeometry and Microgeometry on the Coefficient of Sliding Friction on Ice. Doctoral Thesis. Riga: RTU, 2023. – 127 p.

Iespiests saskaņā ar promocijas padomes RTU P-16 2023. gada 30. janvāra lēmumu, protokols Nr. 1

Published in accordance with the decision of the Promotion Council “RTU P-16” of 30 January 2023, Minutes No. 1

Promocijas darba izstrādi atbalstījuši:
This work has been supported by:

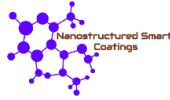
- European Social Fund within the project “The Quest for Disclosing How Surface Characteristics Affect Slideability”.



- National research program “Innovative materials and smart technologies for environmental safety” project No. 6 “Metal surface treatment to reduce friction and wear”.



- Latvian Bobsleigh and Skeleton Federation.
- Latvian Luge Federation.
- Doctoral Grant programme of Riga Technical University.
- Latvian Council of Science project “Carbon-Rich Self-Healing Multifunctional Nanostructured Smart Coatings (NSC) for High-tech Applications Using High-power Confined Plasma Technology for their Deposition”.



- European Social Fund within Project No. 8.2.2.0/20/I/008 “Strengthening of Ph. D. students and academic personnel of Riga Technical University and BA School of Business and Finance in the strategic fields of specialization”.



- Parts of the work were funded by the Austrian COMET Program (Project InTribology, no. 872176) and carried out at the “Excellence Centre of Tribology” (AC2T research GmbH) in collaboration with V-Research GmbH and Riga Technical University. Funding of mobility costs by the Austrian Cooperative Research (ACR) is also gratefully acknowledged.

ACKNOWLEDGMENTS

The author of this Doctoral Thesis primarily wants to thank his scientific supervisors, Iřina Boiko and Kārlis Agris Gross, for their time and knowledge. Without your help and advice, I could not accomplish such a result this soon. I want to thank Iřina Boiko for her help in the administrative work and structuring of the Thesis and Kārlis Agris Gross for his significant contribution to improving my academic writing skill and showing me that I must aim for high-quality publications regardless of the effort needed.

I would also like to thank my colleague Ernest Jansons for being a great research partner in the ice tribology field. Additional thanks to Armands Leitāns and Oskars Liniņš for the frequent discussions on tribology topics that helped me to improve my general knowledge in this research field.

Special thanks to Igor Velkavrh and the V-Research GmbH team for supporting me through the Thesis development process. Without your theoretical and practical help, this Thesis would not be possible in its current form.

Thanks to Dainis Dukurs, Sandis Prūsis, and Mārtiņš Rubenis for including me as a part of your teams and sharing the knowledge and feedback from winter sports athlete point of view. I hope we will continue our collaboration for a long time, ensuring that Latvia has the best equipment for its athletes.

Thanks to Mitutoyo Poland Sp.o.o. for training me in the dimension metrology field.

Thanks to my parents and relatives for always believing in me and supporting my academic career when needed.

ANOTĀCIJA

Promocijas darbā “Pa ledu slīdoša nerūsējošā tērauda virsmas makroģeometrijas un mikroģeometrijas ietekme uz berzes koeficientu”, kurš veidots kā vienotu zinātnisko publikāciju kopa, izveidota jauna metodoloģija pa ledu slīdošu objektu virsmu makroģeometrijas un mikroģeometrijas mērīšanai. Ar jauno metodoloģiju iegūtā informācija par virsmu kontakta laukumu ļauj būtiski uzlabot berzes eksperimentu datu analīzi.

Veikts zinātniskās literatūras apskats un definēti galvenie pētījuma virzieni. Konstatēti būtiski trūkumi līdzšinējā pa ledu slīdošo objektu virsmu makroģeometrijas un mikroģeometrijas metodoloģijā, kas kavē pētījumu tālāku attīstību.

Izstrādāts eksperimentālo pētījumu plans un pielāgots zinātniskais aprīkojums. Dažādos klimatiskajos apstākļos veikti triboloģiskie eksperimenti ar divām dažādām eksperimentālajām iekārtām, un salīdzināti ar tām iegūto rezultātu dati.

Izstrādāta jauna metodoloģija, kas paredz ekeperimentālo paraugu virsmu makroģometriju un mikroģeometrijas mērījumus un datu pēcapstrādi, iegūstot virsmu kontakta laukuma vērtības.

Veikta jaunās metodoloģijas aprobācija paraugiem ar dažādām apstrādes metodēm iegūtām virsmām.

Pētījumu gaita un iegūtie rezultāti apkopoti 17 zinātniskajās publikācijās, no kurām 7 nozīmīgākās iekļautas šajā promocijas darbā.

Atslēgas vārdi: Virsmas makroģometrija, virsmas mikroģometrija, 3D tekstūra, kontaktlaukums, berzes koeficients

ABSTRACT

A new methodology for sliding body surface macrogeometry and microgeometry measurements for the coefficient of friction on ice determination was developed in the Doctoral Thesis " Effect of stainless steel surface macrogeometry and microgeometry on the coefficient of sliding friction on ice.". The Doctoral Thesis has been written as a collection of 7 articles. The information about the surface contact area of the surfaces obtained with the new methodology makes it possible to significantly improve the data analysis of friction experiments.

A review of the scientific literature was carried out, and the main directions of the research were defined. Significant flaws in the existing methodology of macrogeometry and microgeometry of surfaces sliding on ice have been identified, hindering further development of ice tribology.

An experimental research plan was developed, and the necessary infrastructure and scientific equipment were prepared. Tribological experiments were carried out with two different devices in different climatic conditions, and the obtained experimental results were compared.

A new methodology was developed, which requires surface macrogeometry and microgeometry measurements. Contact area values were calculated from surface measurements.

The new methodology was approbated using samples with different surface textures.

The research results are summarized in 17 scientific publications, from which 7 form this Doctoral Thesis.

Keywords: Surface macrogeometry, Surface microgeometry, 3D texture, Contact area, Coefficient of friction on ice

DOCTORAL THESIS PROPOSED TO RIGA TECHNICAL UNIVERSITY FOR THE PROMOTION TO THE SCIENTIFIC DEGREE OF DOCTOR OF SCIENCE

To be granted the scientific degree of Doctor of Science (Ph. D.), the Doctoral Thesis has been submitted for defense at the open meeting of the RTU Promotion Council on July 3, 2023, at 10:00 at the Faculty of Mechanical Engineering, Transport and Aeronautics of Riga Technical University, 1 Paula Valdena Street, Room 106.

OFFICIAL REVIEWERS

Professor Dr. Phys. Aleksejs Kataševs,
Riga Technical University

Dr. Eng. Daniel Grochała,
West Pomeranian University of Technology, Poland

Professor Ph. D. Bojan Podgornik,
University of Ljubljana Slovenia

DECLARATION OF ACADEMIC INTEGRITY

I hereby declare that the Doctoral Thesis submitted for review to Riga Technical University for promotion to the scientific degree of Doctor of Science (Ph. D.) is my own. I confirm that this Doctoral Thesis has not been submitted to any other university for promotion to a scientific degree.

Jānis Lungevičs (signature)

Date:

The Doctoral Thesis is a thematically unified collection of articles. It consists of a summary in Latvian and English and seven publications in SCI-indexed journals. Publications are written in English; the total number of pages is 78, including electronically available supplementary information.

CONTENT

OVERVIEW OF THE THESIS	9
The actuality of the topic	9
Aim and objectives	11
Research methods	11
Scientific novelty	12
Theses to be defended.....	12
Practical significance of the Thesis	13
Approbation of the Doctoral Thesis	13
Structure of the Doctoral Thesis.....	15
MAIN RESULTS OF THE DOCTORAL THESIS.....	19
1. Introduction	19
2. Literature analysis.....	21
3. Experimental research	26
4. New surface macrogeometry and microgeometry measurement methodology	28
5. Approbation of the new methodology	31
CONCLUSIONS AND FUTURE OUTLOOK	38
REFERENCES.....	40
APPENDICES.....	43

OVERVIEW OF THE THESIS

The actuality of the topic

The friction of solid bodies on ice is a relatively little-studied phenomenon influenced by many interrelated factors. These factors range from ambient air and ice temperature, air humidity, movement velocity, the geometry of the sliding body, surface texture orientation, applied pressure, chemical and physical properties of the sliding body, hardness of the ice surface, and others. The interaction of these parameters determines the formation of a thin water layer, known as a liquid-like layer (LLL), on the ice and its thickness [1]–[34]. Despite several attempts by researchers to understand the formation of a liquid-like layer and its influence on the coefficient of friction of the sliding body on the ice, the lack of complex and unified metrological support has impeded a reliable explanation of this phenomenon.

To better comprehend the coefficient of friction on ice, there is a need for holistic information about the interaction between the surfaces of the sliding body and ice and the boundary layer between them. Multiple studies have indicated the significant role played by the sliding body's macrogeometry and microgeometry on the coefficient of friction on ice [3], [16], [24], [29], [31]–[33], [35]–[38], and experimental studies prove it [16], [19], [24], [26], [33], [35], [39]. However, it is still unclear how surface macrogeometry and microgeometry affect the coefficient of friction on ice and which surface geometry component plays a more substantial role.

Theoretically focused studies simplify the texture of the sliding body, considering only the body's form while ignoring waviness and roughness. Such theoretical studies are essential, but the accepted simplifications do not allow analyzing the true nature of the process because macrogeometric bodies, in reality, will always have microgeometric textures that affect the surface contact area between the body and the ice [3], [40]–[43]. On the other hand, experimentally oriented studies [16], [24], [29], [31]–[33], [35]–[37], [44] focus on the sliding body's roughness component, ignoring the macro geometry (shape or form). Literature analysis revealed that in previous studies, the surface of the entire solid body is judged considering only roughness parameters obtained in a small, localized area, typically less than 10 % of the entire body surface [15]. In addition, the texture measurements of this already small area are digitally filtered according to ISO 25178-2 recommendations. With filtering operations, texture form and waviness components are removed, further converting the final texture image and increasing the chances that researchers mislead themselves about the actual texture that interacts with ice (see Fig. 1). Therefore, the author of the Doctoral Thesis perceives the issues mentioned above as significant problems that hinder the progress of ice tribology research.

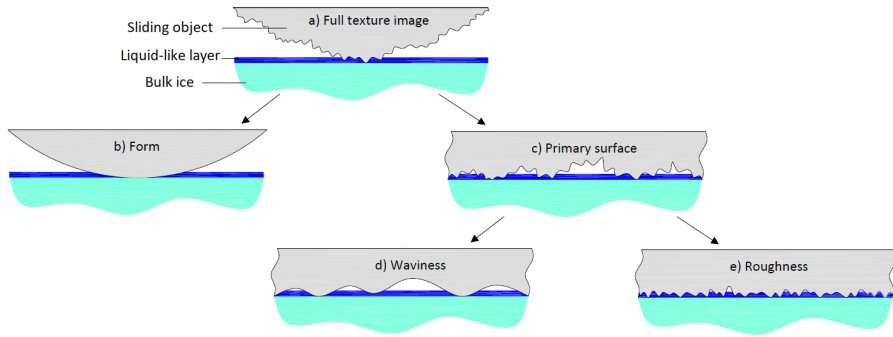


Fig. 1. Schematic representation of sliding body texture components: a) full texture image that represents the true complexity of the surface; b) only the form component of the surface that represents the macrogeometry of the surface; c) primary surface that consists of surface waviness and roughness representing microgeometry of the surface; d) waviness component of the surface; e) roughness component of the surface.

While in reality, full texture defines contact with ice, researchers often use only the filtered roughness component. The schematic representation shows that the contact with ice might be completely misinterpreted by following a standard methodology where only roughness is considered [15]. The author of the Thesis hypothesizes that the interaction of the solid body surface with ice can be reliably evaluated if all surface texture components (form, waviness, and roughness) are considered, as only the combination of these three components provides holistic information about the actual contact area that determines the surface coefficient of friction on ice.

Another factor affecting the ability to analyze macrogeometry and microgeometry influence on the coefficient of friction is the choice of parameters that characterize the surface geometry. So far, the most commonly used are standardized texture parameters (the arithmetic average of profile height deviations from the mean line) R_a or (the arithmetic average of surface height deviation from the mean plane) S_a . However, R_a or S_a values can be identical for differently produced textures with different coefficients of friction on ice (see Fig. 2). This problem highlights that relying only on the roughness parameter to describe the surface contact with ice is insufficient.

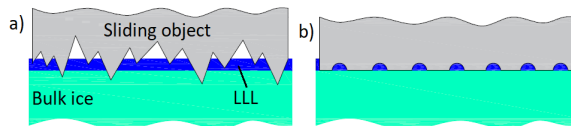


Fig. 2. Schematic representation of the interaction between a sliding body, ice, and liquid-like layer (LLL): a) surface with peaks; b) surface with depressions. In both cases, the surface roughness parameters, such as S_a or R_a , might have the same mathematical value, but the friction on ice differs, i.e., the surface with peaks will increase friction, while the surface with depressions will reduce it [15].

The gathered information hypothesizes that analysis of the surface coefficient of friction on ice is unreliable without complete knowledge of surface macrogeometry and microgeometry and the parameters that characterize it.

Aim and objectives

The Doctoral Thesis aims to develop a new methodology for sliding body surface macrogeometry and microgeometry measurements for the coefficient of friction on ice determination (further referred to as methodology).

The following main tasks were completed to achieve the goal:

1. Analysis of previously known studies and methodologies.
2. Development of experimental procedure.
3. Experimental research.
4. Development of a new methodology of sliding body surface macrogeometry and microgeometry measurements for the coefficient of friction on ice determination.
5. Approbation of the newly developed methodology.

Research methods

To achieve the aim, quantitative and qualitative research methods, and the listed experimental equipment for conducting practical measurements were used.

An auto polisher *334 TI 15 Mecatech* (Presi, France) was used to prepare the experimental sample's initial surfaces. The final sample textures were manufactured using fabric-based sandpapers of different grain sizes (M3, USA), shot blasting equipment *SBC-420* (Power plus, China), a CNC milling machine *Vertical Center Smart 530C* (Mazak, Japan), and *Libra Ti: sapphire* femtosecond laser system (Coherent, USA).

Surface textures were measured and characterized with the following instruments:

- Contact-type profilometer *Form Talysurf Intra 50* with standard stylus *112/2009* (Taylor Hobson, UK).
- Confocal microscope *VK-X250/260* (Keyence International NV/SA, Belgium).
- Optical microscope *Eclipse LV150* (Nikon, Japan).
- Scanning electron microscope *S-4800* (Hitachi, Japan).
- Atomic force microscope *Smena NT-MDT* (NT-MDT Spectrum Instruments, Russia).

Tribological experiments were conducted with two different tribometers:

- *Inclined plane tribometer* (RTU, Latvia). The tribometer records the sample sliding time in defined distances. From these data sliding velocities at various sliding distances were calculated and used as indirect friction describing parameters, i.e., higher velocity values relate to the lower coefficient of friction, and vice versa.
- *V-Research GmbH oscillating type tribometer RVM1000* (Werner Stehr Tribology GmbH, Germany). The tribometer measures the friction force between the ice and the surface of the steel sample. Static and dynamic coefficient of friction (COF) is calculated from the measured friction forces and applied load values.

A *Proscan 520* thermometer (Dostmann, Germany) and a contact-type thermocouple *TP-122-100-MT-K* (Czaki, Poland) were used to measure the ice temperature. Air temperature and air humidity were monitored with *P330 Temp* (Dostmann, Germany).

Sample 3D texture measurements were post-processed in the *Talymap Gold* software (Mountain Maps, France). Statistical methods used in data processing: descriptive/descriptive statistics. Display of results is provided in the form of graphs, pictures, and tables. Tables and graphs were created in *Excel 2018* software (Microsoft, USA). *Solidworks 2022* and *AutoCAD 2022* computer programs were used in image preparation.

Scientific novelty

- A new methodology of sliding body surface macrogeometry and microgeometry measurements was developed for the coefficient of friction on ice determination: both macrogeometry and microgeometry must be included to determine the coefficient of friction on ice.
- It was found that sliding body surface macrogeometry and microgeometry influence on coefficient of friction on the ice must be analyzed considering the sliding body surface temperature: changes in sliding body surface temperature can inverse the coefficient of friction trend for the same surface texture.
- It was proven that surface contact area measurements according to the new methodology allow comparing variously manufactured surface texture influence on the coefficient of friction on ice, which was impossible with previously known methodologies.

Theses to be defended

1. *The newly developed methodology of sliding body surface macrogeometry and microgeometry measurements for determination of the coefficient of friction on ice.* The new methodology includes surface contact area measurements used for contact pressure between the sliding body and ice calculations necessary for tribology experiment result interpretation. According to the new methodology, the whole complexity of the sliding body surface is considered, ensuring a comparison of sliding body surfaces created using various manufacturing methods, which was not possible with previously known methodologies.
2. *Contact area measurements should be used to analyze the coefficient of friction on ice.* The experimental data obtained when contact pressure between the stainless steel surface and ice was higher than 1 MPa proved that the contact area and coefficient of friction have a strong correlation (proportion of variance from 0.9 to 1). The surface texture parameters (Sa, Ssk, Sku, Sds) from previous methodologies have a proportion of variance from 0.5 to 0.9.
3. *The sliding body surface temperature must be considered during the coefficient of friction on ice determination.* It has been proved that in the considered experimental settings, when the contact pressure between the stainless steel surface and ice was higher than 1 MPa, the same surface texture could either increase or reduce the coefficient of friction on ice, depending on the sliding body surface temperature. If the sliding body surface is colder than the ice surface, the reduction of contact areas between the sliding body and ice reduces the

coefficient of friction, but if the sliding body surface is warmer than the ice surface, the reduction of contact areas increases the coefficient of friction.

Practical significance of the Thesis

A new methodology for sliding body surface macrogeometry and microgeometry measurements for the coefficient of friction on ice determination has been developed. This methodology allows analyzing differently manufactured surface macrogeometry and microgeometry that influences the coefficient of friction on ice. This methodology can be used to characterize surface textures manufactured for different functionality, i.e., in some applications coefficient of friction must be increased and in some reduced. Examples where the coefficient of friction should be reduced are:

- Winter sports: Improvement of ice skate blades, bobsleigh runners, skeleton runners, luge runners, curling stones, ski edges, and ice sailing blades. Controlling friction on ice is essential to optimize athlete performance and prevent accidents.
- Construction: Friction on ice is important in constructing and maintaining buildings in cold climates. For example, anti-icing and deicing methods are used to prevent ice buildup on roofs, gutters, walkways, road signs as well as wind turbine blades.
- Transportation: Ice breaker ship front treatment could reduce the friction-caused energy losses while the ship pushes itself on ice to break it. Deicing textures for airplane surfaces would prevent using chemicals that melt the ice.

Some examples where the coefficient of friction should be increased:

- Transportation: Friction between tires and ice affects the handling and safety of vehicles during winter driving.
- Health and safety: Understanding friction on ice is crucial for preventing falls and injuries during winter. Proper footwear with effective treads is essential for maintaining balance and stability.

The new methodology developed in the Doctoral Thesis could also be applied to analyze other tribological pairs, not only metal-ice included in this Doctoral Thesis because the actual contact area determines the coefficient of friction between any surfaces.

The results of the Doctoral Thesis were used to improve the equipment of the Latvian luge team. This is confirmed by the National Luge team coach and head of engineering Mārtiņš Rubenis, in the Appendix 8).

Approbation of the Doctoral Thesis

Presentations at international scientific conferences (*In total, 11 presentations; the 7 most important are listed*)

1. Lungevics, J., Jansons, E., Velkavrh, I., Boiko, I. *Ice tribology investigation using different test setups*. Riga Technical University 63rd International Scientific Conference *Mechanical engineering technology and heat engineering*. Riga, Latvia, 13 October 2022. *Published in Book of Abstracts*.

2. Velkavrh, I., Kafexhiu, F., Wright, T., Lungevics, J., Jansons, E., Boiko, I. *Tribological investigations in a cold environment for winter sports applications: comparative ice friction measurements in different test rigs*. Nordic Tribology Symposium 2022, Alesund, Norway, June 14–17, 2022. *Published in Book of Abstracts*.
3. Lungevics, J., Jansons, E., Boiko, I., Velkavrh I. *Influence of stainless-steel texture on friction properties sliding on ice*. RTU 60th International Scientific Conference. October 14, 2019, Riga, Latvia.
4. Jerane, I., Gross, K. A., Lungevics, J., Pluduma, L. *The Effect of Patterning and Surface Contact on the Sliding Speed over Ice*. The 1st International Conference on Nature Inspired Surface Engineering (NISE 2019). June 11–14, 2019, New Jersey, USA. *Published in Book of Abstracts*.
5. Lungevics, J., Jansons, E., Gross, K. A. *Surface Texture Characterization for Ice Friction Research*. 45th Leeds–Lyon Symposium on Tribology *Smart Tribology Systems*. September 4–7, 2018, Leeds, UK. *Published in Book of Abstracts*.
6. Lungevics, J., Jansons, E., Gross, K. *Skeleton Runner Roughness and Surface Contact Area Influence on Sliding Ability: Field Experiments*. Material Science & Applied Chemistry 2018, October 26, 2018, Riga, Latvia. *Published the conference proceedings indexed in SCOPUS*.
7. Lungevics, J., Jansons, E., Rudzitis, J., Gross, K. A. *Use of Inclined Plane with Additional Time Measurements for Investigating Surface Slidability on Ice*. 12th International Conference *Mechatronic Systems and Materials Intelligent Technical Systems*. July 3–8, 2016, Bialystok, Poland. *Published in Book of Abstracts*.

Patents

1. Jansons, E., Lungevičs, J., Boiko, I. *Portable slip detection device and method*. Patent No. LV15660B, 20.03.2023, owner – RTU.
2. Jansons, E., Lungevičs, J., Leitāns, A., Boiko, I. *Multifunctional equipment and method for assessing the tribological properties of materials and coatings*. Patent application No. LVP2022000037, 29.04.2022, owner – RTU
3. Lungevičs, J., Jansons, E., Stiprais, K., Gross, K. A. *Apparatus and method for determining sliding properties*. Patent application No. LV15305B, 20.03.2018, owner – RTU.

Publications (7 publications that form this Doctoral Thesis are listed. In total, 17 publications are related to the Doctoral Thesis topic. All publications are indexed in SCOPUS or other databases)

1. Gross, K., Lungevics, J., Zavickis, J., Pluduma, L. *A Comparison of Quality Control Methods for Scratch Detection on Polished Metal Surfaces*. Measurement, 2018, Vol. 117, pp. 397–402. ISSN 0263-2241. Available: doi:10.1016/j.measurement.2017.12.022.
2. Jansons, E., Lungevics, J., Gross, K. *Surface Roughness Measure that Best Correlates to Ease of Sliding*. 15th International Scientific Conference *Engineering for Rural Development: Proceedings*. Vol. 15, Jelgava, Latvia, May 25–27, 2016, pp. 687– 695. ISSN 1691-5976. Available: <https://www.tf.llu.lv/conference/proceedings2016/Papers/N127.pdf>.

3. Velkavrh, I., Lungevics, J., Jansons, E., Klien, S., Voyer, J., Ausserer, F. *The Influence of Isotropic Surface Roughness of Steel Sliders on Ice Friction Under Different Testing Conditions*. Lubricants, 2019, Vol. 7, No. 12, pp. 50–63. ISSN 2075-4442. Available: doi:10.3390/lubricants7120106.
4. Velkavrh, I., Voyer, J., Wright, T., Lungevics, J., Jansons, E., Boiko, I. *Variations of ice friction regimes in relation to surface topography and applied operating parameters*, IOP Conf. Ser. Mater. Sci. Eng. 1140 (2021) 012033. Available: <https://doi.org/10.1088/1757-899X/1140/1/012033>.
5. Jansons, E., Lungevics, J., Jerane, I., Gross, K. *A Smaller Bearing Ratio, as a Surface Texture Measure, Promotes Faster Sliding on Ice*. Journal of Tribology, 2021, Vol. 143, No. 11, Article number 111801. ISSN 0742-4787. e-ISSN 1528-8897. Available: doi:10.1115/1.4049704.
6. Lungevics, J., Jansons, E., Boiko, I., Velkavrh, I., Voyer, J., Wright, T. *A Holistic Approach towards Surface Topography Analyses for Ice Tribology Applications*. Frontiers in Mechanical Engineering, 2021, Vol. 7, No. 1, pp. 42–56. ISSN 2297-3079. Available: doi:10.3389/fmech.2021.691485.
7. Gross, K., Lungevics, J., Jansons, E., Jerane, I., Wood, M., Kietzig, A. *Surface Hierarchy: Macroscopic and Microscopic Design Elements for Improved Sliding on Ice*. Lubricants, 2021, Vol. 9, No. 103, Article 103. ISSN 2075-4442. Available: doi:10.3390/lubricants9100103.

Structure of the Doctoral Thesis

The Doctoral Thesis is a collection of seven publications included in SCI journals with a summary in Latvian and English. All publications are written in English, comprising 78 pages, including electronically available supplementary information. Figure 3 is a graphical abstract showing to which Doctoral Thesis tasks each publication refers.

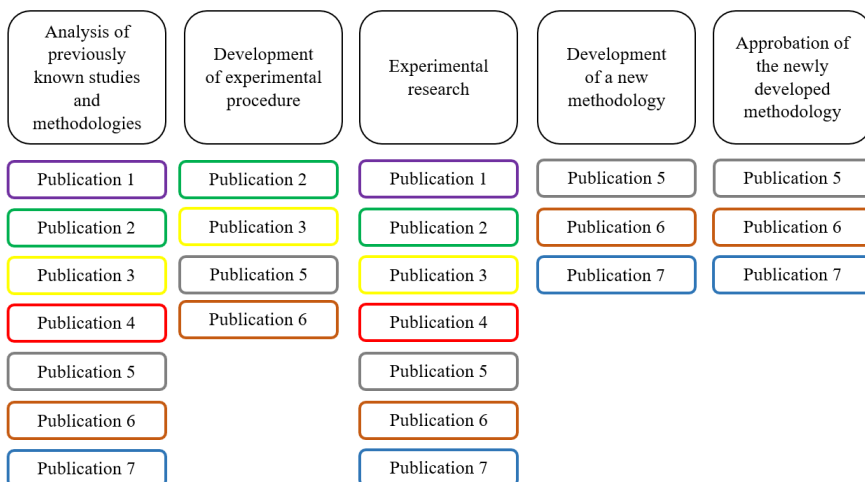


Fig. 3. Graphical abstract of the Doctoral Thesis structure.

The following list highlights each publication's content, results, and the Doctoral Thesis author's personal contribution to these publications. All corresponding authors confirm the Doctoral Thesis authors' personal contribution. Their hand-signed document that proves it is presented in the Appendix 9.

Publication 1

A Comparison of Quality Control Methods for Scratch Detection on Polished Metal Surfaces [45]. The research paper compares various measurement methods for controlling surface quality and analyzing nanometer-scale scratches on mirror-like smooth surfaces. The results showed that AFM ensures the highest resolution and information in three dimensions, but the method is unsuitable for large objects, significantly limiting its usability. It was also concluded that the light microscopy method detected 70 % of scratches visible by AFM, making it an efficient and precise method, but the results are available only in 2D interpretation. The SEM was ideal for detailed observations but had limitations to sample size and preparation. Due to low measured point density and small measured surface area, the contact type 3D profilometer failed to detect nanometer-scale scratches. Still, it provides the ability to obtain 3D surface measurements of large objects, making it suitable for real-life object surface measurements.

Author's personal contribution: conceptualization, investigation, analysis, visualization, writing and reviewing, and editing.

Publication 2

Surface Roughness Measure that Best Correlates to Ease of Sliding [26]. The study analyses why the 2D profilometry method alone may not successfully characterize surface textures that slide on the ice. It was also emphasized that the 2D profile measurement positioning on the surface could cause significant result variation, suggesting that 3D profilometry should be used. The relation to commonly used 2D profilometry parameters and tribology measurements was shown. The Criterion of Contact for surface texture characterization was introduced and compared with the roughness arithmetic mean height parameter. It was concluded that knowledge of the Criterion of Contact ensures defining optimal surface asperity height and spacing ratio that promotes better surface sliding on ice.

Author's personal contribution: conceptualization, investigation, methodology, analysis and validation, writing and preparation of the first draft.

Publication 3

The Influence of Isotropic Surface Roughness of Steel Sliders on Ice Friction Under Different Testing Conditions [6]. Within this study, the same test samples were compared on two different tribometers at various environmental conditions. This Doctoral Thesis is the first known study in ice tribology where the same samples are tested on two setups and the results are compared. Inclined plane type and oscillating type tribometers were used in this study. It was concluded that both setups are sensitive enough to detect texture variation influence on

tribological performance. It was also shown that environmental conditions and sample temperature significantly influence tribological performance.

Author's personal contribution: conceptualization, investigation, methodology, analysis and validation, writing and preparation of the first draft.

Publication 4

Variations of Ice Friction Regimes in Relation to Surface Topography and Applied Operating Parameters [4]. The research aims to study surface textures and surface temperature's influence on tribological performance. The results showed that the changing sliding body surface temperature from +5 °C to –18 °C increased the coefficient of friction on ice four times. It was also discovered that the contact area between the sliding body surface and ice could have an inverse effect on the coefficient of friction at different sliding body surface temperatures, i.e., if the sliding surface temperature were lower, a larger contact area resulted in a higher coefficient of friction. However, if the sliding body surface temperature exceeds the ice temperature, a larger contact area provides a lower coefficient of friction. This study concluded that sliding body surface temperature must be considered during the coefficient of friction on ice determination.

Author's personal contribution: conceptualization, investigation, analysis, visualization, writing and preparation of the first draft.

Publication 5

A Smaller Bearing Ratio, as a Surface Texture Measure, Promotes Faster Sliding on Ice [7]. Newly developed sliding body surface macrogeometry and microgeometry measurement methodology are introduced. The study explains why previously known surface texture characterization methodologies and used parameters are unsuitable for comparing tribological experiments for samples with differently manufactured surface textures. It was proven that a new methodology, where information about the entire surface was considered and expressed as a bearing ratio curve, ensured comparison between differently manufactured surfaces and their tribological performance.

Author's personal contribution: conceptualization, investigation, methodology, analysis and validation, writing and preparation of the first draft.

Publication 6

A Holistic Approach Towards Surface Topography Analyses for Ice Tribology Applications [15]. This paper discusses the newly developed surface macrogeometry and microgeometry measurement methodology in more detail. The paper includes an in-depth analysis of surface characterization methodologies and surface texture parameters used in previous ice tribology studies conducted by other researchers. The benefits of the new methodology were described and validated by analyzing sandblasted surface tribological performance in two different experimental setups. A correlation between various sliding body surface texture parameters and tribology experiment results was demonstrated.

Author's personal contribution: conceptualization, investigation, methodology, analysis and validation, writing and preparation of the first draft.

Publication 7

Surface Hierarchy: Macroscopic and Microscopic Design Elements for Improved Sliding on Ice [5]. Surface macrogeometry and microgeometry influence on sliding body surface tribological performance are discussed, highlighting the importance of considering all surface texture components (form, waviness, and roughness). Practical examples of how sliding body surface macrogeometry and microgeometry combination define final tribological performance are discussed. The benefits of newly developed sliding body surface macrogeometry and microgeometry measurement methodology are discussed and shown graphically.

Author's personal contribution: conceptualization, hierarchy, investigation, visualization, and storyline development with visuals and text.

MAIN RESULTS OF THE DOCTORAL THESIS

1. Introduction

Ice is a crystalline solid composed of water molecules. The most common form of ice is hexagonal ice, referred to as I_h , which contains six-fold symmetry (see Fig. 4 a)) [1], [2]. A repeating pattern of hydrogen bonds between adjacent water molecules characterizes the ice structure. These hydrogen bonds give ice its characteristic properties, including its low density and hardness. Due to its molecular structure, ice is less dense than liquid water. This is because the hydrogen bonds in ice create open spaces between molecules, resulting in a less compact structure. For this reason, ice floats in liquid water [1], [2]. Ice hardness ranges from 15 to 35 MPa depending on ice temperature [1]–[3], [46]. Ice is also brittle and has a low shear strength, which is prone to breaking when subjected to stress. This makes ice a challenging material to work with. Additionally, ice has a low thermal conductivity, meaning it does not transfer heat well [1], [2].

The unique chemical structure of ice gives it a broad range of physical properties, including its slipperiness. This phenomenon can be attributed to several parameters governing its molecular structure and interaction with the surrounding environment and objects. The slipperiness of ice is defined by its low coefficient of friction, which arises due to the presence of a thin layer of water molecules on its surface, known as a liquid-like layer (LLL) [1]–[3], [11], [16], [28], [32]. Ambient conditions and contact with a warmer surface influence the formation of LLL. The thickness of LLL on ice essentially defines the friction regime that will occur during an object sliding on ice. If LLL thickness exceeds sliding body roughness asperity amplitude, a fully hydrodynamic regime with a low coefficient of friction occurs. However, very thin LLL could cause a boundary friction regime where mechanical interlocking of sliding body texture asperities and ice occurs, resulting in a higher coefficient of friction [2], [11], [16], [27], [32]. These principles are summarized in the following Stribeck curve (see Fig. 4 b)), where the coefficient of friction on ice is shown on the vertical axes, and movement velocity is on the horizontal axis.

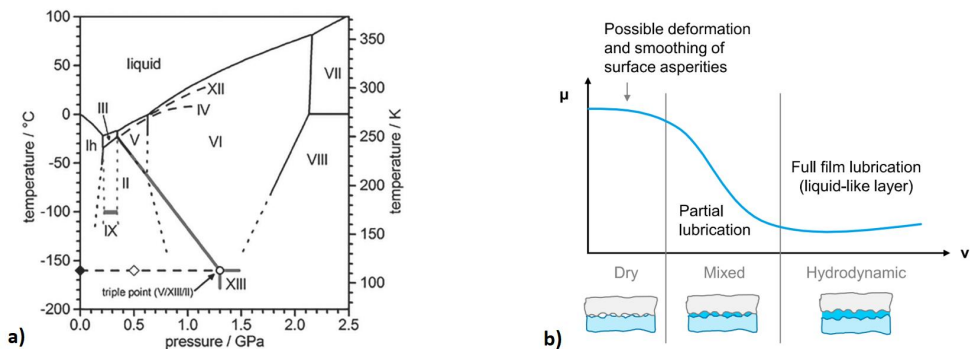


Fig. 4. a) Phase diagram of ice [1]; b) the Stribeck curve for the ice friction. The coefficient of friction on ice is shown on the vertical axes, and movement velocity is on the horizontal axis [6].

The slipperiness of ice is also influenced by the pressure exerted on its surface by external forces and movement velocity [2], [11], [16], [28], [32]. For example, ice can become more slippery when subjected to frictional heating, such as when a skater glides over ice [3], [40], [42], [47], because the friction causes the water molecules in the surface layer to melt, creating a liquid-like layer that further reduces the coefficient of friction.

Another parameter that can significantly influence the slipperiness of ice is its temperature [1]–[3], [16], [19], [32], [48], [49]. As the temperature of ice increases, it starts to melt and form a thicker liquid-like layer, thereby reducing its coefficient of friction. Conversely, as the ice temperature decreases, the water molecules on its surface start to freeze, creating a rougher surface that increases its coefficient of friction.

The coefficient of friction is affected by the contact area between the sliding body and the ice since the contact area directly influences the magnitude of the interfacial forces acting between the two materials. The frictional forces arise primarily due to the interlocking of asperities on the contact surfaces and the materials' deformation at the interface. The contact area controls the number of asperities in contact and the extent of deformation, thereby determining the overall frictional resistance. A larger contact area leads to a greater number of interlocking asperities. Conversely, a smaller contact area would result in less interlocking. The contact area also plays a role in heat dissipation during sliding, where a larger area allows for more intense heat transfer from the sliding body to the ice. Hence, the contact area is a crucial parameter in determining the frictional behavior of sliding bodies on ice, and carefully controlling it is essential for surface engineering for various applications.

Figure 5 summarizes the most influential parameters that define surface friction on ice.

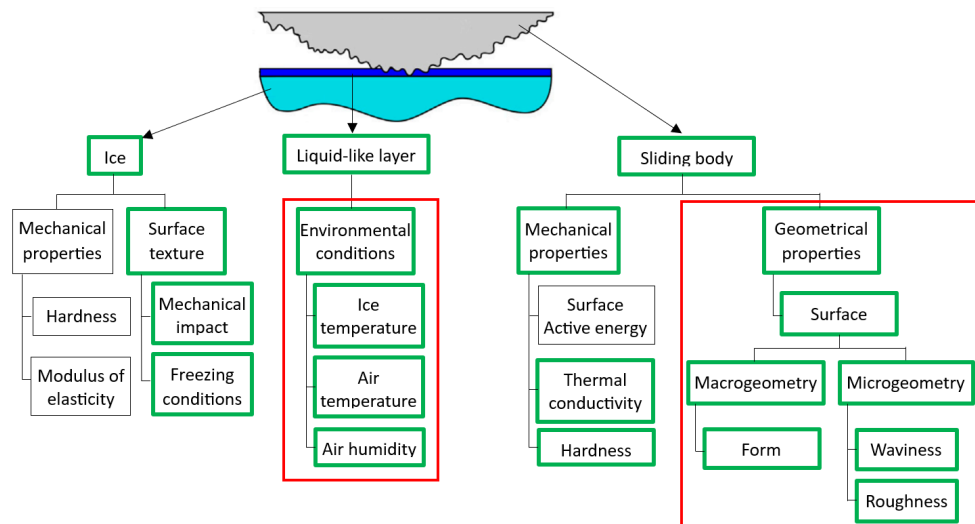


Fig. 5. Most influential parameters that define surface friction on ice. The parameters marked green are considered in the Doctoral Thesis. The parameters marked red highlight parameters primarily addressed in the Doctoral Thesis.

In conclusion, the slipperiness of ice is due to the formation of a thin layer of water molecules on its surface, which reduces its surface coefficient of friction. The parameters that

influence the slipperiness of ice include ambient air and ice temperature, air humidity, movement velocity, the contact area between the sliding body and the ice, surface texture orientation, contact pressure, chemical properties of the sliding body, hardness of the ice surface, and others. A better understanding of these parameters and their interconnection can improve the design of products that can enhance or reduce friction in various applications. Primarily the Doctoral Thesis focuses on sliding body geometrical property measurements and characterization to improve understanding of surface interaction with ice and liquid-like layer.

2. Literature analysis

Within the doctoral Thesis, a new methodology for sliding body surface macrogeometry and microgeometry measurements and analysis was developed and approved. The Thesis author realized that such a method is necessary after noticing that many times in his experiments, identical test samples with the same roughness values, which should perform the same in friction tests, had a noticeably different tribological performance. This observation made the author hypothesize that some crucial information about the test sample geometry was missing, hiding the explanation of why these apparently identical test samples have different friction with ice. Knowing this problem, the Doctoral Thesis author researched how other scientists have measured and characterized their test sample surfaces in ice friction studies. The literature review summarized in **Publications 1, 2, 5, and 6** [7], [15], [26], [45] concluded that each research group working on this topic has its unique approach, equipment, and methods for preparing, measuring, and interpreting test sample geometry. Unfortunately, none of these methods included holistic information about the test sample geometry. Mostly only the roughness of the surface was considered, suggesting that other research groups might face the same issues with unreliable test surface description, so the work on a new surface macro geometry and microgeometry measurement and post-processing method began.

The first step in new methodology development was finding the most suitable measurement tool for the task. Different measurement tool capabilities, advantages, and disadvantages were compared and examined in **Publications 1 and 6** [15], [45]. Table 1 summarizes the measurement tool comparison presented in **Publication 6**.

Table 1 [15]

Limitations of the surface topography measurement tools (symbols +, ?, and X stand for “measurement is possible”, “measurement might be possible”, and “measurement is not possible”, respectively)

	Form	Waviness	Roughness	Limitations	Typical measurement limits
2D measurements					
Profilometer – contact	+	+	+	Stylus tip radius > 1 μm	Profile length: 100 mm Height: 2 mm
Optical microscope	X	?	+	Surface reflection, contrast	Area: 200 \times 200 mm
SEM	X	?	+	Sample preparation	Area: 5 \times 5 mm
3D measurements					
Coordinate measurement machine	+	?	X	Stylus tip diameter > 300 μm	Produced in small and large sizes
Contour measurement machine	+	+	?	Stylus tip radius > 25 μm	200 x 100 mm Height: 60 mm
Non-contact profilometer	+	+	+	Light absorption Reflection Steep asperity slopes	Area: 150 \times 200 mm Height: 2 mm
Contact profilometer	+	+	+	Stylus tip radius > 1 μm	200 \times 100 mm Height: 2 mm
AFM	X	?	+	Limited sample size	Area: 200 \times 200 μm Height: 50 μm

Even though all compared measurement tools are useful and have their advantages, it was concluded that the contact-type profilometry is best suited for this task due to the following reasons:

- All three surface components (form, waviness, and roughness) can be measured. This approach provides the possibility to perform one measurement, which can afterward be analyzed using all surface components together or separately if needed.
- A broad measurement range is possible, allowing work with larger objects that can later be used in field tests.
- Heavy samples can be measured (up to 10 kg), ensuring that large test objects like bobsleigh or skeleton runner can be measured.

It was also concluded that a 3D contour measurement machine and 3D coordinate measurement machine (CMM) would be the best complementary tool for larger amplitude form measurements, and an atomic force microscope (AFM) is needed if minor amplitude scratches or patterns on small polished surfaces with very great details must be examined [45].

The next step was investigating what type and size samples were used in known studies, how their geometry was measured, and which parameters were used to characterize the geometry. Comparison is discussed in **Publication 6**. It was concluded that only a tiny fraction of the whole sliding body surface was typically measured (see Table 3), meaning that

information about the investigated surface's entire geometry was missing. Table 2 summarizes surface texture parameters other researchers have used in the ice tribology field.

Table 2 [15]

Texture parameters used in the known ice tribology studies

2D parameters	
Ra	The arithmetical mean deviation of the assessed profile. Defines surface asperity average height [10], [26], [29], [37].
Rdq	Root mean square (RMS) slope of profile. Defines the steepness of the asperities [10].
Rsm	The mean width of the roughness profile elements [26], [37], [50]. Defines how densely packed or stretched roughness asperities are.
3D parameters	
Sa	Arithmetical mean deviation of the assessed surface [26], [45], [50].
Sq	RMS roughness [16].
Ssk	The skewness of the surface. Characterizes whether a sample has asperities on top of the flat surface or dimples/scratches below the flat surface [24], [33].
Sku	Kurtosis of the surface. The measure of the asymmetry of the probability distribution of a real-valued random variable about its mean [24], [33].
S10z	Ten-point height. Indicates surface height calculated using only 5 highest asperities and 5 lowest valleys. It gives better insight into texture asperity's actual amplitude. Due to the involvement of the 5 highest asperities, this parameter might change rapidly if the sample starts to wear [24].
Sz	The maximum amplitude of the surface texture. Indicates the height between the surface's highest asperity and deepest valley. As far as only the highest and lowest points are used, this parameter will change rapidly if the sample wears [22].
Sfd	Fractal dimension. Characterizes the complicity of texture. If the parameter value aspires to the number 2, the surface is smooth and less complex. If the parameter aspires to the number 3, the surface is more complex and thus has a larger theoretical contact surface [33], [35].
Non-standardized parameters	
β	Attack angle. The angle between the sample surface, which is considered flat, and snow (ice) roughness asperity slope [35].
KK	The criterion of contact. It is calculated as Rsm/Sa ratio. Indicates the steepness of asperities, i.e., a larger ratio represents smoother surfaces with low and wide asperities, but a smaller ratio represents high and densely packed asperities [26].

Besides the parameters described in Table 2, the bearing ratio curve (Abbot–Firestone curve) has been used to characterize sliding surfaces in ice tribology [7], [10], [36]. It describes the cumulative probability density function of the surface profile height.

Table 3 summarizes the data used by other research groups in their studies of experimental samples, surface measurement methods, and surface parameters.

Table 3 [15]

Examples of sample geometry, surface measurement equipment, and obtained surface texture parameters used by other research groups (abbreviations: n/s – not stated, L – length, W – width, H – height, R-radius)

Sample type and dimensions (mm)	Measured lengths/areas (mm)	Equipment	Calculated parameters	Ref.
Pin: Diameter = 3	0.4 × 2.8	Confocal microscopy	Ra, Rq, Rsk, Rku	[10]
Pin, dimensions: n/s	0.5 × 0.5	Stylus 3D profilometer	Ra, Rdq, Ssk, Sku, Sfd (D)	[33]
Ring type slider: outer diameter = 25.4; inner diameter = 23.4; H = 1	Profilometer: n/s AFM: n/s SEM: 0.2 × 0.2	Non-contact profilometer, AFM, SEM	Ra, microscale bump diameter	[29]
Steel ski: L = 487.5; W = 30; H = 30	1.7 × 1.8	Focus variation microscope	Sa, Sz, Ssk, Sku	[22], [24]
	3.3 × 3.3			
	8.2 × 7.8 11.3 × 11.3			
Steel runner: L = 150; W = 8; H = 20; runner transversal radius = 4	0.05 × 0.05	AFM	Sa, St	[22]
UHMWPE polymer samples: n/s	0.4 × 0.5	Interferometer, SEM	Attack angle	[35]
UHMWPE ski sole on aluminum body: L = 65; W = 40; H = n/s	0.5 × 1	Confocal microscopy	Width of the ridges	[9]
Laser textured skis with attachable metallic base plate: L = 200; W = 20; H = 0.5	0.6 × 0.6	SEM, Optical profilometer	Dimple diameter and depth	[8]
Silicon carbide spheres: R = 0.75; 6.00 Soda-lime glass spheres: R = 1.84 Sapphire sphere: R = 1.59 Model ice skate: R ≈ 22	0.2 × 0.2	laser-scanning confocal microscopy	Sq	[16]
Steel block: L = 35; W = 18; H = 14	2 × 2	Interferometer Contact type profilometer	Ra, Rsm, Rz, Rpk, Sa, KK, Sdq, Ssk, Sku	[6], [7], [26]
	20 × 10 32 × 16			

The literature review indicated that 12 different surface geometry describing parameters had been used. A common problem with these parameters is that they are calculated for the roughness component of the surface using different filter (cut-off) values, and roughness amplitude can be only a fraction of the whole surface texture amplitude. Figure 6 shows an example of different interpretations about the surface one can get if full surface measurement is available and what is visible if only a small section of the entire surface is measured. Previously known methods suggest small section measurement with the following roughness component filtration.

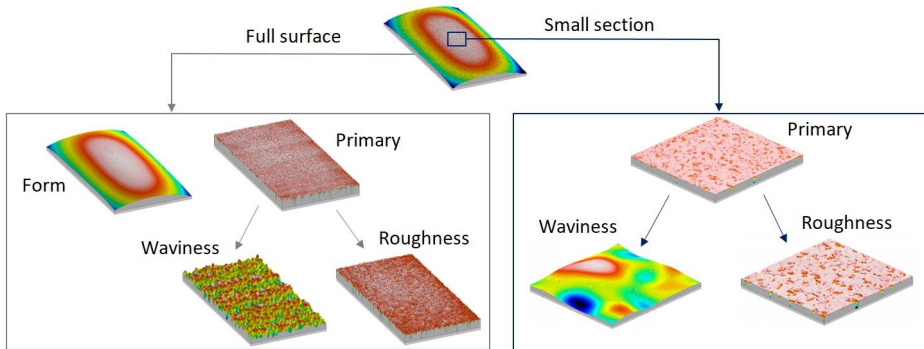


Fig. 6. Sample surface observation possibilities depend on the measured area of the sample. Full surface measurements provide essential information about surface macrogeometry (form) and microgeometry (waviness and roughness). On the other hand, small section measurements might have a higher measured point density, thus providing more details about the microgeometry, but information about the form is unavailable [15]. Missing information on the surface form can reduce the possibility of analyzing surface interaction with ice.

Figure 7 shows a workflow for the most common surface measurement approach and obtained result post-processing in the ice tribology research field. The measured surface is filtered multiple times during this approach, and only the filtered roughness component is considered, neglecting all information about the surface macrogeometry that might have the largest impact on the surface's final tribological performance.

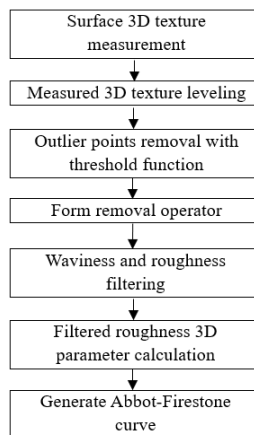


Fig. 7. Previously used 3D topography processing methodology.

Literature analysis concluded that a new unified approach for surface macrogeometry and microgeometry measurements and analysis was needed to include whole surface complexity in the research process.

3. Experimental research

Development of this Doctoral Thesis was based on conducting multiple practical experiments on two different tribometer setups. This study is the first known in the ice tribology research field when the same samples are tested on different tribometer setups, providing the unique possibility of comparing the observations from different methods. Such testing possibilities were possible due to the designed experimental sample size and geometry described below. The obtained tribology experiment results provided information on surface macrogeometry and microgeometry influence on friction on ice and allowed to compare tribology measurements from different test setups to double check surface geometry influence tendencies.

Experimental samples

All experimental samples of the Doctoral Thesis that were tested on tribometers were made as rectangular blocks with the following dimensions: 35 mm length, 18 mm width, and 14 mm height (see Fig. 8). The samples were processed in the same batch to ensure that the initial geometry was identical. Sharp edges and corners of the blocks were rounded to reduce edge collision with ice bumps.

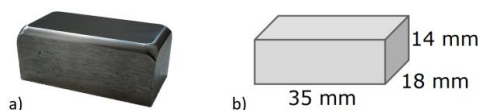


Fig. 8. a) Photo of experimental sample; b) sketch of experimental sample geometry.

The samples were made from the high corrosion resistance stainless steel Ramax HH (Uddeholm, Sweden) with the following chemical composition and physical properties.

Table 4

Uddeholm Ramax HH stainless steel chemical composition [51]

Element	C	Si	Mn	Cr	Mo	Ni	V	S
%	0.12	0.2	1.3	13.4	0.5	1.6	0.2	0.1

Table 5

Uddeholm Ramax HH stainless steel physical properties [51]

Property	At 20 °C
Density, kg/m ³	7700
Modulus of elasticity, Mpa	215000
Coefficient of thermal expansion per °C from 20 °C	10.8×10^{-6}
Thermal conductivity, W/m °C	24
Specific heat capacity, J/kg °C	460
Tensile strength Rm, MPa	1140
Yield strength Rp _{0.2} , MPa	990
Elongation A ₅ , %	12
Hardness, HB	330 ± 5

The experimental sample's test surface was polished with auto polisher *334 TI 15 Mecatech* (Presi, France). Detailed information about the polishing process is given in **Publication 7**.

The final sample textures were manufactured using different methods, i.e., abrading with fabric-based sandpapers (**Publications 2, 4, and 5**), shot blasting (**Publications 3, 4, 5, and 6**), CNC engraving (**Publications 5, and 7**), and femtosecond laser system engraving (**Publication 7**).

Tribology experiments

Two different types of tribometers were used to test the experimental sample's tribological performance. Both setups could control ambient conditions around the machine, allowing one to set different environmental conditions.

The inclined plane tribometer (see Fig. 9), developed by Riga Technical University engineers, measures the sample's sliding time in defined distances. Average sliding velocities at various sliding distances were calculated using known distances and measured time and used as indirect tribological performance describing parameters, i.e., higher velocity values mean lower coefficient of friction and vice versa. The inclined plane tribometer working principle and used experimental settings are described in **Publications 2, 3, 4, 5, 6, and 7**. During the Doctoral Thesis research, the inclined plane tribometer underwent several phases of improvement. Each improvement ensured a more stable climate around the tribometer and improved the resolution of the obtained result and ergonomics during the tests.

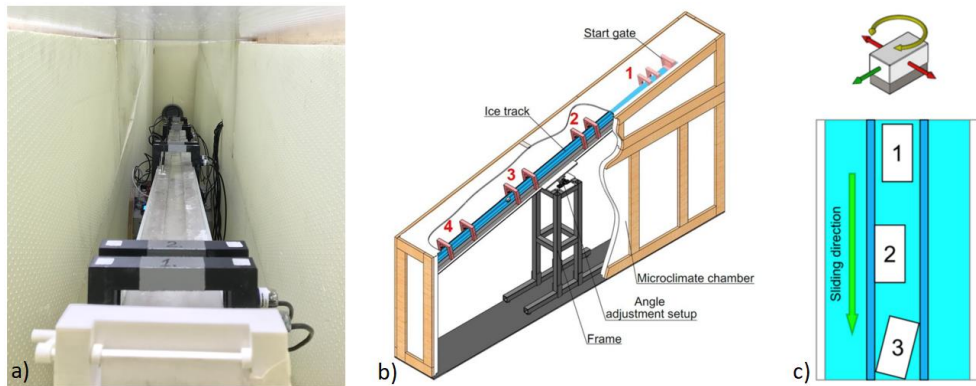


Fig. 9. a) Photo of the inclined plane tribometer; b) a schematic sketch of the inclined plane tribometer [7]; c) degrees of freedom of the steel samples during the tests on the inclined plane tribometer: 1 – ideal movement position; 2 – unwanted lateral translation of the sample; 3 – unwanted rotation of the sample [6].

The second tribometer used in the Doctoral Thesis was an oscillating type tribometer (see Fig. 10) *RVM1000* (Werner Stehr Tribology GmbH, Germany) located in the *V-Research GmbH* (Dornbirn, Austria) tribology laboratory. The oscillating tribometer measured the friction force between the ice and the surface of the steel sample. Static and dynamic coefficients of friction were calculated from the measured friction forces and applied load values. Calculated coefficients of friction were used to compare sample tribological

performances. The tribometer working principle and used experimental settings are described in more detail in **Publications 3, 4, and 6**.

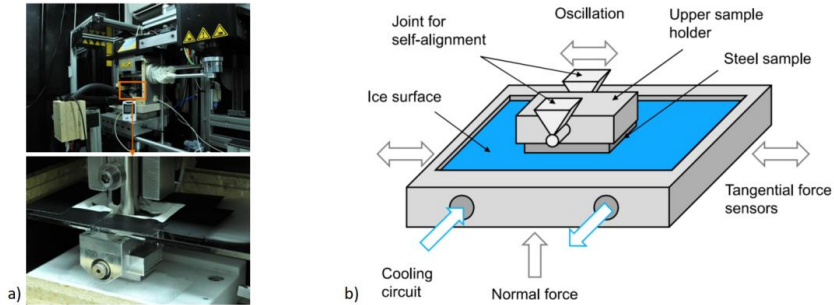


Fig. 10. a) Photo of an oscillating type tribometer *RVM1000*; b) a schematic sketch of an oscillating type tribometer [6].

Experimental sample 3D surface geometry measurements

Within the Doctoral Thesis, experimental sample surface geometry was measured and characterized with different instruments. The contact type profilometry was considered the most important and usable measurement tool to achieve the main goal, i.e., develop a new surface micro and macrogeometry measurement methodology. The 3D profilometry results were post-processed in *TalyMap Gold* software (Mountain Maps, France).

The following list shows which measurement tools were used in the publications of the Doctoral Thesis.

- Contact-type profilometer *Form Talysurf Intra 50* with standard stylus *112/2009* (Taylor Hobson, UK). **Publications 1, 2, 3, 5, 6, and 7.**
- Confocal microscope *VK-X250/260* (Keyence International NV/SA, Belgium). **Publications 3, 4, and 6.**
- Optical microscope *Eclipse LV150* (Nikon, Japan). **Publication 1.**
- Scanning electron microscope *S-4800* (Hitachi, Japan). **Publication 1.**
- Atomic force microscope *Smena NT-MDT* (NT-MDT Spectrum Instruments, Russia). **Publication 1.**

4. New surface macrogeometry and microgeometry measurement methodology

A new methodology that defines a general strategy of surface texture measurements and results interpretation in this Doctoral Thesis is graphically shown in Fig. 11. This methodology and its advantages over previously used methods are described in more detail in **Publications 5, 6, and 7**. The main advantage of the new methodology is the possibility of calculating surface contact area containing the full surface complexity (form, waviness, and roughness), providing the missing data for contact pressure calculations between the sliding surface and ice. This information ensures a better explanation for surface texture's influence on friction on ice.

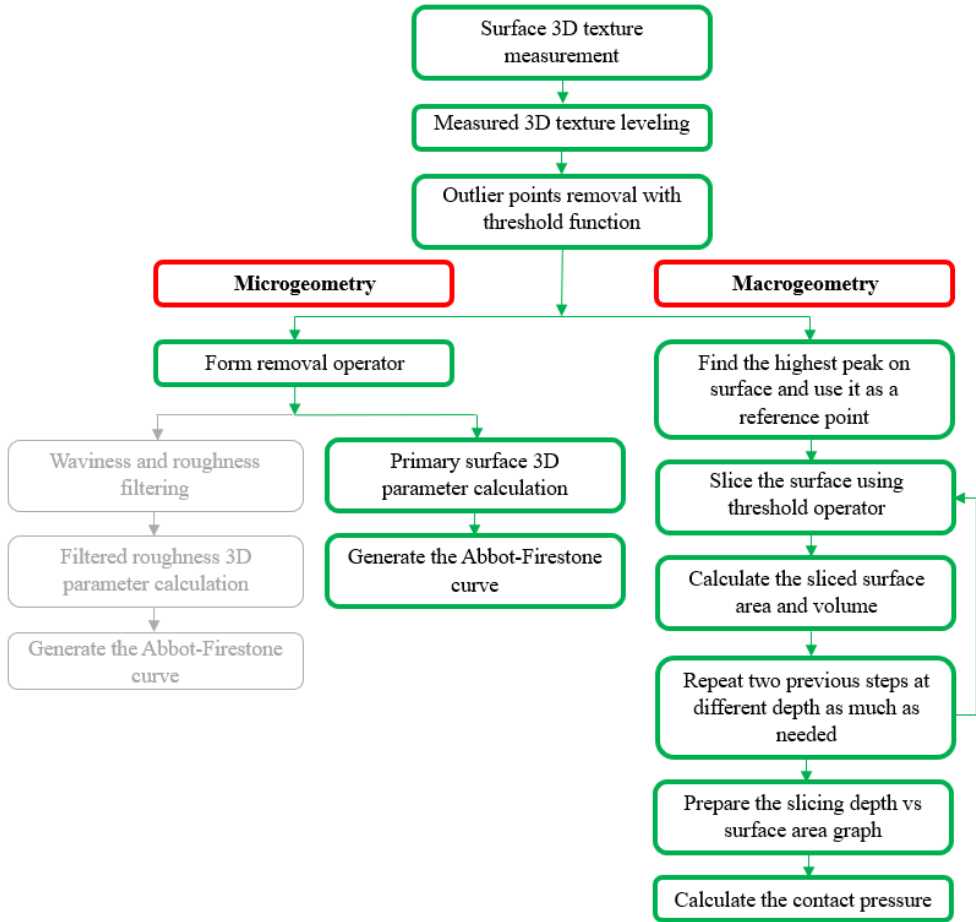


Fig. 11. A graphical interpretation of new surface macrogeometry and microgeometry measurements and result processing methodology. The block in grey shows the previously used approach, while the blocks in green show the new methodology steps.

The Thesis author proposes to perform surface virtual slicing using the "Threshold" operator in 3D surface analysis software. First, the measured 3D surface must be leveled, and the highest texture point must be used to define the virtual slicing plane reference. The highest point is used as a reference because this point will be the first one in contact with ice during the tribology experiments. An external force applied to the sample along with the heat transfer causes the ice to melt, resulting in the surface plowing into ice, increasing the contact area. By performing the proposed virtual slicing method, measuring the contact area at different sample plowing depths in the ice is possible, providing necessary information for contact pressure calculations. Figure 12 shows a schematic principle of surface virtual slicing.

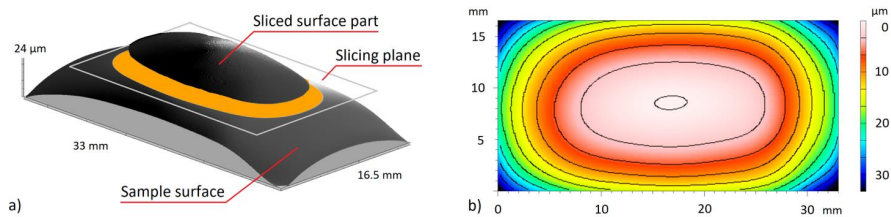


Fig. 12. a) Representation of the surface virtual slicing using the "Threshold" operator. Virtual slicing plane separates the surface segment from the entire surface, and its surface area and volume can be calculated. b) Contour map example of a sliced surface. A 3 μm step between the virtual planes was used in this example. The obtained contours show which parts of the entire surface would contact ice at various plowing depths. If the surface has curvature, as shown in this example, the actual contact area with ice is significantly smaller than the nominal surface area [15].

Calculated contact area values at different heights from the highest point can be used to calculate the contact pressure between the sliding body and the ice providing essential information for analyzing how significantly the sliding surface will plow in the relatively soft ice. Figure 13 shows how measured contact area is used to calculate contact pressures for tribometer setups used in this Doctoral Thesis.

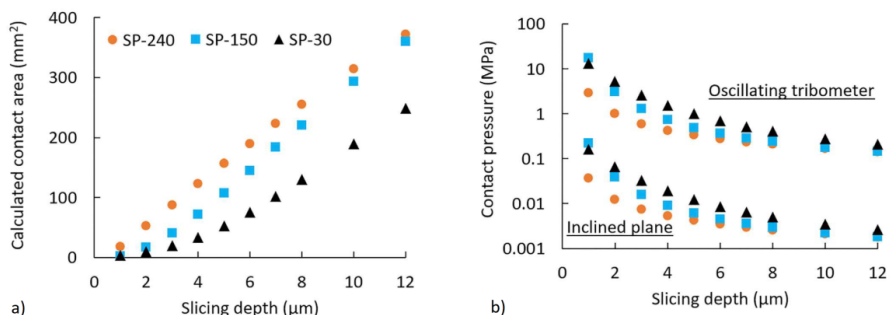


Fig. 13. a) Examples of measured surface contact area values at different slicing depths from the surface's highest point. Due to the sample surface curvature, the contact area increases at a lower slicing depth. The smoothest sample (SP-240) has the largest contact area and thus the lowest contact pressure, while the roughest sample (SP-30) has the highest contact pressure. b) Calculated contact pressure (shown in logarithmic scale) at various slicing depths for two experimental setups (oscillating tribometer and inclined plane tribometer). The most significant differences in contact pressure between the samples occur at smaller slicing depths, where surface asperities play a more prominent role. If the sample surface were sliced at 12 μm below the highest surface peak, the contact pressure evens for all samples [15].

Information about the actual contact area and the calculated contact pressure is a major improvement in the ice tribology research field because the results can be used in the theoretical coefficient of friction calculation models, which previously used only nominal values of the

surface geometry. With the new methodology, the actual contact area is known and can be directly used in further calculations. A visual example of surface measurement post-processing according to the new methodology is shown in the Appendix 10.

5. Approbation of the new methodology

New surface macrogeometry and microgeometry measurement methodology was approbated comparing it with the previously used surface characterization methods. Experiments and comparisons are described in **Publications 5, 6, and 7**. The following chapters highlight the most important results of the methodology approbation experiments.

Comparison of surfaces produced with different manufacturing methods

The most significant benefit of the newly developed sliding surface macrogeometry and microgeometry measurement methodology is the possibility to reliably compare surfaces produced with different manufacturing methods, which was impossible using previously known methods.

For example, patterned surfaces with deep grooves can be manufactured, as shown in the Figure 14 section Milled surfaces. However, how to reliably characterize such surfaces using only surface roughness parameters is unclear.

One may try performing a surface measurement between the grooves, but there might not be enough space for 3D measurement if the grooves are tightly spaced. Another option would be the contact area theoretical calculations knowing the sample's initial surface and subtracting the grooved area. However, this approach could result in a significant error due to the imperfections of the surface, which caused the need for a new surface characterization method in the first place. Another issue is the potential material pile-ups on the edges of the grooves, as shown in Fig. 17. Without proper surface texture measurements, it is not possible to detect them. These issues raise many questions on how to measure such complex surfaces reliably. The solution is a newly developed surface macrogeometry and microgeometry measurement method that includes whole surface complexity (form, waviness, and roughness). This methodology removes none of the surface components during the comparison, providing a more realistic interpretation of the comparable surfaces. It does not matter if the surface is manufactured by milling, shot blasting, laser texturing, etc. The new methodology needs a complete 3D texture measurement that gets to be virtually sliced afterward and calculated contact areas or bearing ratios used as surface geometry characterizing parameters.

In **Publication 5**, eight differently manufactured surfaces (see Fig. 14) were, first, described using the bearing ratio curves, and to compare the new methodology with the previously used, surface roughness parameters S_a , S_{dq} , S_{sk} , and S_{ku} were also measured for all surfaces.

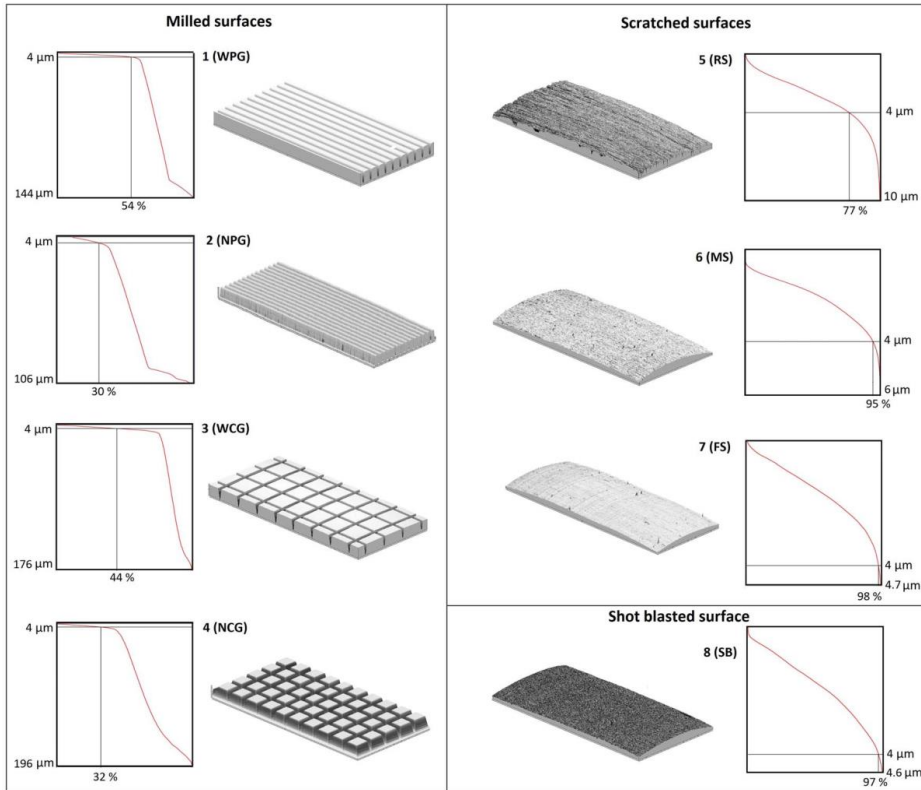


Fig. 14. Examples of differently manufactured surface 3D textures. Milling patterned samples WPG, NPG, WCG, NCG, scratched samples RS, MS, FS, and shot blasted sample SB. Graphs next to the 3D textures show the bearing ratios of these textures at $4\ \mu\text{m}$ from the highest point. Obtained results show that differently produced surfaces can have significantly different contact areas at the same plowing depth in the ice, resulting in different contact pressures that influence the coefficient of friction on ice [7]. (Copyright ASME)

Then samples were tested on an inclined plane tribometer setup at different ambient conditions. Experiment No. 1 was conducted at 64 % air humidity, $-2.5\ ^\circ\text{C}$ air temperature, and $-9\ ^\circ\text{C}$ ice temperature, and Experiment No. 2 was conducted at 78 % air humidity, $+1\ ^\circ\text{C}$ air temperature, and $-4\ ^\circ\text{C}$ ice temperature. The obtained sample sliding speed results were used to compare sample tribological performance. A higher average speed means a lower coefficient of friction. Then, tribology experiment results were compared with sample texture parameters and bearing ratio values. The comparison results are shown in Fig. 15.

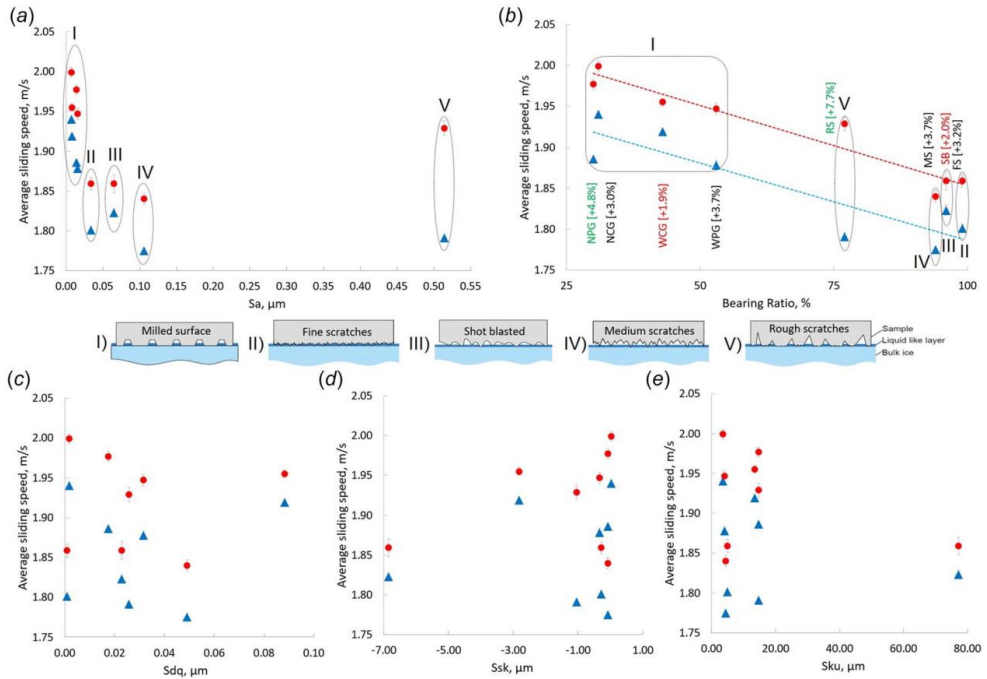


Fig. 15. Comparison between (a) average sliding speed and surface roughness parameter S_a , (b) average sliding speed and the bearing ratio at 4 micrometers from the highest surface point, (c) average sliding speed and surface roughness parameter S_{dq} , (d) average sliding speed and surface roughness parameter S_{sk} , and (e) average sliding speed and surface roughness parameter S_{ku} . Triangles, Experiment No. 1 (64 %, -2.5 °C, -9 °C); Dots, Experiment No. 2 (78 %, $+1$ °C, -4 °C). Circled areas and Roman numerals represent different surface textures shown in sketches below the graphs [7]. (Copyright ASME)

The obtained results showed a linear trend between the bearing ratio and sliding speed in these experimental settings. Changes in the ambient conditions shifted the tribology experiments' overall values, but the trendline remained the same. In such experimental settings, smaller contact areas promoted better tribological performance. Remembering that the inclined plane tribometer setup has low contact pressure (<1 MPa), it is vital to remember that a significant contact pressure increase could result in different results due to the sample plowing in the ice.

The observed correlation between average sliding speed and surface roughness parameter S_a was not as good. The results proved that the surface roughness parameter S_a is not the best parameter for ice tribology research to describe the surface texture. Additionally, it was proven that there were no logical trends between average sliding speed and surface roughness parameters S_{dq} , S_{sk} , and S_{ku} . The obtained results showed great potential to use the bearing ratio as a surface characterization parameter instead of S_a if the experimental sample surfaces have different surface textures. However, if the surface manufacturing method is the same and

only manufacturing parameters are slightly changed, the surface roughness parameter Sa can also be used.

Comparison of surfaces produced with the same manufacturing process

After the differently manufactured surface comparison described above, the new surface macrogeometry and microgeometry measurement methodology was also approved on samples produced with the same manufacturing method to see if also, in such cases, there are noticeable benefits compared to the previously known method. This study is fully described in **Publication 6**, but the following chapter will highlight the study's main results.

Experimental samples of this study were prepared by combining sandblasting and polishing to produce smooth surfaces with randomly distributed dimples. In Fig. 16, the prepared surfaces are shown.

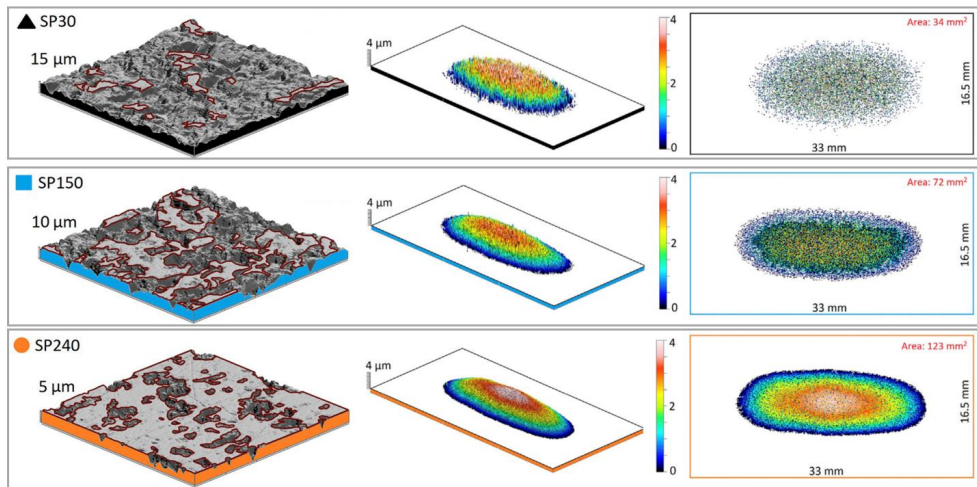


Fig. 16. Shotblasted samples. The 3D texture closeup (500 × 500 μm) is shown on the left. Sample virtually sliced surface parts at 4 μm from the highest point are shown in the middle.

The projected surface areas of the sliced surface part are shown on the right [15].

Table 6 shows a calculated proportion of variance (RSQ) between the measured surface parameters and the coefficient of friction measurements from the oscillating tribometer. The closer the RSQ value gets to 1, the better the correlation between the compared parameters. For a graphic representation, RSQ values are prepared in a color scale, reaching from red (value 0) to yellow (value 0.5) and green (value 1). Red shades represent areas with low correlation, while green shades represent areas with high correlation. For more details, please see **Publication 6**.

Table 6 [15]

The proportion of variance (RSQ) between surface roughness/contact pressure and the measured coefficients of friction (COF) on the oscillating tribometer

Information about sample surface																			
Contact Pressure, [MPa]	Slicing depth, [μm]	SP30	SP150	SP240															
	1	13.18	17.57	2.93															
	2	5.27	3.10	0.99															
	3	2.64	1.29	0.60															
	4	1.55	0.73	0.43															
	5	0.99	0.49	0.34															
	6	0.69	0.36	0.28															
	7	0.52	0.29	0.24															
	8	0.41	0.24	0.21															
	10	0.28	0.18	0.17															
12	0.21	0.15	0.14																
Texture parameters	Sa (R), μm	3.2	2.4	1.0															
	Sa (P), μm	1.7	1.1	0.4															
	Ssk (P)	-0.6	-1.2	-2.9															
	Sku (P)	3.0	3.8	12.0															
	Sds (P), pks/mm ²	4272	5622	10881															
Oscillating tribometer tests																			
Velocity, [m/s]	incr./decr.	COF values			Contact Pressure VS COF, [RSQ]								Texture VS COF, [RSQ]						
0.02	Increase	0.079	0.028	0.014	0.18	0.91	0.98	1.00	1.00	1.00	1.00	0.99	0.98	0.76	0.89	0.70	0.52	0.64	
0.04		0.057	0.023	0.014	0.17	0.90	0.98	1.00	1.00	1.00	1.00	0.99	0.98	0.75	0.88	0.70	0.52	0.63	
0.10		0.045	0.024	0.015	0.25	0.95	1.00	0.99	0.99	0.99	0.98	0.98	0.96	0.95	0.83	0.94	0.78	0.61	0.72
0.15		0.041	0.023	0.016	0.23	0.94	1.00	1.00	1.00	0.99	0.99	0.98	0.97	0.95	0.81	0.93	0.76	0.59	0.70
0.19		0.043	0.028	0.023	0.20	0.93	0.99	1.00	1.00	1.00	0.99	0.99	0.98	0.97	0.79	0.91	0.74	0.56	0.67
0.29		0.029	0.019	0.017	0.14	0.88	0.97	0.99	1.00	1.00	1.00	1.00	0.99	0.99	0.71	0.85	0.66	0.47	0.59
0.39		0.033	0.020	0.016	0.19	0.92	0.99	1.00	1.00	1.00	1.00	0.99	0.98	0.97	0.78	0.90	0.72	0.54	0.66
0.29		0.030	0.019	0.015	0.18	0.94	0.99	1.00	1.00	1.00	0.99	0.99	0.97	0.96	0.80	0.92	0.75	0.58	0.69
0.19		0.039	0.024	0.018	0.24	0.95	1.00	1.00	1.00	0.99	0.99	0.98	0.97	0.95	0.82	0.93	0.77	0.60	0.71
0.15	Decrease	0.040	0.023	0.016	0.24	0.95	1.00	1.00	0.99	0.99	0.98	0.96	0.95	0.82	0.93	0.78	0.60	0.71	
0.10		0.044	0.023	0.016	0.20	0.93	0.99	1.00	1.00	1.00	0.99	0.98	0.97	0.79	0.91	0.74	0.56	0.67	
0.04		0.051	0.023	0.015	0.18	0.91	0.98	1.00	1.00	1.00	1.00	0.99	0.98	0.76	0.89	0.71	0.53	0.64	
0.02		0.059	0.023	0.015	0.15	0.89	0.99	0.99	1.00	1.00	1.00	0.99	0.99	0.73	0.86	0.67	0.49	0.60	

Obtained results proved that the new method of using the calculated contact area of the entire sliding body surface provides a better correlation between the surface geometry and friction on ice. A more detailed explanation of this can be found in **Publication 6** [15].

Microgeometry impact on coefficient of friction on ice

Experimental studies have proven that macrogeometry has a more significant role in the friction process, suggesting that optimizing this geometry component must be prioritized. However, the neglect of microgeometry components may cause a significant friction increase. This problem is explained in Publication 7. In this study, the sample surface area with ice was reduced by milling parallel grooves. During this machining process, material pile-ups formed on the edges of the grooves, as shown in Fig. 17 (top left). The pile-ups varied in height and were unsymmetrical on each ridge, extending 8 μm to 20 μm from the top surface. After milling the grooves, these samples were tested on an inclined plane tribometer, and their tribological performance was compared to a polished surface without grooves with a larger contact area with ice. From the previously discussed results, the grooved surface with a smaller

contact area should slide faster, but experimental results showed that grooved surfaces had approximately 8 % slower sliding speed than the reference (see Fig. 17, bottom left). These results proved that focusing on macrogeometry without considering microgeometry will not provide the desired surface tribological performance.

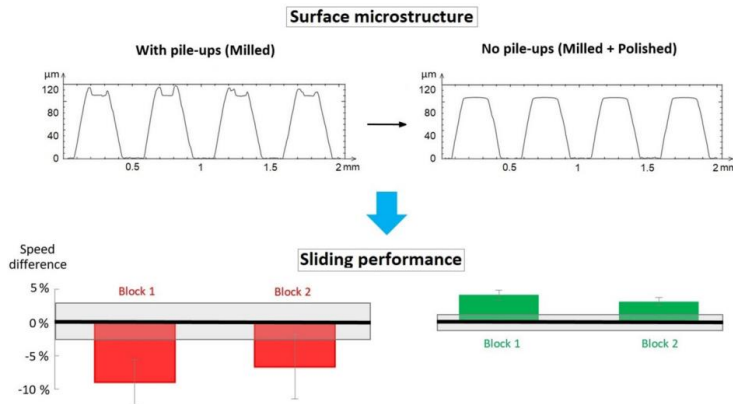


Fig. 17. The experimental sample profile directly after groove milling is shown in the top left side of the image, and the profile from the same surface location after additional repolishing is shown in the top right side. The sliding speed of the sample with pile-ups was slower relative to the polished, flat surface reference (a grey area in the graph) but faster when the pile-ups was removed by polishing [5].

After initial experiments, additional polishing was performed for the grooved samples. The polishing process removed the pile-ups, flattened, and rounded the edges. The groove width increased from about 0.175 mm to 0.190 mm, introducing a gentle rounding at the edge of each groove, as seen in Fig. 17 (top right). Polishing out the pile-ups removed the microscopic aspect and returned a nanoscopic roughness on the ridge surface to 13 nm.

Then these samples were tested one more time on the inclined plane tribometer. With the pile-ups removed, the sliding speed was approximately 4 % faster than the polished reference surface. Simply repolishing resulted in a 12 % difference in surface tribological performance. This significant sliding performance difference emphasized the influence of both microscaled and macroscale contact areas on the sliding speed. A more detailed discussion of this can be found in **Publication 7** [5].

Sliding body surface temperature influence on friction on ice

It was already known that sliding body temperature significantly influences the sliding ability on the ice. Historically winter sports athletes used to heat their equipment before the competition to increase the ice surface melting, which in most cases resulted in better results. Because of the temperature's significant influence, preheating winter sports equipment in many sports is forbidden. For example, in bobsleigh, skeleton, and luge competitions, sleigh runner temperature is monitored before the start and cannot exceed the reference temperature.

What was not known was how specific changes in sliding object geometry at different temperatures influence friction properties. The question was whether one should increase the

contact area with ice or reduce it depending on the ambient temperature and humidity, ice temperature, and sliding body temperature to improve sliding performance. Two practical experiments were conducted using samples with different contact areas at different temperatures. The ice temperature ($-9\text{ }^{\circ}\text{C}$) was kept the same, but the sample temperature was first reduced to $-18\text{ }^{\circ}\text{C}$, and during the second set of tests sample temperature was kept at $+5\text{ }^{\circ}\text{C}$. See more details in **Publications 3, 4, and 6** [4], [6], [15]. Figure 18 shows the coefficient of friction value differences at these test conditions.

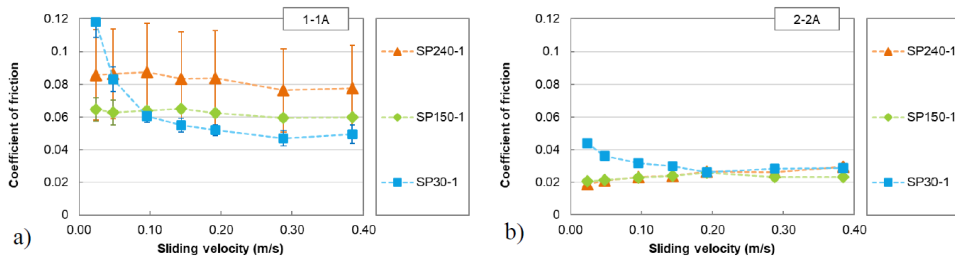


Fig. 18. Coefficient of friction measurements. a) For test setup 1-1A, where the sample temperature was $-18\text{ }^{\circ}\text{C}$, the coefficient of friction decreased with sliding velocity increase, and friction was higher for samples with a larger contact area with ice. Also, it was noticed that the surface contact area significantly impacts the measured friction value. b) For test setup 2-2A, where the sample temperature was $+5\text{ }^{\circ}\text{C}$, the overall friction value significantly decreased compared to test setup 1-1A, as logically predicted, but the influence of surface contact area is not as pronounced. However, it has an inverse effect on friction, as in test setup 1-1A, i.e., in this case, friction was higher for surfaces with smaller contact areas [4].

Obtained results highlight the overall surface temperature influence on sliding on ice and show that surface preparation might have an inverse effect on the process, so both parameters should be considered as a system to improve sliding on ice. These observations and the possibilities of new surface area measurements and thermal image recordings of the friction process might provide proof for surface temperature and contact area interaction explanation. Such a study is planned for the future.

CONCLUSIONS AND FUTURE OUTLOOK

The objective of the Doctoral Thesis was to develop a new methodology of sliding body surface macrogeometry and microgeometry measurements. The scientific literature review revealed that ice tribology studies never simultaneously considered sliding body surface macrogeometry (form) and microgeometry (waviness and roughness). According to previously known surface measurement methodologies, which considered only microgeometry, experimental sample surface area measurements included less than 2 % of the entire sliding body surface. Besides, sliding body surface macrogeometry was only considered in purely theoretical studies, which consider surface microgeometry ideally smooth. As a result, the sliding body surface contact area with ice cannot be determined. See **Publication 6**.

The objective of the Doctoral Thesis was achieved, and the main findings are the following:

1. A new methodology of sliding body surface macrogeometry and microgeometry measurements was developed. The new methodology contains measurements of sliding body surface form, waviness, and roughness components, which are further used in the sliding body surface and ice contact area determination. It was proved that the sliding body contact area with ice and coefficient of friction have a strong correlation (proportion of variance from 0.9 to 1). See **Publications 5, 6, and 7**.
2. The newly developed methodology of sliding body surface macrogeometry and microgeometry measurements allows for comparing the tribological performance of sliding body surfaces produced with various manufacturing methods, including abrasion, shot blasting, patterning with a milling or laser, chemical etching, and others. With the previously known methodology, tribological performance could be compared only for the samples manufactured with the same manufacturing method. See **Publication 5**.
3. It was proved that sliding body surface macrogeometry and microgeometry must be considered to ensure the previously specified coefficient of friction on ice. It was observed that sliding body surface macrogeometry (form) influences the contact area between the sliding body and ice. A study discussed in **Publication 5** proved that a 60 % increase in contact area reduced the sample average sliding speed by 7 %. However, microgeometry imperfections (high micro spikes and sharp edges) also influence the contact area. A study discussed in **Publication 7** proved that simple micro asperity removal from the sliding body surface could improve its average sliding speed by 12 %.
4. It was concluded that sliding body surface temperature must be considered during the coefficient of friction on ice determination. Experiments reported in **Publications 3 and 4**, with contact pressure between the sliding body surface and ice higher than 1 MPa, proved that for sliding body surfaces with temperature 9 °C below ice temperature, a reduction of contact area between the body and ice by 30 % reduced the coefficient of friction two times. However, if the sliding body surface temperature was 14 °C higher than the ice temperature, the same 30 % contact area reduction resulted in a two times higher coefficient of friction, inverting the surface texture influence trend. See **Publications 3 and 4**.

Considering the findings of the Doctoral Thesis, future research on surface texture influence on the coefficient of friction on ice should implement the new methodology of sliding body surface macrogeometry and microgeometry measurements along with thermal imaging recordings of the friction experiments. The combination of the sliding body surface geometry and thermal observations contains information for a better explanation of sliding surface interaction with ice. The developed methodology should be tested on different size and shape samples in various experimental settings not included in this Doctoral Thesis.

REFERENCES

- [1] I. Olovsson, “Snow, ice and other wonders of water: A tribute to the hydrogen bond,” *Snow, Ice And Other Wonders Of Water: A Tribute To The Hydrogen Bond*, pp. 1–86, Dec. 2015, doi: 10.1142/9928/SUPPL_FILE/9928_CHAP01.PDF.
- [2] “Physics and Chemistry of Ice,” *Physics and Chemistry of Ice*, 2007, doi: 10.1039/9781847557773.
- [3] F. Du, P. Ke, and P. Hong, “How ploughing and frictional melting regulate ice-skating friction,” *Friction* 2022, pp. 1–23, Mar. 2023, doi: 10.1007/S40544-022-0711-9.
- [4] I. Velkavrh, J. Voyer, T. Wright, J. Lungevičs, E. Jansons, and I. Boiko, “Variations of ice friction regimes in relation to surface topography and applied operating parameters,” *Proceedings of the International Conference of DAAAM Baltic*, vol. 2021-April, 2021, doi: 10.1088/1757-899X/1140/1/012033.
- [5] K. A. Gross, J. Lungevics, E. Jansons, I. Jerane, M. J. Wood, and A. M. Kietzig, “Surface hierarchy: Macroscopic and microscopic design elements for improved sliding on ice,” *Lubricants*, vol. 9, no. 10, p. 103, Oct. 2021, doi: 10.3390/LUBRICANTS9100103/S1.
- [6] I. Velkavrh, J. Lungevičs, E. Jansons, S. Klien, J. Voyer, and F. Ausserer, “The Influence of Isotropic Surface Roughness of Steel Sliders on Ice Friction Under Different Testing Conditions,” *Lubricants* 2019, Vol. 7, Page 106, vol. 7, no. 12, p. 106, Nov. 2019, doi: 10.3390/LUBRICANTS7120106.
- [7] E. Jansons, J. Lungevics, I. Jerane, and K. A. Gross, “A smaller bearing ratio, as a surface texture measure, promotes faster sliding on ice,” *J Tribol*, vol. 143, no. 11, Nov. 2021, doi: 10.1115/1.4049704/1095466.
- [8] F. Ripamonti *et al.*, “Dynamic behaviour of miniature laser textured skis,” <https://doi.org/10.1080/02670844.2018.1512730>, vol. 36, no. 12, pp. 1250–1260, Dec. 2018, doi: 10.1080/02670844.2018.1512730.
- [9] R. Böttcher, M. Seidelmann, and M. Scherge, “Sliding of UHMWPE on ice: Experiment vs. modeling,” *Cold Reg Sci Technol*, vol. 141, pp. 171–180, Sep. 2017, doi: 10.1016/J.COLDREGIONS.2017.06.010.
- [10] M. Scherge, R. Böttcher, A. Spagni, and D. Marchetto, “High-Speed Measurements of Steel–Ice Friction: Experiment vs. Calculation,” *Lubricants* 2018, vol. 6, no. 1, p. 26, Mar. 2018, doi: 10.3390/LUBRICANTS6010026.
- [11] B. Weber *et al.*, “Molecular Insight into the Slipperiness of Ice,” *J. Phys. Chem. Lett*, vol. 9, pp. 2838–2842, 2018, doi: 10.1021/acs.jpcllett.8b01188.
- [12] C. A. Brown, “Surface Metrology Principles for Snow and Ice Friction Studies,” *Front. Mech. Eng.*, vol. 7, p. 98, Dec. 2021, doi: 10.3389/FMECH.2021.753906/BIBTEX.
- [13] J. von Schleinitz, L. Wörle, M. Graf, and A. Schröder, “Modeling ice friction for vehicle dynamics of a bobsled with application in driver evaluation and driving simulation,” *Tribol. Int.*, vol. 165, p. 107344, Jan. 2022, doi: 10.1016/J.TRIBOINT.2021.107344.
- [14] N. S. Vracas, D. Short, J. Banks, D. J. Taunton, and S. R. Turnock, “A trajectory simulation model to analyse the factors influencing the descent of a Skeleton athlete,” *Proc. Inst. Mech. Eng. P. J. Sport. Eng. Technol.*, p. 175433712211508, Jan. 2023, doi: 10.1177/17543371221150820.
- [15] J. Lungevics, E. Jansons, I. Boiko, I. Velkavrh, J. Voyer, and T. Wright, “A Holistic Approach Towards Surface Topography Analyses for Ice Tribology Applications,” *Front. Mech. Eng.*, vol. 7, p. 56, Jun. 2021, doi: 10.3389/FMECH.2021.691485/BIBTEX.
- [16] R. W. Lieferrink, F.-C. Hsia, B. Weber, and D. Bonn, “Friction on Ice: How Temperature, Pressure, and Speed Control the Slipperiness of Ice,” *Phys. Rev. X*, vol. 11, no. 1, p. 011025, Feb. 2021, doi: 10.1103/physrevx.11.011025.

- [17] I. Stafeca, L. Pluduma, J. Lungevics, and K. A. Gross, *Effect of surface modification on the wettability and static coefficient-of-friction between steel and ice*, vol. 800 KEM. 2019. doi: 10.4028/www.scientific.net/KEM.800.293.
- [18] S. Kim, H. Kang, D. Kim, Y. Z. Lee, and J. Lee, "Measurement of sliding friction coefficient of micro-line patterned surfaces on ice," *Appl. Phys. Lett.*, vol. 111, no. 21, p. 211601, Nov. 2017, doi: 10.1063/1.4995493.
- [19] E. Jansons, J. Lungevics, K. Stiprais, L. Pluduma, and K. A. Gross, "Measurement of sliding velocity on ice, as a function of temperature, runner load and roughness, in a skeleton push-start facility," *Cold. Reg. Sci. Technol.*, vol. 151, 2018, doi: 10.1016/j.coldregions.2018.03.015.
- [20] S. Bengaluru Subramanyam, V. Kondrashov, J. Ruhe, and K. K. Varanasi, "Low Ice Adhesion on Nano-Textured Superhydrophobic Surfaces under Supersaturated Conditions," *ACS Appl. Mater. Interfaces*, 2016, doi: 10.1021/acsami.6b01133.
- [21] N. Maeno, M. Arakawa, A. Yasutome, N. Mizukami, and S. Kanazawa, "Ice-ice friction measurements, and water lubrication and adhesion-shear mechanisms," *Can. J. Phys.*, vol. 81, no. 1–2, pp. 241–249, Jan. 2003, doi: 10.1139/p03-023.
- [22] M. Scherge, R. Bottcher, M. Richter, and U. Gurgel, "High-Speed Ice Friction Experiments under Lab Conditions: On the Influence of Speed and Normal Force," *ISRN Tribology*, vol. 2013, pp. 1–6, Dec. 2013, doi: 10.5402/2013/703202.
- [23] F. Braghin, E. Belloni, S. Melzi, E. Sabbioni, and F. Cheli, "Friction Between Runner and Ice," in *The Engineering Approach to Winter Sports*, New York, NY: Springer New York, 2016, pp. 33–51. doi: 10.1007/978-1-4939-3020-3_3.
- [24] S. Rohm *et al.*, "Friction Between Steel and Snow in Dependence of the Steel Roughness," *Tribol. Lett.*, vol. 59, no. 1, p. 27, Jul. 2015, doi: 10.1007/s11249-015-0554-x.
- [25] J. J. de Koning, G. de Groot, and G. J. van Ingen Schenau, "Ice friction during speed skating," *J. Biomech.*, vol. 25, no. 6, pp. 565–71, Jun. 1992.
- [26] E. Jansons, J. Lungevics, and K. A. Gross, "Surface roughness measure that best correlates to ease of sliding", in *Engineering for Rural Development*, 2016.
- [27] G. Amit and Gilead, "Why is ice slippery?" *New Sci. (1956)*, vol. 227, no. 3037, p. 38, Sep. 2015, doi: 10.1016/S0262-4079(15)31136-2.
- [28] A. Mills and Allan, "The coefficient of friction, particularly of ice," *Phys. Educ.*, vol. 43, no. 4, pp. 392–395, Jul. 2008, doi: 10.1088/0031-9120/43/4/006.
- [29] A. M. Kietzig, S. G. Hatzikiriakos, and P. Englezos, "Ice friction: The effects of surface roughness, structure, and hydrophobicity," *J. Appl. Phys.*, vol. 106, no. 2, p. 024303, Jul. 2009, doi: 10.1063/1.3173346.
- [30] A. M. Kietzig, S. G. Hatzikiriakos, and P. Englezos, "Ice friction: The effect of thermal conductivity," *Journal of Glaciology*, vol. 56, no. 197, pp. 473–479, Aug. 2010, doi: 10.3189/002214310792447752.
- [31] A.-M. Kietziga, M. N. Mirvakilia, S. Kamalb, P. Englezosa, and S. G. Hatzikiriakosa, "Nanopatterned Metallic Surfaces: Their Wettability and Impact on Ice Friction," *J. Adhes. Sci. Technol.*, vol. 25, no. 12, pp. 1293–1303, Jan. 2011, doi: 10.1163/016942411X555872.
- [32] A. M. Kietzig, S. G. Hatzikiriakos, and P. Englezos, "Physics of ice friction", *J. Appl. Phys.*, vol. 107, no. 8, p. 081101, Apr. 2010, doi: 10.1063/1.3340792.
- [33] A. Spagni, A. Berardo, D. Marchetto, E. Gualtieri, N. M. Pugno, and S. Valeri, "Friction of rough surfaces on ice: Experiments and modeling", *Wear*, vol. 368–369, pp. 258–266, 2016, doi: 10.1016/j.wear.2016.10.001.
- [34] R. S. Pritchard, G. S. Knoke, and D. C. "Skip" Echert, "Sliding friction of sea ice blocks," *Cold Reg. Sci. Technol.*, vol. 76–77, pp. 8–16, 2012, doi: 10.1016/j.coldregions.2011.04.001.
- [35] S. Ducret, H. Zahouani, A. Midol, P. Lanteri, and T. G. Mathia, "Friction and abrasive wear of UHMWPE sliding on ice," in *Wear*, 2005, pp. 26–31. doi: 10.1016/j.wear.2004.09.026.

- [36] L. Baurle, T. U. Kaempfer, D. Szabo, and N. D. Spencer, "Sliding friction of polyethylene on snow and ice: Contact area and modeling," *Cold Reg. Sci. Technol.*, vol. 47, no. 3, pp. 276–289, 2007, doi: 10.1016/j.coldregions.2006.10.005.
- [37] S. Sukhorukov and A. Marchenko, "Geometrical stick-slip between ice and steel," *Cold Reg. Sci. Technol.*, vol. 100, pp. 8–19, 2014, doi: 10.1016/j.coldregions.2013.12.007.
- [38] B. Weber *et al.*, "Molecular Insight into the Slipperiness of Ice," *Journal of Physical Chemistry Letters*, vol. 9, no. 11, pp. 2838–2842, Jun. 2018, doi: 10.1021/ACS.JPCLETT.8B01188/SUPPL_FILE/JZ8B01188_SI_002.WMV.
- [39] J. Lungevics, E. Jansons, and K. A. Gross, *Skeleton runner roughness and surface contact area influence on sliding ability: Field experiments*, vol. 800 KEM. 2019. doi: 10.4028/www.scientific.net/KEM.800.303.
- [40] E. P. Lozowski and K. Szilder, "Derivation and new analysis of a hydrodynamic model of speed skate ice friction," *International Journal of Offshore and Polar Engineering*, vol. 23, no. 2, pp. 104–111, 2013.
- [41] E. Lozowski, K. Szilder, and L. Poirier, "A bobsleigh ice friction model," *International Journal of Offshore and Polar Engineering*, vol. 24, no. 1, pp. 52–60, 2014, [Online]. Available: <http://www.scopus.com/inward/record.url?eid=2-s2.0-84883697973&partnerID=40&md5=99c2f74e6a8d18d646d46b27f63c4c4c>
- [42] E. Lozowski, K. Szilder, and S. Maw, "A model of ice friction for a speed skate blade," *Sports Engineering*, vol. 16, no. 4, pp. 239–253, Dec. 2013, doi: 10.1007/s12283-013-0141-z.
- [43] L. Poirier, E. P. Lozowski, S. Maw, D. J. Stefanyshyn, and R. I. Thompson, "Experimental analysis of ice friction in the sport of bobsleigh," *Sports Engineering*, vol. 14, no. 2–4, pp. 67–72, Dec. 2011, doi: 10.1007/s12283-011-0077-0.
- [44] E. J. Y. Ling, V. Uong, J. S. Renault-Crispo, A. M. Kietzig, and P. Servio, "Reducing Ice Adhesion on Nonsmooth Metallic Surfaces: Wettability and Topography Effects," *ACS Appl. Mater. Interfaces*, vol. 8, no. 13, pp. 8789–8800, Apr. 2016, doi: 10.1021/acsami.6b00187.
- [45] K. A. Gross, J. Lungevics, J. Zavickis, and L. Pluduma, "A comparison of quality control methods for scratch detection on polished metal surfaces," *Measurement*, vol. 117, pp. 397–402, Mar. 2018, doi: 10.1016/j.measurement.2017.12.022.
- [46] L. Poirier, E. P. Lozowski, and R. I. Thompson, "Ice hardness in winter sports," *Cold Reg. Sci. Technol.*, vol. 67, no. 3, pp. 129–134, Jul. 2011, doi: 10.1016/j.coldregions.2011.02.005.
- [47] E. Lozowski, K. Szilder, and S. Maw, "A model of ice friction for a speed skate blade," *Sports Engineering*, vol. 16, no. 4, pp. 239–253, Dec. 2013, doi: 10.1007/s12283-013-0141-z.
- [48] S. C. Colbeck, L. Najarian, and H. B. Smith, "Sliding temperatures of ice skates," <http://jobs.aapt.org/>, 1998, doi: 10.1119/1.18576.
- [49] D. D. Higgins, B. A. Marmo, C. E. Jeffree, V. Koutsos, and J. R. Blackford, "Morphology of ice wear from rubber-ice friction tests and its dependence on temperature and sliding velocity," *Wear*, vol. 265, no. 5–6, pp. 634–644, 2008, doi: 10.1016/j.wear.2007.12.015.
- [50] J. Lungevics, E. Jansons, and K. A. Gross, "An Ice Track Equipped with Optical Sensors for Determining the Influence of Experimental Conditions on the Sliding Velocity," *Latvian Journal of Physics and Technical Sciences*, vol. 55, no. 1, 2018, doi: 10.2478/lpts-2018-0007.
- [51] Uddeholm, "Uddeholm Ramax ® HH".

APPENDICES

APPENDIX 1
PUBLICATION 1

Gross K., Lungevics J., Zavickis J., Pluduma L. *A Comparison of Quality Control Methods for Scratch Detection on Polished Metal Surfaces*. Measurement, 2018, Vol.117, pages 397-402. ISSN 0263-2241.

Available: doi:10.1016/j.measurement.2017.12.022

Open access

© 2017 Elsevier Ltd. All rights reserved.



A comparison of quality control methods for scratch detection on polished metal surfaces



Karlis Agris Gross*, Janis Lungevics, Juris Zavickis, Liene Pluduma

Faculty of Materials Science and Applied Chemistry, Riga Technical University, Latvia

ARTICLE INFO

Keywords:

Polished surfaces
Scratch
Scratch detection
Microscopy
Quality control

ABSTRACT

Scratch detection and the location of the scratch on the surface is important in the quality control of multi-layered, functional and polished surfaces. Visual examination in good lighting conditions has been previously used to detect scratches, but interest to see finer scratches and their location should consider use of the optical microscope, and compare it with other imaging methods at the same magnification. Stainless steel was polished, scratched and then one specific location analyzed at the same magnification with all methods to determine the level of scratch detection. Atomic force microscopy, as the technique with a higher resolution, was used to determine the mean depth of every scratch as a reference. An image was then recorded with the different techniques and the number of visible scratches counted. Profilometry did not clearly identify scratches due to limitation of the 2 μm probe size. Light microscopy provided the fastest and most appropriate technique for quality control, detecting 70% of the scratches. Scanning electron microscopy only showed 35% of the scratches at the same magnification, but provided a good 2-D image of the scratch and the resulting metal pile-up.

1. Introduction

Quality control of polished surfaces is essential to maintain the longevity and performance in a range of engineering applications. Quality control presently relies on careful inspection in good lighting conditions by the naked eye, but there is a limit to the detection of defects seen by the naked eye [1], and so this initiates the inquiry of the best scratch detection method at a higher magnification. This study will use the highest magnification common to the selected imaging methods, to determine the best quality control method.

Scratches are best detected against a highly polished surface. A high surface finish can be attained by mechanical polishing [2], chemical polishing [3,4] or high temperature treatment (vapour [5], laser [6] and flame polishing [7]). Keeping scratch-free surfaces is important; for image quality on films in the film industry [8], for file storage in magnetic disk storage devices [9], and for maintaining low wear on CoCr hip prostheses [10]. Scratches are the most common form of surface degradation, but previous studies on scratches cannot be readily found, and despite extensive reports on scratch resistance, a Web of Science search – using search terms “surface imaging” and “scratch”, “imaging” and “scratch”, “microscope” and “scratch” – does not provide

the requested information.

After knowing that a scratch is present, the size, location and orientation of the scratch can offer further useful information. This is important for understanding the damage to multilayered surfaces and thin films covering underlying sensors, but also for surfaces where the scratch orientation can influence the interaction with radiation, water flow, air flow or movement over other surfaces. Methods such as interferometry do not show scratches smaller than about 0.5 μm [11,12] and so will not be considered. This investigation will address non-contact methods (optical microscopy and scanning electron microscopy) and contact methods (profilometry and atomic force microscopy). Examination conditions that improve the level of detection, but distort the scratch size and location of one scratch relative to another scratch will not be used. This rules out placing the surface at an angle to the incident electron beam in scanning electron microscopy, that otherwise improves the quality of the image.

The best measurement method should assess large areas, be portable and fast. Larger areas are more easily assessed by light microscopy and profilometry. Other optical methods such as vertical scanning interferometry [13] and digital holography [14] are also available for detecting scratches on large surfaces, but will not be considered since it is

* Corresponding author.

E-mail address: kgross@rtu.lv (K.A. Gross).

Table 1
A comparison of scratch detection methods.

	Light microscopy	Electron microscopy	Profilometry	Atomic force microscopy
<i>Practical considerations</i>				
Portability	✓	✓	✓	x
Speed	Fast	Slow	Slow	Slow
Evaluate large areas	✓	x	✓	x
<i>Advantages/disadvantages</i>				
Advantages	Works in air and liquids, Possible to differentiate chemical phases	High magnif., Large depth of field, Elemental analysis	3D image, Clear wave profile	3D image, High magnif., High resolution
Disadvantages	Lowest resolution, 2D image, Lowest magnif.	2D image, Difficult to locate scratch	Stylus wear, Scratches surface, Vertical features not accurate	< 20 µm high features, Small scan area, Stylus wear, Difficult to locate scratch

not as portable like optical microscopy and profilometry, Table 1. A fast assessment of the surface is only provided by optical microscopy. This then raises the question of how effective optical microscopy is for detecting scratches. What is the level of scratch detection by optical microscopy?

Scratching could create pile-ups at the side of the scratch and so assist in the detection of scratches by modifying the intensity of the signal in light and electron microscopy. Scratches from a symmetrical 1 µm wide diamond probe have aided the detection of scratches due to the light reflection from pile-ups, when viewed by the naked eye under good lighting conditions [15]. There is a high likelihood of the pile-up since symmetrical hard asperities only need to be tilted by 5° to create pile-up [14], and the source of scratches such as grains of sand will always be non-symmetrical, thus increasing the likelihood of metal pile-up. Consequently, metal pile-up could be used to identify scratches in images from light microscopy and electron microscopy.

Polished surfaces are being investigated to determine the effect of scratches on the movement of polished metal over cold surfaces. For this reason, a fast surface evaluation method is required for evaluating small polished metal blocks in laboratory tests and larger objects in field experiments. Since a fast assessment of each surface is required, then optical microscopy is the obvious choice, and so a comparison to other imaging techniques is required.

The objective of the investigation is to determine the ability of optical microscopy to locate scratches, in comparison to other methods used at the same magnification. Higher magnification methods such as atomic force microscopy and scanning electron microscopy will be used to collect additional information on the depth of the groove and the presence of pile-ups. These features will be mentioned during the discussion on the limits of light microscopy.

2. Methods

2.1. Preparation of metallic surfaces

A sectioned austenitic stainless steel block (62% Fe, 16% Ni, 14% Cr, 4.5% Mo, 1.4% Co, 1.25% Mn, 0.8% Cu) was hot mounted in a MecaTech 334 hot press (Presi, Bri et-Angonnes, France) to form a 30 mm diameter disc. The mounted steel sample was then ground on a Reflex Max 120 surface rotating at 250 rpm under a load of 40 N for 120 s, and then on a Reflex Max 220 surface with the same conditions. Polishing was conducted with 9 µm, 3 µm and 1 µm diamond suspensions (together with a Reflex Lub lubricant) on Reflex MedB, Reflex Ram and Reflex NT surfaces, under loads of 40 N, 35 N and 30 N, for 5 min, 4 min and 2 min, respectively. Reference scratches were introduced, indentations made to frame the area of investigation and then

the surface was cleaned with ethanol before applying the different scratch detection methods.

2.2. Visual examination

Three areas of investigation were marked on the polished surface with indentations from a Vickers indenter. Indentation marks spaced 100 µm from each other helped to maintain sample orientation as well as the same field of view for the different imaging methods. Images were taken with a light microscope, a scanning electron microscope, an atomic force microscope and a profilometer.

A Nikon LV150 Eclipse light microscope (Tokyo, Japan) collected an image in darkfield imaging conditions of the surface through a 100× objective lens (0.9 NA) to capture the scattered light from the scratches. The contrast and brightness of the image was then adjusted on the computer screen.

A Hitachi S-4800 scanning electron microscope (Tokyo, Japan) with a field emission electron source was operated at 15 kV and 1 nA to view the surface. An image at the highest resolution of 5120 × 3840 pixels was obtained at the same magnification as the optical microscope image. The sample surface was kept at 90° to the electron beam to prevent distortion of the image and maintain the same distance between scratches in the x and y directions.

A Smena NT-MDT atomic force microscope (NT-MDT Spectrum Instruments, Moscow, Russia) with a 10 nm sized probe scanned the surface along 1024 lines to obtain a 60 µm × 60 µm view. To optimize the resolution, a smaller total vertical movement was chosen by not including the indent within the imaging area. Since AFM is the most sensitive in detecting scratches, the total number of scratches, the position and depth of each scratch was determined from the AFM image as a reference to see how effective other methods would reveal the scratches.

A Talysurf Intra 50 (Taylor Hobson, UK) profilometer scanned the surface with a 112/2009 stylus (4 µm tip diameter). Calibration was conducted with a 112/2062-D-4148-04 ball (25 µm diameter). The precision of the profilometer verified with a Taylor Hobson Reference 112/1534 ($R_a = 6 \mu\text{m}$ and $R_{sm} = 0.133 \text{ mm}$) and a surface roughness standard comparator Flexbar Composite Pocket set No 16008 gave a 10% error in the recorded values. Data on the probe position was recorded for a total of 800 points by 800 points with an area outlined by a 1.8 × 1.8 mm rame at a speed of 0.5 mm/s. A 12 nm vertical resolution and a 1 µm horizontal resolution were recorded from measurements on the calibration ball.

The total number of scratches detected by each method, was expressed as a percentage of the total number of scratches, obtained from the AFM image. Scratch profiles from the AFM traces were used to

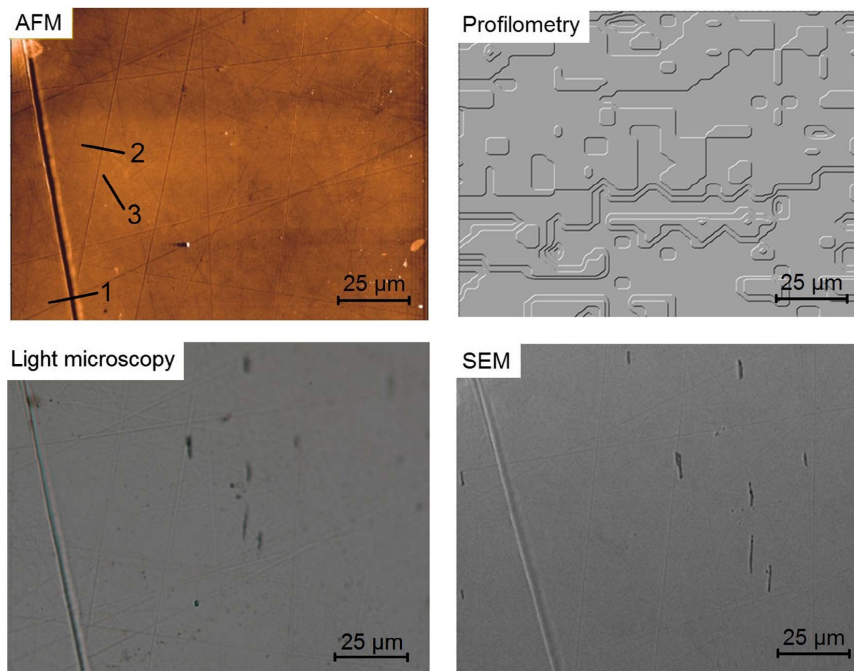


Fig. 1. A comparison of contact methods (AFM and profilometry) and non-contact methods (dark-field light microscopy and SEM) for imaging minor scratches on polished metal. The large scratch, labeled as 1, is made for reference. The three labels reference the scratch profiles shown in Fig. 2.

determine the depth of scratches detected by each imaging method.

2.3. Data analysis

Scanning Probe Image Processor (SPIP) software was used to ensure that the data obtained from the AFM and the profilometer is processed in the same manner. This removed the error associated with data processing from software provided by each equipment supplier. The image was placed on a level background by removing the slope using the *Global Leveling* function and was made flat by removing the curviness with the *Form Removal* function.

The total number of scratches was determined by AFM. The number of identifiable scratches were counted on the computer screen in images from the light microscope, SEM, AFM and profilometer. A comparison was then made to determine the number of scratches detected by the contact and non-contact imaging methods.

For quantitative analysis, the scratch profile from the 3D image was extracted along the length of the scratch with the *Cross Section Profile* function in the SPIP software. For more statistically reliable data on the scratch depth, the *Average Profile* function mathematically averaged the scratch depth and determined the average scratch shape.

3. Results and discussion

3.1. Detection of minor scratches on a polished surface

Only three imaging methods detected scratches at a magnification of $1000\times$, when the image was taken at the highest resolution. Both

non-contact methods (light microscopy and scanning electron microscopy) and atomic force microscopy displayed scratches.

The $2\mu\text{m}$ probe on the profilometer limited the measurement capability and so did not clearly show the small scratches, Fig. 1. A smaller $0.2\mu\text{m}$ radius probe has been used for greater sensitivity in other studies [16], but the large step size of the measuring method further limits the ability to detect scratches.

Image resolution and contrast are required for the best detection ability. Atomic force microscopy has the highest resolution and showed the most scratches. The SEM image had poor contrast and did not show small scratches when imaged at the same $1000\times$ magnification as the optical microscope. The large vertical reference scratch, at the left side of the image, was easily seen in the SEM due to the larger depth of the scratch and the pileup on both sides of the scratch. Higher magnification is required to detect scratches with the SEM, but the need to refocus, and the difficulty of finding scratches on the surface is not suitable for quality control in a timely manner, even in a more affordable benchtop scanning electron microscope.

The smallest visible scratch size, imaged at a magnification of $1000\times$ was detected with the AFM; further analysis provided the depth of each scratch. From a total of 24 scratches, 7 scratches (3 nm and deeper) were easily detected by all three microscopy methods (AFM, SEM and light microscopy), 13 scratches (1 nm to 3 nm deep) were visible, but four scratches at a depth of 1 nm could not be seen. The ease of viewing is appreciated by matching the scratches in Fig. 1 with the depth profiles in Fig. 2. The light microscope detected 70% of the scratches recorded by the AFM, but the SEM only showed 35% of the scratches seen by the AFM.

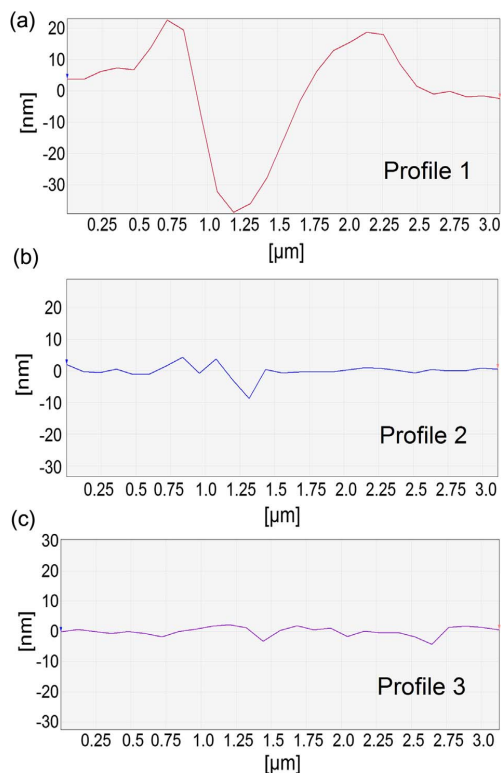


Fig. 2. The profile of three scratches as marked on the AFM image in Fig. 1.

Compared to previous studies, the optical microscope showed 500 times smaller scratches than the naked eye, as referenced to the study of scratches made by a nanoindenter and viewed by the naked eye [1]. This makes the optical microscope a powerful tool to inspect larger objects, quickly examine the surface, and detect 10 nm deep scratches on the polished steel surface. It would seem logical that a $1000\times$ magnification will show $1000\times$ smaller objects but this relies on tilting the surface to provide the best angle of light reflection for seeing the scratch. It is not possible to readily tilt polished steel objects on the light microscope at higher magnifications.

3.2. Characterization of scratches

The polished steel abraded by the 3000 grade sandpaper contained similar sized scratches on the surface, and showed that optical microscopy is the most appropriate quality control method. The black line arising from the pile-up next to the scratch showed the location of the scratch; brighter areas in the AFM image arose from the difference in height associated with the scratch, and the bright line in the SEM arose from a greater electron emission, Fig. 3. So, pile-up next to the groove provided easier scratch detection, Fig. 4. Absence of the pile-up makes it difficult to identification scratches.

After detecting the scratch, complementary information can be

obtained from the pile-up with SEM and AFM. Preferred plastic deformation from an unsymmetrical sand grain led to a higher pile-up on one side of the scratch, Fig. 3. Previous studies have also shown that the pile-up in front of a scratch may be up to three times higher than the pile-up on the sides of the scratch [9]. These pile-ups in front of the scratch will not be easily seen, since the elevated peak will be more difficult to detect than the line of pile-ups on the surface.

Atomic force microscopy together with scanning electron microscopy can provide a more complete interpretation of the scratch and the associated pile-up. The AFM probe shows shallower depths of narrow scratches and peak rounding [17–19]. This occurs from “stylus flanking” where the edge of the stylus cone makes contact with the highest point [20]. Selection criteria for the tip radius have been proposed to improve the reproduction of the surface topography [21]. Scanning electron microscopy is recommended for complementary information on the pile-up, providing a good 2-D map of the surface, as well as retrieving elemental information. The true geometry of the pile-up and the groove provides an insight into the process of scratching, the groove depth, and the pile-up, Fig. 4.

Metal pushed out from the groove can offer information about the applied load and damage to the surface. At low loads, only a groove is formed, at intermediate loads a pile-up on the side of the groove will appear, but at higher loads the plastically deformed metal pushed out of the groove will chip and occasionally be released [22]. The absence of pile-up on the side of the scratch makes it more difficult to identify scratches. A pressure of 16 kPa on the 3000 grade sandpaper was sufficient to cause chipping and loose debris on the abraded surface.

Lower yield point metals will scratch more easily and are likely to have deeper scratches, making it easier to identify scratches. The ease of scratch detection on plastics has been reported to depend on the size of the scratch, the roughness of the scratch and the gloss of the background [23]. This study was focused on an austenitic stainless steel. Further work could determine the ease of scratch detection from different types of particles and loading conditions. Additional work may look at how the polished surfaces hardness influences the ease of scratching.

This investigation addressed alterations to the surface, but it should be noted that scratch formation could also change the subsurface. Plastic deformation from scratching will change the number and arrangement of subsurface dislocations [24], that will change the yield strength or hardness.

This study has shown that polished surfaces can be quickly assessed for scratches by light microscopy, firstly in the darkfield imaging mode to identify the fine scratches on the polished steel, and then in the brightfield imaging mode to show larger scratches. More detailed characterization with AFM provides scratch depth, but further analysis with the SEM will show metal pile-up or chipping. Such an approach can be used both for assessing a polished surface and for determining the performance of smooth surfaces in different environments.

4. Conclusions

A comparison of different imaging methods showed that light microscopy is best suited for quality control. Light microscopy identified 70% of the scratches imaged by the atomic force microscope on the same scratched area. The ability to detect scratches as shallow as 3 nm in the light microscope is attributed to the pile-up next to the scratches. When samples are small, the scratch depth and adjoining pile-up may be obtained by atomic force microscopy, and a more detailed 2-D view seen by scanning electron microscopy.

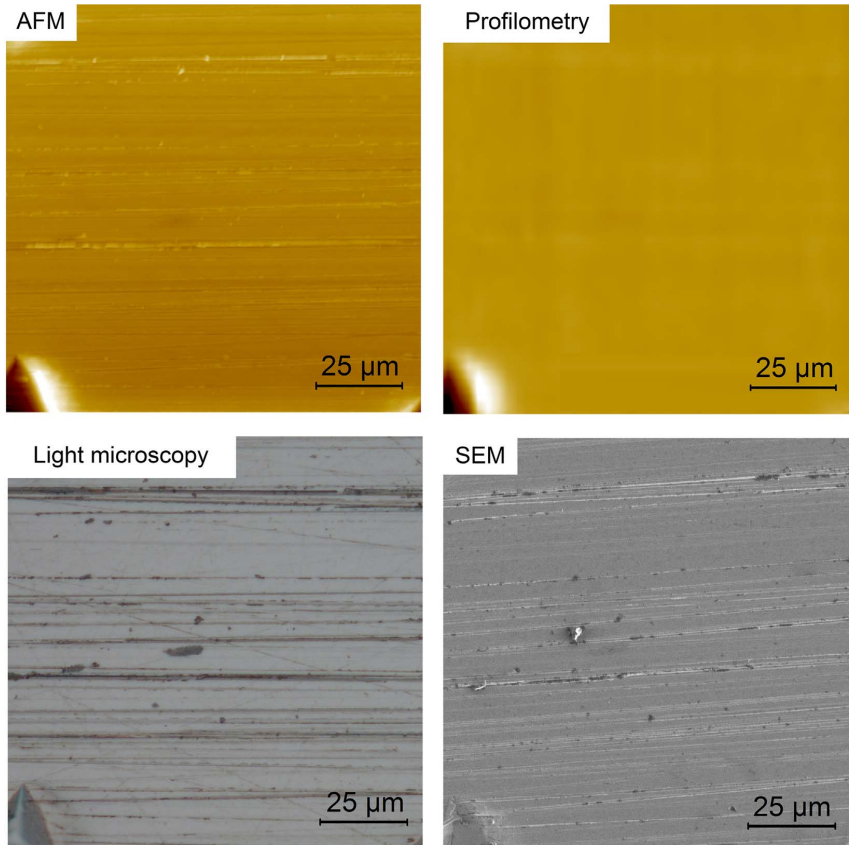


Fig. 3. A 3000 grade sandpaper scratched metal surface as seen by contact imaging methods (AFM and profilometry) and non-contact imaging methods (light microscopy and SEM).

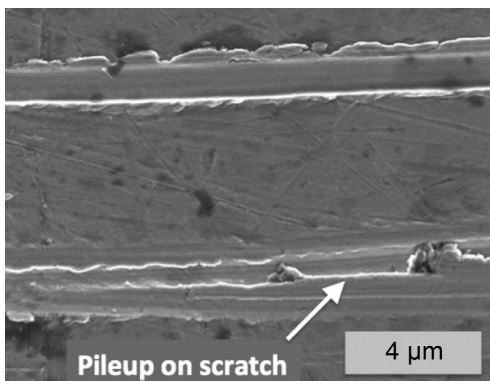


Fig. 4. Pile-up on the side of a scratch after abrasion with 3000 grade sandpaper. The bottom scratch shows only pile-up on the upper side of the scratch and a trapped abrading particle with a higher pile-up at the front.

Acknowledgements

The authors thank Klavs Stiprais and Pavels Gavrilovs for polishing. Project “IMATEH: Innovative Materials and Smart Technologies for Environmental Safety” from the Latvian State Research Programme

funded the project titled “Modification of metal surfaces for the reduction of friction and wear”.

References

- [1] T. Puntous, S. Pavan, D. Delafosse, M. Jourlin, J. Rech, Ability of quality controllers to detect standard scratches on polished surfaces, *Precis. Eng.* 37 (2013) 924–928.
- [2] L.E. Samuels, *Metallographic Polishing*, ASM International, Materials Park, Ohio, 2003.
- [3] T. Hryniewicz, P. Konarski, K. Rokosz, R. Rokicki, SIMS analysis of hydrogen content in near surface layers of AISI 316L SS after electrolytic polishing under different conditions, *Surf. Coat. Technol.* 2015 (2011) 4228–4236.
- [4] C.E. Johnson, Chemical polishing of diamond, *Surf. Coat. Technol.* 68 (1994) 374–377.
- [5] Lee Ks, H.L.T. Le, R.J. Ram, Polymer waveguide backplanes for optical sensor interfaces in microfluidics, *Lab Chip* 7 (2007) 1539–1545.
- [6] F. Vega, N. Lupon, J.A. Cebrian, F. Laguarda, Laser application for optical glass polishing, *Opt. Eng.* 37 (1998) 272–279.
- [7] F.P. Mallinder, B.A. Proctor, The strengths of flame-polished sapphire crystals, *Phil. Mag.* 13 (1966) 197–208.
- [8] K. Kim, E.Y. Kim, Film line scratch detection using texture and shape information, *Pattern Recogn. Lett.* 31 (2010) 250–258.
- [9] Z. Liu, J. Sun, W. Shen, Study of plowing and friction at the surfaces of plastic deformed metals, *Tribol. Int.* 35 (2002).
- [10] D. de Villiers, A. Traynor, S.N. Collins, J.C. Shelton, The increase in cobalt release in metal-on-polyethylene hip bearings in tests with third body abrasives, *Proc. Inst. Mech. Eng. H J. Eng. Med.* 229 (2015) 611–618.
- [11] H.W. Lippincott, Stark, Optical digital detection of dents and scratches on specular metal surfaces, *Appl. Opt.* 21 (1982) 2875–2881.
- [12] T.V. Vorburger, H.G. Rhee, T.B. Renegar, J.F. Song, A. Zheng, Comparison of optical and stylus methods for measurement of surface texture, *Int. J. Adv. Manufact. Technol.* 33 (2007) 110–118.

- [13] R.J. Hocken, N. Chakraborty, C. Brown, Optical metrology of surfaces, *Cirp Ann. – Manuf. Technol.* 54 (2005) 705–719.
- [14] K.B. Seo, B.M. Kim, E.S. Kim, Digital holographic microscopy based on a lateral modified chearing interferometer for three-dimensional visual inspection of nanoscale defects on transparent objects, *Nanoscale Res. Lett.* 9 (2014) 471.
- [15] C. Shi, H. Zhao, H. Huang, S. Wan, Z. Ma, C. Geng, et al., Effects of probe tilt on nanoscratch results: An investigation by finite element analysis, *Tribol. Int.* 60 (2013) 64–69.
- [16] C. Poon, B. Bhushan, Comparison of surface roughness measurements by stylus profiler, AFM and non-contact optical profiler, *Wear* 190 (1995) 76–88.
- [17] J.I. McCool, Assessing the effect of stylus tip radius and flight on surface topography measurements, *J. Tribol. Trans. ASME* 106 (1884).
- [18] E.L. Church, P.Z. Takacs, Effects of non-vanishing tip size in mechanical profile measurements, *Proc. SPIE* 1332 (1991) 504–514.
- [19] K.H. Kwon, N.G. Cho, Assessing the effect of stylus tip radius on surface roughness measurement by accumulation spectral analysis, *Int. J. Prec. Eng. Manuf.* 7 (2006) 9–12.
- [20] **Exploring Surface Texture: A Fundamental Guide to the Measurement of Surface Finish, 7th ed. Taylor Hobson Ltd., 2011.**
- [21] D.H. Lee, Three dimensional profile distortion measured by stylus raw surface profilometer, *Measurement* 46 (2013) 803–814.
- [22] J.M. Wheeler, J. Wehrs, G. Favaro, J. Michler, In-situ optical oblique observation of scratch testing, *Surf. Coat. Technol.* 258 (2014) 127–133.
- [23] P. Rangarajan, M. Sinha, V. Watkins, K. Harding, J. Sparks, Scratch visibility of polymers measured using optical imaging, *Polym. Eng. Sci.* 43 (2003) 749–758.
- [24] F.A. Ponce, Q.Y. Wei, Z.H. Wu, H.D. Fonseca, C.M. Almeida, R. Prioli, D. Cherns, Nanoscale dislocation patterning by scratching in an atomic force microscope, *J. Appl. Phys.* 106 (2009) 076106.

APPENDIX 2
PUBLICATION 2

Jansons E., Lungevics J., Gross K. *Surface Roughness Measure that Best Correlates to Ease of Sliding*. 15th International Scientific Conference "Engineering for Rural Development": Proceedings. Vol.15, Jelgava, Latvia, May 25-27, 2016. Pages 687-695. ISSN 1691-5976.

Available: <https://www.tf.llu.lv/conference/proceedings2016/Papers/N127.pdf>

Open access

SURFACE ROUGHNESS MEASURE THAT BEST CORRELATES TO EASE OF SLIDING

Ernests Jansons, Janis Lungevics, Karlis Agris Gross

Riga Technical University, Latvia

ernests.jansons91@gmail.com, janis.lungevics@rtu.lv, kgross@rtu.lv

Abstract. Despite the long history on the study of friction and ease of sliding, there are few studies on friction of metal with smooth surfaces such as ice. The aim of this study was to determine the best surface roughness measure that correlates with the ease of sliding. Ice was chosen as the smooth surface since it is easy to produce. Stainless steel blocks were abraded with different grades of sandpaper to produce parallel scratches in the metal surface. Single roughness measures (R_a , S_a , S_{sk} , S_{ds} , S_{dq} , and R_{Sm}) and R_{Sm}/S_a that is related to the Criterion for Contact were extracted from a 3D profilometry measurement on metal blocks scratched with 400 to 3000 grades of sandpaper. The scratched metal blocks were slid down an ice-track to determine the sliding speed of blocks with different roughness. The relationship between the roughness parameters and sliding velocity was then investigated. It was shown that the best correlation between the surface roughness and the sliding speed was for the "Criterion for Contact" roughness measure, R_{Sm}/S_a . A critical value of roughness was essential for achieving the best sliding. A method was established for measuring and characterizing the roughness of a surface for applications requiring low friction.

Keywords: surface roughness, scratches, surface topography, 3D roughness, slidability.

1. Introduction

If one is planning to investigate how solid objects slide on the ice it is essential to understand that the object surface that comes into contact with ice contains small asperities (otherwise defined as roughness). Asperities first of all penetrate into the underlying ice surface, thus possibly "anchor" the sliding object and secondly they determine wettability characteristics for the specific surface [1-4]. This means that roughness influences the ease of sliding from two important and inseparable aspects. Even though scientists agree that roughness plays an important role in friction processes only few of them have done deeper investigation in this field [3; 5-7].

The first step for doing such research is to make sure that the experimental sample surfaces are properly manufactured and characterized. Literature analysis shows that surface roughness is most likely characterized by using single 2D roughness parameter R_a , but, as shown in Fig. 1, such parameter alone cannot properly characterize the surface texture, therefore, it is important to find a better characterization technique. The first step on finding such technique starts with replacing most commonly used 2D roughness measurements with 3D surface roughness measures, because such approach provides statistically more reliable data than roughness measures obtained from single profiles across a surface. Secondly, one must find, which of these parameters are most likely usable for ice friction surface characterization, therefore, in this article the authors are analyzing different methods of surface characterizations and comparing the obtained roughness measurements with sample slidability on ice.

As important as proper surface characterization is also the development of a method for slidability detection. While most of the studies use different kinds of tribometers, rheometers, etc. [2; 3; 5] for metal and ice friction coefficient measurements, the authors in this a simple incline plane [8] that is equipped with additional optical sensors. Additional sensors on the side of the plane, combined with the data logging and analysing system, allow to maintain experimental sample sliding time measurements along the inclined plane. Time measurements can be used directly or indirectly as sliding velocity, calculated from time measurements and distances between the sensors, for comparing how different surface modifications affect slidability. It is proposed that such device can achieve better detection of roughness influence on slidability, because the result (sliding time or average sliding velocity differences), not the cause of it (friction coefficient change), is measured and compared afterwards.

The objective for this research is to investigate how different surface roughness characterization methods correlate with slidability measurements, which are maintained on inclined plane.

2. Materials and Methods

Surface roughness characterization

So far known scientific researches in roughness influence on ice friction [3; 5; 6] use only two dimensional (2D) roughness parameters like arithmetical mean deviation of the roughness profile R_a or root mean square deviation of the roughness profile R_z which are calculated from independently measured roughness profiles, but experience shows that individual profile measurements cannot be considered as enough informative data to describe the actual surface texture. For instance, Fig. 1 clearly shows that completely different profile shapes can give same roughness parameter R_a value but it is obviously clear that if such surfaces with so different texture are involved in the sliding process, their slidability will be different. As a result, there are no conditions for the reference plane, and this can be along the top of the surface (Fig. 1B) or along the bottom from which peaks are formed (Fig. 1C). The large degree of freedom for the R_a measure does not adequately describe the surface, and this emphasizes the requirement for investigating other possible measures.

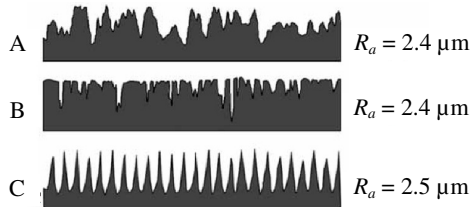


Fig. 1. **Roughness profile examples:** A – grounded surface;
B – honed surface; C – turned surface

In order to improve surface roughness characterization precision, first of all it is more adequate to use three dimensional (3D) roughness measurements to describe the surface texture instead of just measuring 2D profiles. Relatively newly developed 3D roughness standard ISO 25178 [9] defines more than 30 different roughness parameters, which are categorized in four large groups: height parameters, spatial parameters, hybrid parameters and functional parameters. The authors analyzed all the parameters defined on specific standard from surface mechanic aspect and it was concluded that following 3D roughness parameters can be considered for characterizing the surface involved in sliding:

- S_a – arithmetical mean height of the scale limited surface;
- S_{Sk} – symmetry of the distribution curve of depth;
- S_{ds} – density of peaks;
- S_{dq} – mean quadratic slope of the surface.

The arithmetic mean is the most commonly used roughness characterization indicator that describes surface asperities in vertical direction, and so it was included. S_{Sk} describes the structure of the surface, i.e. it shows whether the surface consists of relatively smooth reference plane, which mostly has pits (similar to Fig. 1B) or peaks (similar to Fig. 1C) on it. As far as the actual surface contact area varies according to the surface peak the density parameter S_{ds} theoretically should allow to characterize this factor. S_{dq} characterizes how steep the peaks of the surface are, thus allowing to define whether surface asperities are sharp or shallow.

Although 3D roughness parameters seem to provide good characterization for the investigated surfaces, the authors offer to use the Criterion of Contact (KK) (see equation 1) instead [10].

$$KK = \frac{R_{Sm} \cdot H_{\mu}}{S_a \cdot E}, \quad (1)$$

- where R_{Sm} – mean spacing between the peaks at the mean line, mm;
- H_{μ} – surface microhardness, MPa;
- S_a – arithmetical mean height of the scale limited surface (this parameter can be theoretically replaced with R_a – the arithmetic average of the absolute values in the roughness profile, but this parameter is statistically less reliable), μm ;

E – Young’s modulus of the metal, MPa.

KK generally was developed to analyze two metallic surface contact to see whether the contact is elastic or plastic, but in this article the authors investigate opportunity to use this criterion simplified version (see Equation 2) for determining how surface roughness affects its slidability. Opportunity for equation 1 simplification arises because KK consists of two fundamentally different parameter groups:

1. surface physical properties (H_μ, E);
2. surface roughness (R_{Sm}, S_a).

If all examined surfaces are made of one material, it is possible to consider material property component as identical constant thus allowing the following equation (1) simplification:

$$KK_R = \frac{R_{Sm}}{S_a}, \quad (2)$$

where KK_R – Criterion of Contact roughness parameter component.

Equation 2 contains only two roughness parameters:

1. S_a – arithmetic mean height of the scale limited surface that describes surface roughness level in the asperity direction (shown as H in Fig. 2);
2. R_{Sm} – mean spacing between the profile peaks at the mean line (in the sliding direction) that describes surface asperity width (shown as W in Fig. 2).

R_{Sm}/S_a defines the steepness of the asperity and is related to W/H (see Fig. 2), thus combining the surface roughness texture in the vertical and horizontal direction. A larger ratio represents flatter asperities, thus resulting to smoother surface.

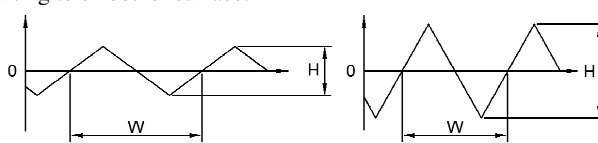


Fig. 2. **Roughness asperity slope steepness:** H – asperity height (S_a in equation 2);
 W – asperity width (R_{Sm} in equation 2)

Surface preparation of experimental samples

Stainless steel with good corrosion resistance was chosen to maintain the surface characteristics during testing. The steel contained Iron (Fe), Carbon (C), Chromium (Cr), Nickel (Ni), Manganese (Mn), Silicon (Si), Vanadium (V) and Sulfur (S). The samples were prepared as rectangular blocks with dimensions of 35x18x14 mm and a weight of 67 ± 0.5 g.

The samples went through three preparation stages; the blocks were milled, polished and scratched. An automated polisher – a *Mecatech 334 TI 15* – finely ground and polished the blocks to an average surface roughness, S_a , value of ~ 8 nm. For obtaining a scratched surface with parallel scratches, the metal blocks were abraded on different grades of sandpaper (400, 600, 2000 and 3000). A special device was made with rails on both sides to guide the block without rotation during the scratching operation (see Fig. 3). A load of 10 N was placed on the block while traversing the scratch path length L (120 mm) in both a forward and backward direction for a total of 20 times to cover the total distance of 2400 mm.

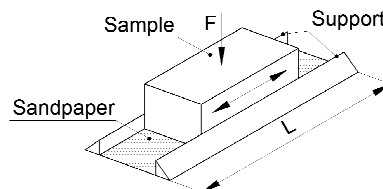


Fig. 3. **Sample scratching principle**

After scratching, the surface roughness was measured for the blocks scratched on 400, 600, 2000 and 3000 grades of sand paper and the scratch lines were also viewed with a *BA310Met* optical microscope (Motic, CHN) to verify how parallel and evenly distributed the grooves appeared from scratching.

Measurement of surface roughness

A *Talysurf Intra 50* profilometer (Taylor Hobson, UK) collected data from the travel of the stylus across the sliding surface to characterize the surface roughness. A total of 10 samples were measured for roughness – scratched with different grit size sandpaper (400, 600, 2000 and 3000) taking account the recommendations in [9-11]. The measurement settings are shown in Table 1, but actual R_a , R_{Sm} and S_a parameter average values (calculated from separate measurements for statistically reliable data) can be seen in Table 2, where the effect of roughness on the ease of sliding is shown.

Table 1

Surface roughness measurement settings

Stylus	Stylus Arm 112/2009, tip radius 2 μ m
Number of points (Y)	400
Data length (Y)	2 mm
Number of points (X)	400
Length of traverse (X)	2 mm
Measurement speed	0.5 mm \cdot s ⁻¹
Cut-off	0.25 mm

3D roughness measures were determined by the following steps:

1. the surface was levelled and the form error was removed to correct for positioning inaccuracy;
2. waviness and roughness were filtered using the same Gaussian filter with a 0.25 mm cut-off according to the standard ISO 25178;
3. filtered roughness surface 3D parameters were calculated to determine S_a , S_{St} , S_{ds} and S_{dq} ;
4. ten separate profiles extracted from 3D surface (perpendicular to the sample sliding direction) were used to calculate R_a ;
5. ten separate surface profiles extracted from 3D surface (in the sample sliding direction) were extracted to calculate R_{Sm} . The profiles were located on top of surface asperities, which likely made contact with ice (see Fig. 4);
6. R_{Sm}/S_a was calculated by using equation 2.

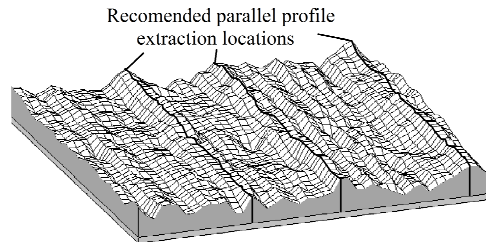


Fig. 4. Selected profile scan locations

Measurement of metal slidability

To obtain reproducible sliding conditions for the investigated samples, an inclined plane with smooth ice surface was used. The experiments were conducted in a cold room with the temperature set to -5.5 °C. The samples were placed on a 16° slope and allowed to slide a distance of 3.3 m to measure the sliding time. The time was measured after passing by optical sensors at the start and end of the track. Repetitive measurements showed that a precision of 0.01s was achieved. The experiment was repeated 80 times for each sample to obtain a representative sliding time. For each surface condition, the experiment was repeated with two or three samples prepared in the same way. For sample

slidability comparison the sample sliding velocity was used instead of the sample total sliding time (see Table 2).

3. Results and discussion

All metal blocks were milled, polished and scratched on different sandpapers. The change in the surface condition can be seen in Figure 5.

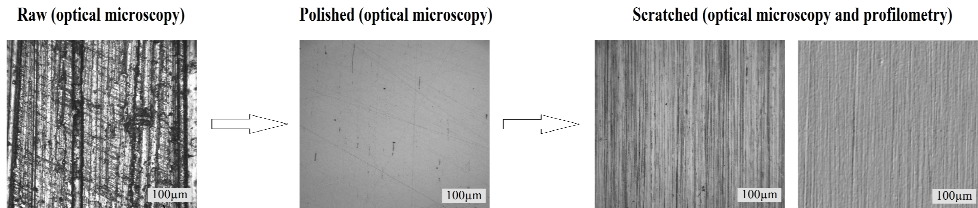


Fig. 5. Experimental sample surface during all preparation steps

The surface roughness measurements show that rougher surfaces (from abrasion on sandpaper with larger grains) are more anisotropic. Waviness appears in the sample scratching direction that is particularly evident after treatment on 400 and 600 sandpaper (see Fig. 6). For example, the metal surface abraded with 400 grit paper shows a slow decline over the first 0.45 mm, and then a rise over the next 0.45mm. A ridge is no longer present along this distance and this could be attributed to a small sideways shift of the ridge, or the removal of the metal that is built up on the side of the scratch. Other studies with a scanning electron microscope support the latter interpretation, where built up metal on the side of the scratch is not always present and could be removed as a result of continued abrasion that removed built up metal and superimposes new scratches on top of the existing scratches.

Mechanistically, this change in waviness can be explained by the removal of larger metal volumes by larger grains. There is an accompanying increase in convexity on the side of the scratches that also produces a more uneven surface perpendicular to the scratching direction. The amplitude in the perpendicular direction seems to be about 0.4 microns, with an occasional jump representing locations where the repeated abrasion by the 30 micron particles on the 400 grade sandpaper may excavated deeper valleys or built up metal may remain on the sides. There could be a correlation between sandpaper grit designation and waviness it creates on the metal surface, but this requires further investigations with an accent on the depth of the groove, the height of the built up metal. Furthermore, one should keep in mind that profilometry with a 2 micron tip does not accurately reproduce the true topography in case where the probe end cannot completely survey the detailed vertical oscillations that occur over horizontal distance of less than 1 micron, but for cases when relatively large surfaces need to be scanned (as in the case of sample roughness influence on slidability investigations) profilometry is still the most relevant method.

An increase in surface anisotropy is also observed with the 3D roughness parameter S_r – ratio of texture aspect. The value can lie in the interval from 0 to 1. A value closer to 0 represents a more anisotropic surface. The parameter S_r varied from $S_r = 0.009$ for metal abraded on 400 grade sandpaper to $S_r = 0.4$ for metal abraded on 3000 grade sandpaper. An anisotropic surface meant that the mean spacing between the profile peaks at the mean line R_{Sm} was measured in the scratch direction, Fig. 4.

The use of surface roughness S_a seems to be more reliable than the roughness of one profile, R_a . Surfaces scratched with 3000 and 2000 sandpaper were similar and displayed a roughness of $S_a \approx 0.014\mu\text{m}$ and $0.023\mu\text{m}$, respectively. An intermediate roughness from 600 sandpaper provided a 5 time greater roughness ($S_a \approx 0.08\mu\text{m}$), but 400 sandpaper showed the greatest roughness $S_a \approx 0.185\mu\text{m}$ (see Table 2). Roughness R_a when averaged from 10 evenly distributed profiles approached the S_a values. Since S_a is easily determined, and it represents the entire surface, then S_a is recommended as the measure of roughness.

Table 2 also contains information on the average sliding velocity, v , of metal blocks with a different surface roughness. The sliding velocity is calculated by dividing the separation distance between the sensors (3.3 m) by the time necessary for the sample to slide this distance. It is important to

inform that the sample velocity value shown in Table 2 is an average value out of 3 different experiment day measurements and each day experiments consist of 80 individual slidability measurements for each sample, thus meaning that 240 slidability measurements were done for each sample.

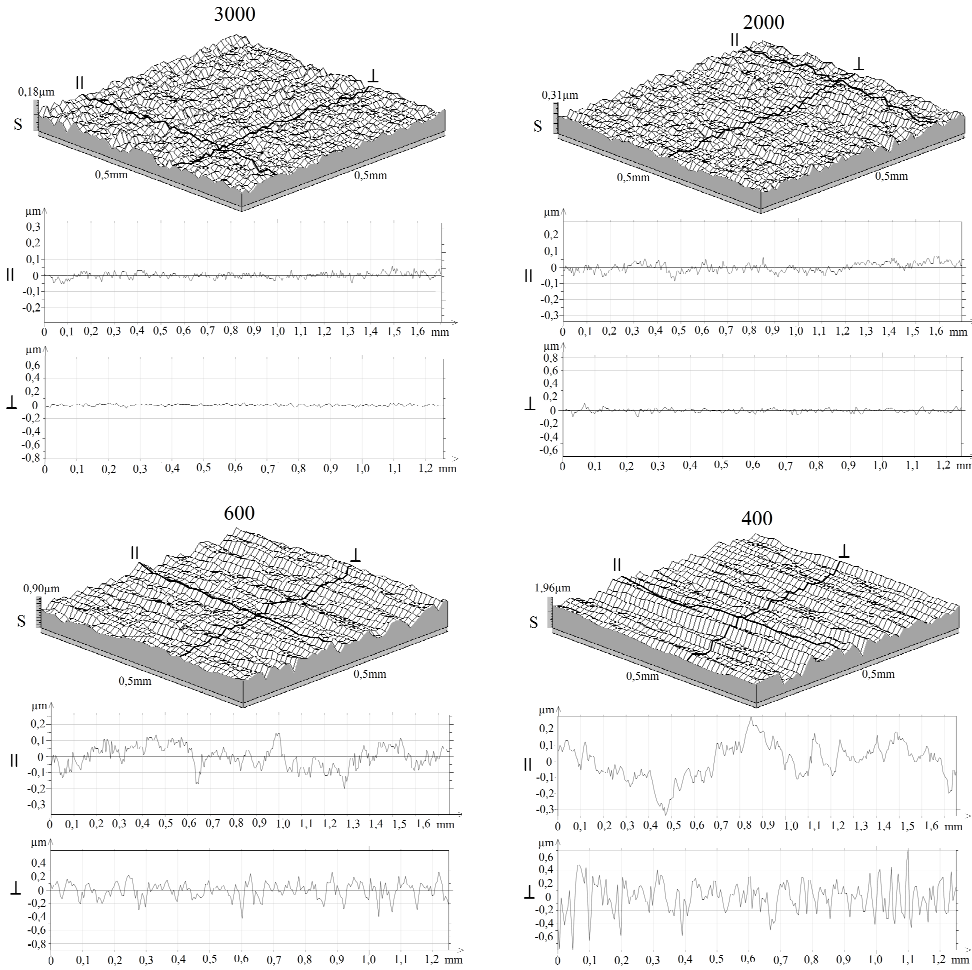


Fig. 6. Sample surface after treatment with different sandpapers: S – 3D surface roughness image; II – profile parallel to treatment direction; I – profile perpendicular to treatment direction

To evaluate the relationship between different roughness measures on the ease of sliding, a graph was constructed to learn about the most informative roughness parameter. Graphs of sliding velocity versus S_a and R_a were constructed in Figure 7, but sliding velocity versus R_{Sm}/R_a and R_{Sm}/S_a in Figure 8. Less useful roughness measures were discussed.

The simplest search for a correlation between roughness and the sliding velocity starts by plotting the sliding speed versus the roughness parameter, R_a and S_a . The roughness parameter R_a in this case is taken perpendicular to the sample scratching direction as recommended in the ISO 2D roughness standard 4287. Furthermore, the measure of R_a is taken from the 3D profile, and this reduces the variability that would otherwise arise from a line profile. There appears to be a very loose correlation between the roughness and the sliding speed, Fig. 7. The scatter in results is very large.

The graph trend lines show an apparent linear correlation between roughness and the sliding velocity, Fig. 7. The same tendency is seen for both cases R_a and S_a . A closer examination will show that the roughness parameter S_a shows a slightly larger roughness than R_a , that is more emphasized with rougher surfaces.

Table 2

Slidability and roughness measurements

Sample No.	Sandpaper grit designation	Roughness parameters					$V, \text{m}\cdot\text{s}^{-1}$
		R_{Sm}, mm	$S_a, \mu\text{m}$	$R_a, \mu\text{m}$	R_{Sm}/S_a	R_{Sm}/R_a	
1	3000	0.031	0.014	0.011	2214	2818	2.327
2	“	0.028	0.013	0.012	2154	2333	2.335
3	“	0.028	0.015	0.011	1867	2545	2.376
4	2000	0.027	0.024	0.021	1125	1286	2.343
5	“	0.033	0.023	0.021	1435	1571	2.343
6	600	0.045	0.094	0.087	478	517	2.323
7	“	0.042	0.060	0.049	700	857	2.317
8	“	0.048	0.094	0.085	510	565	2.285
9	400	0.062	0.180	0.160	344	387	2.237
10	“	0.05	0.194	0.175	257	258	2.249

Despite a possibly correct interpretation of the roughness data with respect to R_a and S_a , these parameters do not accurately reflect the surface topography. Figure 1 showed completely different interpretations of a surface with the same R_a value. The criterion for contact shows a different measure that could be plotted against the sliding velocity. Rudzitis has previously used such an expression for the static contact between two metal surfaces, but it has not been explored for a motion of roughened metal surface on ice.

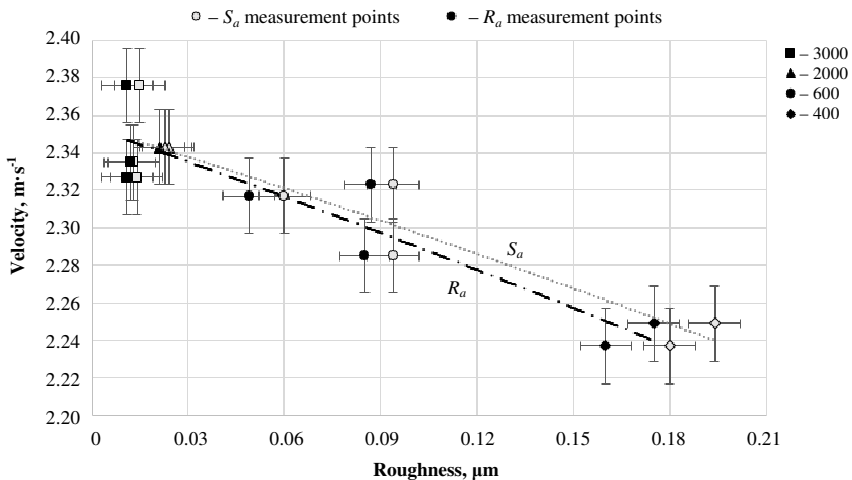


Fig. 7. Surface roughness influence on sample sliding velocity characterizing sliding surface with parameters R_a and S_a

The use of the “Criterion of Contact” approach divides the curve into two parts; from 0 to 1000, where an increase in the sliding speed is connected to the use of smoother surfaces, and from 1000 to 2500, where there is no change in the sliding velocity with further changes in the roughness. The second part exhibiting a close to linear relationship between roughness and the sliding velocity infers that there is no need for polishing metallic surfaces with smoothness higher than R_{Sm}/R_a or R_{Sm}/S_a of 1000. There is no economic benefit for more highly polished surfaces.

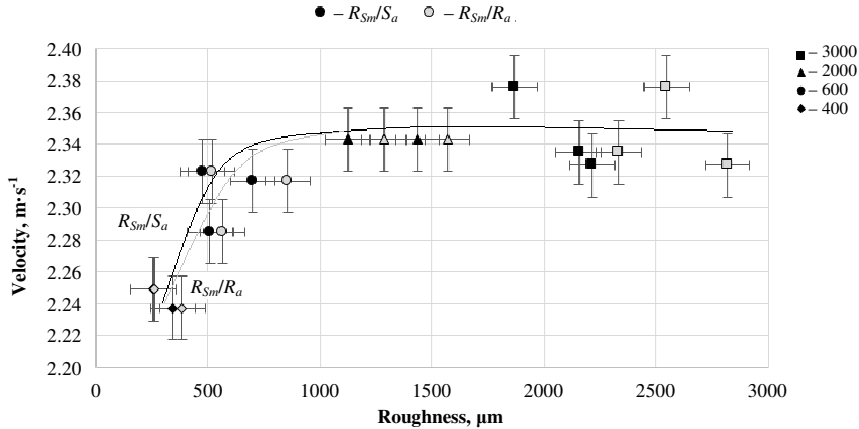


Fig. 8. Surface roughness influence on sample sliding velocity characterizing sliding surface with parameter R_{sm} and R_a or S_a ratio (using Criterion of Contact)

Both R_{sm}/R_a or R_{sm}/S_a show similar trendlines suggesting no need for R_{sm}/S_a , where a more time-consuming 3D measurement is necessary. Due to the inability to acquire R_{sm} parallel to the scratching direction on the top of a ridge in a 2D profile measurement, it is necessary to conduct a 3D measurement. 2D measurements cannot find the ridges and cannot ensure the profile along the ridge. This can be done precisely in a 3D measurement, where the location for determining the roughness can be chosen. Sliding surface characterization thus requires the use of a 3D profilometer.

Further work will investigate the linear region in more detail and determine the location of the turning point in Figure 8. It is possible that a larger surface adhesion results on smoother surfaces will play a larger role on the ease of sliding. These experiments could be conducted with larger loads to verify if the same tendency holds.

The correlation between the roughness parameters S_{sk} , S_{ds} and S_{dq} and the sliding velocity was also investigated. It was observed that the roughness parameter S_{dq} shows the same trend as the parameter S_a – this parameter is obtained from the same data from which S_a is calculated. The parameters S_{sk} , S_{ds} do not show any correlation at all. Despite the ability to extract S_{dq} from the roughness data, it has no practical usefulness, since surfaces cannot be made or controlled to satisfy a given S_{dq} value.

Conclusions

1. The Criterion of Contact (with roughness measures in the vertical and the sliding direction) is a better indicator of the surface roughness than R_a or S_a , for controlling the sliding velocity;
2. The roughness parameters S_{dq} and S_a show the same curve with the sliding speed, but there is no practical use for S_{dq} since surfaces cannot be made according to this surface roughness measure;
3. The parameters S_{sk} , S_{ds} do not show an useful correlation with the sliding velocity;
4. There is no need for polishing metallic surfaces with higher smoothness than R_{sm}/S_a of 1000, as shown by the horizontal linear region for values greater than 1000.

Acknowledgement

JL and EJ acknowledge the discussions with Janis Rudzitis on the use of the Criterion of Contact, according to the previous studies. This paper was prepared by EJ, JL and KAG. Project “IMATEH: Innovative Materials and Smart Technologies for Environmental Safety” from the Latvian State Research Programme funded the research for reducing friction of metal surfaces against smooth surfaces.

References

1. Makkonen L., Tikanmaki M. Modeling the friction of ice. Cold Regions Science and Technology 102, 2014, pp. 84-93.

2. Liang H., Martin J.M., Mogne T.L. Experimental investigation of friction on low-temperature ice. *Acta Mater.* 51, 2003, pp. 2639-2646.
3. Kietzig A.M., Hatzikiriakos S.G., Englezos P. Ice friction: The effects of surface roughness, structure, and hydrophobicity. *Journal of Applied Physics* 106 (2009) 024303.
4. Bowden F.P., Hughes T.P. The mechanism of sliding on ice and snow. *Proc. Roy. Soc. A*, 172, 1939, pp. 280-298.
5. Koinar V.N., Brushan B. Effect of scan size and surface roughness on microscale friction measurements. *Journal of Applied Physics* 81, 1997, pp. 2472-2479.
6. Manning D.P., Jones C., Rowland F.J., Roff M. The surface roughness of rubber soling material determines the coefficient of friction on water-lubricated surfaces. *Journal of Safety Research* 29, 1998, pp. 275-83.
7. Penny A., Lozowski E., Forest T et al. *Physics and chemistry of ice*. Royal Society of Chemistry, 2009, pp. 495-504.
8. Lungevics J., Kumermanis M., Rudzitis J., Linins O., Avisane A., Boiko I., Lipenitis J. *Equipment For Measuring Static Coefficient of Friction and Surface Slip Properties*. (2013) Patent No LV 14795 B.
9. *Geometrical product specifications (GPS) - Surface texture: Areal - Part 2: Terms, definitions and surface texture parameters (ISO 25178-2:2012)*.
10. Rudzitis J., Oditis I., Konrads G., Torims T. 3D roughness effects on tribology of sliding surfaces. *Proceedings of 10th International Conference "Metrology and Properties of Engineering Surfaces"*, France, Saint Étienne, 4-7 July, 2005. Saint-Étienne, 2005, pp. 110-112.
11. Ohlson R., Goran B., Westberg J. *The interrelationship of 3D surface characterization techniques with standardized 2D techniques*. *Advanced Techniques for Assessment Surface Topography*. ISBN 1903996112, 2003, pp. 197-220.

APPENDIX 3
PUBLICATION 3

Velkavrh I., Lungevics J., Jansons E., Klien S., Voyer J., Ausserer, F. *The Influence of Isotropic Surface Roughness of Steel Sliders on Ice Friction Under Different Testing Conditions*. Lubricants, 2019, Vol. 7, No. 12, pages 50-63. ISSN 2075-4442.

Available: doi:10.3390/lubricants7120106

Open access

© 2019 by the authors. Licensee MDPI, Basel, Switzerland. This article is an open access article distributed under the terms and conditions of the Creative Commons Attribution (CC BY) license



Article

The Influence of Isotropic Surface Roughness of Steel Sliders on Ice Friction Under Different Testing Conditions

Igor Velkavrh ^{1,*}, Jānis Lungevičs ², Ernests Jansons ², Stefan Klien ¹, Joël Voyer ¹ and Florian Ausserer ¹

¹ V-Research GmbH, Stadtstrasse 33, Dornbirn 6850, Austria; stefan.klien@v-research.at (S.K.); joel.voyer@v-research.at (J.V.); florian.ausserer@v-research.at (F.A.)

² Department of Mechanical Engineering and Mechatronics, Riga Technical University, Kipsalas str. 6b, Riga 1048, Latvia; janis.lungevics@rtu.lv (J.L.); ernests.jansons_1@rtu.lv (E.J.)

* Correspondence: igor.velkavrh@v-research.at; Tel.: +43-5572-394159-28

Received: 30 October 2019; Accepted: 21 November 2019; Published: 26 November 2019



Abstract: Ice friction is affected by various system and surface-related parameters such as ice temperature, ambient air temperature and humidity, relative sliding velocity, specific surface pressures and surface texture (waviness, roughness) as well as the macroscopic geometry of the samples. The influences of these parameters cannot be easily separated from each other. Therefore, ice friction is a very complex tribological system and it is challenging to draw sound conclusions from the experiments. In this work, ice friction experiments with stainless steel samples that have different isotropic surface roughness values were carried out. Two tribological experimental setups were used: (i) an inclined ice track where the sliding velocity of the freely sliding steel samples was determined and (ii) an oscillating tribometer, where the coefficient of friction was assessed. For both experimental setups, the environmental parameters such as air temperature, relative humidity and ice surface temperature as well as the test parameters such as normal load and surface pressure were kept as constant as possible. The results of the experiments are discussed in relation to the ice friction mechanisms and the friction regimes.

Keywords: ice friction; friction regime; coefficient of friction; sliding velocity; surface roughness; steel

1. Introduction

Depending on ice and ambient temperatures, sliding velocity and surface contact pressure, different mechanisms prevail that divide ice friction into different friction regimes. An important parameter influencing friction regimes, especially in the context of the present study, is the presence and thickness of a liquid-like layer on the ice surface in relation to the roughness of the ice and the slider [1,2]. Figure 1 shows a schematic representation of the Stribeck curve for ice friction. With regard to the thickness of the liquid-like layer, three different friction regimes are typically distinguished: dry, mixed and hydrodynamic friction. Dry friction describes the sliding contact of two surfaces without any intermediate layer—friction coefficient is typically high. However, in ice tribology, such conditions are extremely rare because a thin liquid-like layer is always present on the ice surface when ice temperature is above around $-35\text{ }^{\circ}\text{C}$ (depending on the contact pressure) [3]. Mixed friction occurs when the surface temperature at some points within the contact zone rises above the melting point of ice and the thickness of the liquid-like layer is still lower than the characteristic roughness of the mating surfaces—friction coefficient decreases with the thickness of the liquid-like layer. If in the contact zone the temperature is higher than the melting point of the ice and the thickness of the

liquid-like layer is greater than the height of the mating surface asperities, the friction regime is called hydrodynamic—here, friction coefficient increases with the liquid-like layer thickness due to increased viscous friction. The liquid-like layer formation is also influenced by the contact pressure, the relative velocity of the sliding bodies and the humidity.

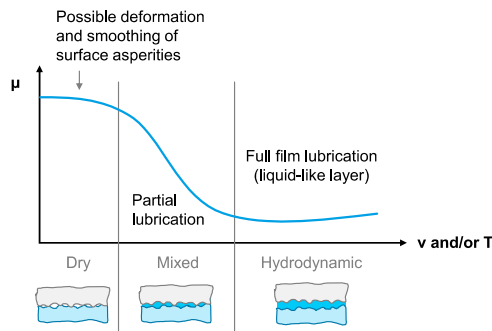


Figure 1. Schematic representation of the Stribeck curve for ice friction.

For different ice friction regimes, different influences of surface roughness have already been reported for polymer [4] or steel [5–9]. Under dry/mixed friction conditions, friction typically increased with increasing roughness of the slider or ice due to increased deformative friction [4–7]. On the other hand, friction under hydrodynamic friction conditions typically decreased with increasing roughness of the slider [6,8], which was ascribed to the suppression of capillary bridges. Although the asperities facilitate the formation of capillary bridges, rougher surfaces have more volume available for the propagation of meltwater compared to smooth surfaces and also result in a smaller contact area. Therefore, with decreasing roughness, the contact area and thus the adhesion as well as the friction in liquid-like layer increase. Thus, under hydrodynamic friction conditions with lower roughness, the overall friction is higher, despite the lower deformative friction component, than with higher roughness. However, for the hydrodynamic friction conditions conflicting results have also been reported. In Reference [9], smoother bobsled runners provided lower friction than the rougher ones, which was more pronounced at temperatures of -3 and -5 °C than at -10 °C. It should be noted that in the mentioned study, the coefficient of friction was calculated through the difference of initial and final sliding velocities, that is, under the presumption that higher friction results in a more pronounced reduction of velocity.

In order to address the ambiguities present in the available literature and to gain deeper understanding of the influence of surface roughness of steel sliders under different testing conditions and/or different ice friction regimes, experimental studies were performed in the present study on stainless steel samples with different isotropic surface roughness values using two different experimental setups and test parameter sets, which has according to the knowledge of the authors previously not been performed yet. The results are discussed from the perspective of the known ice friction mechanisms in terms of friction regimes.

2. Materials and Methods

In this study, steel samples (Uddeholm Ramax HH) having dimensions of $35 \text{ mm} \times 18 \text{ mm} \times 14 \text{ mm}$ ($L \times W \times H$) at a deviation of $\pm 0.01 \text{ mm}$ and weight of $67 \pm 0.1 \text{ g}$ were machined and their test surfaces polished with a semi-automatic polisher 334 TI 15 Mecatech (Presi, Eybens, France) to a surface roughness of $R_a < 0.1 \text{ } \mu\text{m}$. Before polishing, sample sharp edges were rounded to avoid their sticking in ice during experiments. Two of the polished samples were used as reference samples. The rest of the samples additionally had their test surfaces treated by sandblasting which was followed by additional

polishing using three different re-polishing times (30, 150 and 240 s) to obtain three different isotropic surface roughness values. Additional polishing ensured that the sharp asperity peaks which formed during sandblasting were removed thereby creating relatively flat surfaces with randomly distributed valleys/dimples which act as reservoirs for the meltwater. The described surface treatment procedure was selected with the aim to verify whether this relatively affordable and well-accessible technology can be applied for effective modification of steel surfaces for sliding on ice. The surface topographies of the samples were characterized by laser scanning microscopy (VK-X250/260, Keyence International NV/SA, Mechelen, Belgium) and the macroscopic surface geometry/form of the samples were characterised by a contact type 3D profilometer (Talysurf Intra 50, Taylor Hobson, United Kingdom). Table 1 lists the surface treatments used to generate the topographies of the differently treated steel samples and their relevant roughness parameters and Figure 2 shows their surface topographies. From the Ra and Rz values (Table 1), it is clear that the applied surface treatments produced four distinct surface roughness categories. It should be noted that re-polishing after sandblasting affects the Abbott-Firestone curve and also the corresponding core roughness Rk, reduced peak height Rpk and reduced valley depth Rvk values [10]. For comparative purposes, the Rpk values describing the average height of the protruding peaks above the roughness core profile are listed in Table 1. In Figure 3, a typical macroscopic surface geometry/form of the steel samples is shown. It is clear that due to polishing, sample surfaces had a noticeable curvature which reduced the nominal contact area. Since the curvature of all samples was very similar, for the purpose of the present study, its influence on the sliding properties of the samples was not taken into account.

Table 1. Differently treated steel samples and their roughness values Ra, Rz and Rpk (listed in decreasing roughness order).

Surface Treatment	Sample Number	Ra (μm)	Rz (μm)	Rpk (μm)
Polishing, sandblasting and additional polishing for 30 s	SP30-1	3.0	18.3	1.6
	SP30-2	2.7	17.5	1.5
Polishing, sandblasting and additional polishing for 150 s	SP150-1	2.3	15.3	1.2
	SP150-2	2.0	14.0	1.1
Polishing, sandblasting and additional polishing for 240 s	SP240-1	1.0	10.9	1.0
	SP240-2	0.8	8.4	0.7
Polishing	P-1	<0.1	1.0	0.2
	P-2	<0.1	0.7	0.1

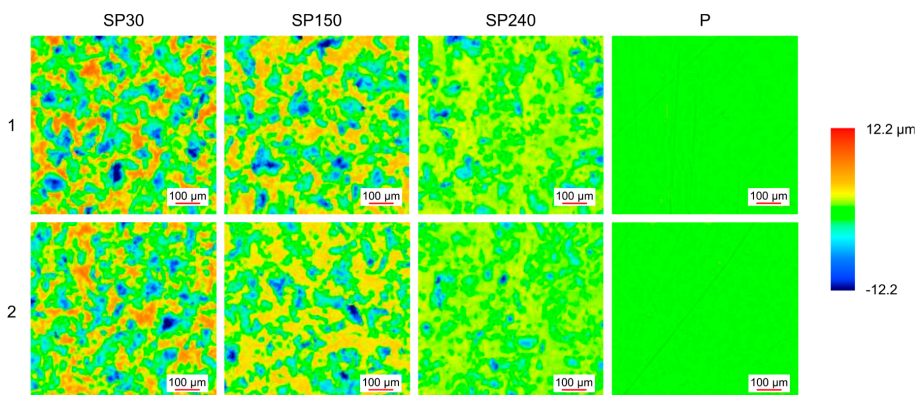


Figure 2. Surface topographies of differently treated steel samples.

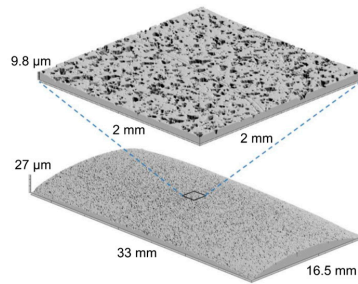


Figure 3. Typical macroscopic surface geometry/form of the steel samples after polishing (sample SP240-1). Magnification of a 2 mm × 2 mm area is shown for scale comparison.

Two tribological test setups were used—(i) an inclined ice track tribometer in which the steel sample slides freely after lifting the start gate while its sliding time is measured by 4 pairs of optical sensors (Figure 4a) and (ii) a modular tribometer (RVM1000, Werner Stehr Tribology GmbH, Germany) used in oscillating mode (Figure 4b).

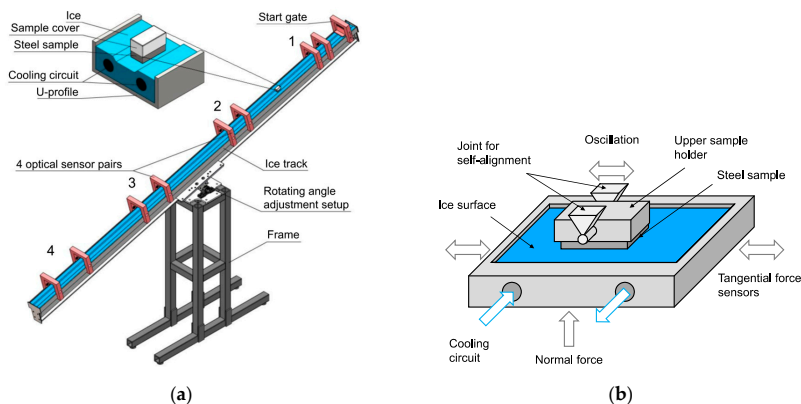


Figure 4. Schematic representation of the test setups used (a) inclined ice track tribometer, (b) oscillating tribometer.

2.1. Tests on the Inclined Ice Track Tribometer

The inclined ice track tribometer was designed as a miniature model of the skeleton field experiment [11]. It was developed to enable the comparison of the sliding velocities of steel runners from field experiments with the velocities of test samples achieved under controlled laboratory conditions. The tribometer consists of a closed, 3300 mm long U-profile with a built-in cooling system for ice formation. It is possible to achieve and maintain ice temperatures of 0 down to $-20\text{ }^{\circ}\text{C}$ which allows the simulation of different ice conditions. The tribometer is located in a climate simulation room that allows temperature control from 30 down to $-20\text{ }^{\circ}\text{C}$. The positions of the four sensor pairs used to measure the sliding time of the steel sample were as follows (measured from the start gate, see Figure 4a): 90–140 mm, 1030–1130 mm, 1920–2070 mm and 2740–2940 mm. The steel sample thus glides over 4 different distances (with a length of 50, 100, 150 and 200 mm) over which the sliding time is measured with a precision of 1 ms. From the time measurements, four momentaneous sliding velocities were calculated. During the experiments, the ice track was tilted at an angle of 16° , which is slightly above the minimum to initiate the sliding motion of the test samples and is at the same time

sufficient to prevent from adhesive sticking of the samples in the starting position. More information on the working principle of the inclined ice track tribometer can be found in Reference [12]; however it should be noted that the latest device updates include a stronger frame, improved optical sensors and an additional climate chamber surrounding the device for minimization of the changes in temperature and humidity which occur due to the heat emitted by the researcher/operator who is present inside the climate simulation chamber during the experiments.

Before the tests, the ice surface was levelled with a specially designed planner, which can move linearly along the ice track over rolling bearings. During ice levelling, a shallow groove is formed in the middle of the ice track surface which helps to guide the sample in a straight line (see detail in Figure 4a). After levelling, remaining ice particles were carefully removed with a moist sponge and ice left untouched for a couple of minutes so it can recrystallize. Experiments were conducted at two different ice and ambient temperature conditions: (i) ice $-2\text{ }^{\circ}\text{C}$ and ambient $0\text{ }^{\circ}\text{C}$ and (ii) ice $-7\text{ }^{\circ}\text{C}$ and ambient $-4\text{ }^{\circ}\text{C}$. In all experiments, the relative humidity was between 60% and 80%. Temperature and humidity were controlled using 4 thermocouples (one located in air approximately 10 mm above the ice surface and the other embedded in the ice) and hygrometer (located in air approximately 10 mm above the ice). The steel samples were cooled together with the ice track before the tests in the climate simulation room. An isolating plastic sample cover was used to avoid temperature transfer from the operators' hands to the sample during the experiments. For each sample, two series of experiments were carried out in one day to minimize the influences of ambient fluctuations. Each series of experiments consisted of at least 20 measurements so that for each sample at least 40 measurements were performed at the defined ice and ambient temperatures. For the evaluation, three measurements with the highest and three measurements with the lowest velocity were not considered (Figure 5a) and the final result is calculated as the average value of the remaining measurements. In all experiments conducted on the same day, the same ice surface was used. It should be noted that during free sliding, steel sample has 3 degrees of freedom (2 linear, 1 rotational), therefore unwanted lateral translation (Figure 5b, position 2) and rotation (Figure 5b, position 3) can occur which can affect the scattering of the results. It could be observed that in the cases where the unwanted translational or rotational movement of the sample occurred (this behavior was purely stochastic), slightly lower sliding velocities were typically achieved compared to the cases where the unwanted movement did not occur. However, since in the performed experiments these deviations were smaller than the differences which occurred due to the applied surface treatments of the samples, no detailed analyses of the sample movement were conducted.

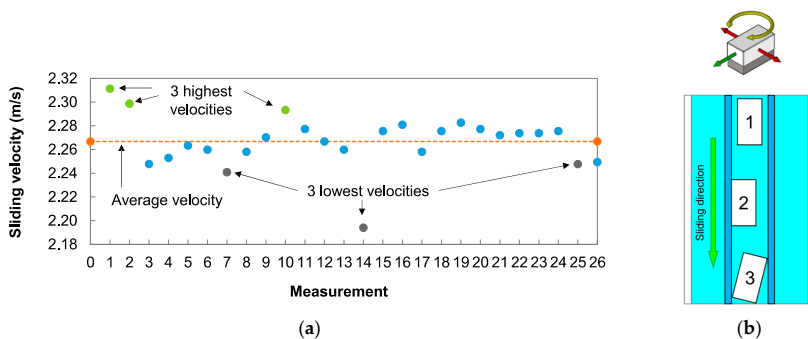


Figure 5. (a) Example of the results from a single series of experiments on the inclined ice track tribometer and their post-processing (3 highest and 3 lowest velocities were not considered); (b) degrees of freedom of the steel samples during tests on the inclined ice track tribometer: 1—ideal movement position, 2—unwanted lateral translation of the sample, 3—unwanted rotation of the sample.

2.2. Tests on the Oscillating Tribometer

The modular tribometer is equipped with an insulated test chamber, which is continuously flooded with dry, cool air and enables the establishment of the required environmental conditions (low temperatures at defined humidity). The steel sample is mounted in the upper sample holder, which allows self-alignment in the direction of movement. The steel sample moves against an ice surface having dimensions of 80 mm × 20 mm × 5 mm. To produce the ice, 18 mL of distilled water was used to which 0.5 mL of tap water was added to accelerate ice formation. Due to the expansion of the water volume at sub-zero temperatures, the ice had a convexly curved surface, so the surface was first flattened with an aluminum plate (45 mm × 28 mm) before the experiment. The smoothing was performed at a normal force of 692 N and an average sliding velocity of 0.08 m/s until the height difference between the left and right sides of the ice surface was lower than 100 μm. The flatness of the ice surface was measured with a built-in tribometer dial gauge. During the experiments, the ice temperature at the surface was $-8\text{ }^{\circ}\text{C}$ (measured with a thermocouple), with the relative humidity being $27 \pm 3\%$ and the ambient temperature being $4 \pm 1\text{ }^{\circ}\text{C}$. These were measured with a thermometer/hygrometer inside the test chamber.

Experiments were carried out at a constant normal load of 52 N and a stroke of 24 mm. The steel samples were stored in a freezer at $-18\text{ }^{\circ}\text{C}$ for 24 h prior to testing. For each test, a run-in period of 60 s at 0.10 m/s was first performed to adjust the sample temperature to the ice temperature. Afterwards, experiments were carried out at 7 velocity levels (average sliding velocities of 0.02, 0.05, 0.10, 0.14, 0.19, 0.29 and 0.38 m/s)—during each experiment, friction measurements at all velocity levels were performed twice—once at increasing and once at decreasing velocity (Figure 6a). At each velocity level, at least 10 cycles (one cycle consisting of one forward and one backward stroke) were performed. For each sample, three experiments were carried out one after the other on the same ice surface without removing the steel sample. The first test was carried out with the test chamber closed by a transparent plastic plate so that the contact between the steel sample and the ice could be visually assessed. The second test was performed with a closed and sealed test chamber to allow even lower humidity values. The third test was carried out with an opened test chamber to allow higher humidity values. The coefficient of friction was measured continuously during the tests, while for the evaluation, 5% of the friction signal was omitted at the beginning and at the end of each stroke to eliminate the influence of static friction (Figure 6b). In Table 2, the average ambient temperatures and relative humidity values from the three sequential tests are listed and in Figure 6 modification of sliding velocities during each experiment (Figure 6a) and friction signal from a single oscillating cycle (Figure 6b) are presented.

Table 2. Average ambient temperatures and relative humidity values from three sequential tests conducted on the oscillating tribometer.

Test	Ambient Temperature	Relative Humidity
Test 1 (chamber with plate)	$8 \pm 1\text{ }^{\circ}\text{C}$	$41 \pm 7\%$
Test 2 (closed chamber)	$4 \pm 1\text{ }^{\circ}\text{C}$	$27 \pm 3\%$
Test 3 (opened chamber)	$7 \pm 1\text{ }^{\circ}\text{C}$	$70 \pm 4\%$

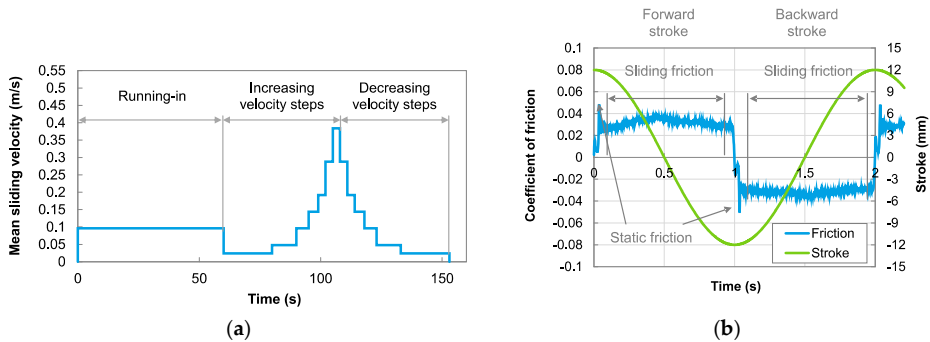


Figure 6. (a) Modification of the sliding velocities during each experiment performed on the oscillating tribometer and (b) measured friction signal from a single oscillating cycle.

3. Results

3.1. Sliding Velocities Measured on the Inclined Ice Track Tribometer

Figure 7 shows the velocities measured on the inclined ice track tribometer. During sliding, the sliding velocity of all samples was increasing with the sliding distance due to the accelerated movement (free sliding downwards) so that in position 1 (Figure 7a) the velocities were the lowest and in position 4 (Figure 7d) they were the highest (note that for a clearer representation of the measured differences, y-scale is different in every diagram). From Figure 7 it is clear that in all measurement positions (1-4) and at both ice and ambient temperatures, the velocity of the steel samples was approximately inversely proportional to their roughness: the samples with the highest roughness, SP30-1 and SP30-2, reached the lowest velocities, while the sample with the lowest roughness, P-1, reached the highest velocity. In the existing literature, a reduction of friction with decreasing surface roughness has typically been reported for the dry/mixed friction regimes and attributed to reduced deformative friction [4–7]. This may also be the case with the experiments conducted on the inclined ice track tribometer.

The difference between the sliding velocities of rough and smooth samples was more pronounced at low velocities (positions 1 and 2) than at high velocities (positions 3 and 4). This could be associated with higher deformative friction at lower velocities and stronger adhesion between the ice and the steel sample surfaces. Increasing velocity inhibits the formation of capillary bridges between mating surfaces thus reducing adhesion. In all measuring positions, the sliding velocities were somewhat lower at higher ice and ambient temperatures (ice $-2\text{ }^{\circ}\text{C}$, environment $0 \pm 0.5\text{ }^{\circ}\text{C}$) than at lower ice and ambient temperatures (ice $-7\text{ }^{\circ}\text{C}$, environment $-4 \pm 0.5\text{ }^{\circ}\text{C}$). At the same time, the influence of roughness on velocity was somewhat less pronounced at lower ice and ambient temperatures, especially the samples with higher roughness (samples SP30 and SP150) showed a less pronounced decrease in velocity. It is worth mentioning that also in the previous research of the authors, the influence of surface texture of the sliders on their velocity typically decreased at lower ice and ambient temperatures which was true for tests on the inclined ice track tribometer [12] as well as for skeleton field tests [11]. Similar observations were made independently by the winter sports athletes who collaborated in the skeleton field tests.

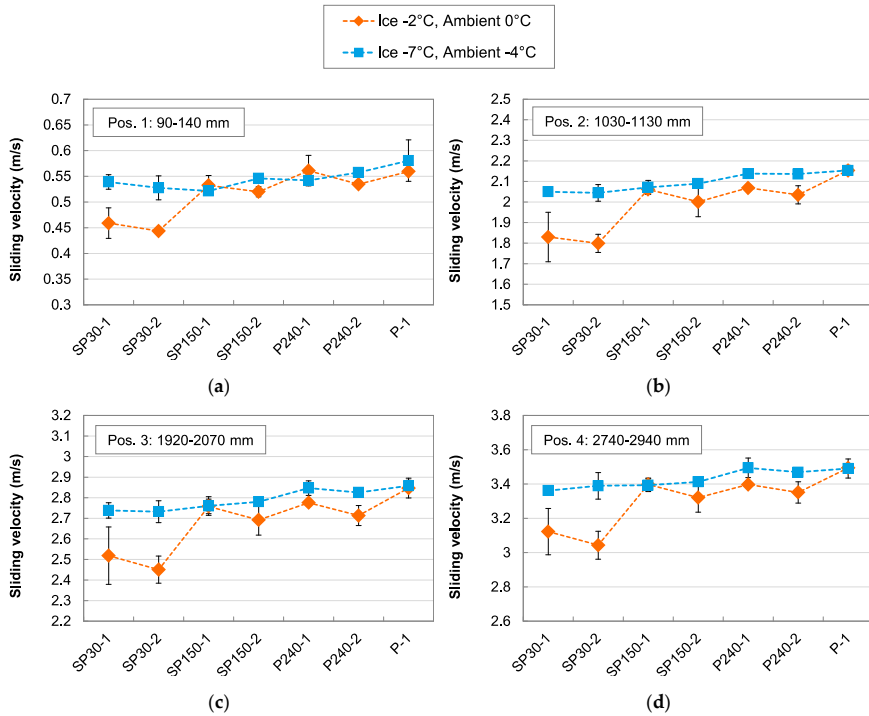


Figure 7. Velocities measured on the inclined ice track tribometer for 4 different measuring positions (a) position 1: 90–140 mm, (b) position 2: 1030–1130 mm, (c) position 3: 1920–2070 mm and (d) position 4: 2740–2940 mm. Results at two environmental conditions are shown: (i) ice temperature -2 ± 0.5 °C and ambient temperature 0 ± 0.5 °C and (ii) ice temperature -7 ± 0.5 °C and ambient temperature -4 ± 0.5 °C. Note that for a clearer representation of the measured differences, y-scale is different in every diagram.

3.2. Coefficients of Friction Measured on the Oscillating Tribometer

Figure 8 shows the coefficients of friction measured on the oscillating tribometer. It can be seen that in all tests friction increased with decreasing surface roughness. The lowest coefficients of friction of approximately 0.04 were measured with samples SP30-1 and SP30-2. With samples SP150-1, SP150-2, SP240-1 and SP240-2 slightly higher coefficients of friction of 0.06 to 0.08 were measured, while samples P-1 and P-2 provided the highest coefficients of friction of 0.1 to as high as 0.24. Assuming that lower friction leads to a higher velocity (due to lower resistance during sliding), the results from the oscillating tribometer (Figure 8) show a reverse tendency compared to the results from the inclined ice track tribometer (Figure 7). In the existing literature, an increase in friction with decreasing surface roughness has typically been reported for the hydrodynamic friction regime and attributed to higher viscous friction [6,8]. This may also be the case with the experiments conducted on the oscillating tribometer.

From Figure 8 it is also clear that for all samples, coefficient of friction was the highest in Test 1 (Figure 8a,b), slightly lower in Test 2 (Figure 8c,d) and the lowest in Test 3 (Figure 8e,f). This was the most pronounced for the smoothest samples, P-1 and P-2 and the least pronounced for the roughest samples, SP30-1 and SP30-2. Most probably, this effect is correlated with the properties of the ice surface. Since the Tests 1–3 were conducted on the same ice surface, one after another without unmounting the steel sample, the ice surface was being gradually smoothed and affected by frictional heating which enabled easier the formation of the liquid-like layer. Therefore, during Test 3, the formation of the

liquid-like layer was more efficient than during Test 1. In Test 3, where the lowest friction values were measured, most likely, the higher ambient humidity (Table 2) acted as an additional factor for efficient liquid-like layer formation.

Generally, no difference in friction was detected between the increasing and decreasing velocity levels.

In Figure 8, a slight decrease in coefficient of friction values with increasing velocity is also visible. This effect was the most pronounced for the smoothest samples, P-1 and P-2, while for the rougher samples it is almost absent (this is especially true for Tests 2 and 3). A decrease in friction with increasing sliding velocity is typically reported for the dry and mixed friction regimes, since at higher velocities more frictional heat is generated, resulting in more efficient production of the liquid-like layer which facilitates easier sliding [1,2]. In the dry/mixed friction regime the velocity dependence of the friction coefficient is described with the following equation:

$$\mu \propto 1 / \sqrt{v} \tag{1}$$

where μ is the coefficient of friction and v is the sliding velocity.

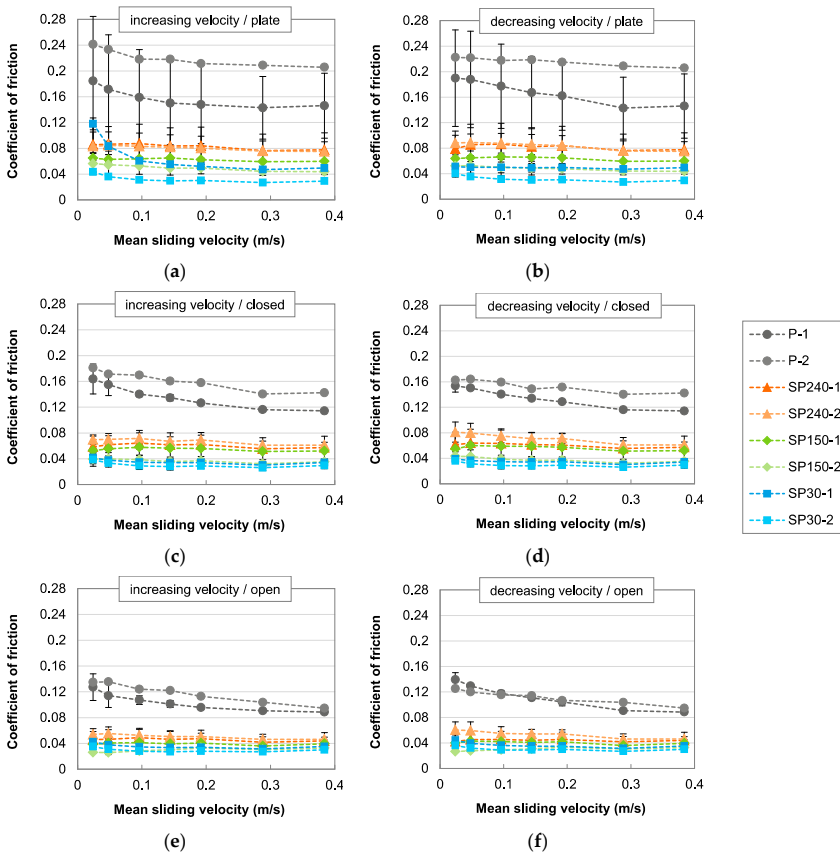


Figure 8. Coefficients of friction measured on the oscillating tribometer: (a,b) Test 1: test chamber closed by a transparent plastic plate, (c,d) test chamber closed and sealed, (e,f) test chamber opened; (a,c,e) increasing velocity levels, (b,d,f) decreasing velocity levels.

4. Discussion

Table 3 shows a comparison between the experimental parameters and the contact conditions on the inclined ice track tribometer and on the oscillating tribometer. Due to the different test parameters and sliding conditions, different friction regimes may have occurred on both test rigs. The formation of the liquid-like layer on the ice surface is largely influenced by the ambient temperature, ice temperature, surface pressure, sliding velocity and relative humidity. In the present study, the dynamics of movement may have had a strong influence on the liquid-like layer formation and the friction regime. On the inclined ice track tribometer, the steel specimen constantly in contact with a fresh ice surface and possibly the formation of the liquid-like layer (also because of the low surface pressure) was insufficient, resulting in dry or mixed friction regime. On the other hand, on the oscillating tribometer, the steel sample was in continuous oscillating contact with the ice surface, which was most likely covered with a liquid-like layer due to frictional heat, resulting in the hydrodynamic friction regime.

In Figure 9, the influence of surface roughness on the shape of the Stribeck curve for ice friction based on results from different studies (estimated on the basis of the properties of the ice surface) is presented schematically:

- In References [4–7], under dry/mixed friction conditions, friction increased with roughness. Correspondingly, in the present study on the inclined ice track tribometer (mixed friction conditions), friction increased with the roughness of the steel sliders.
- In References [6,8] under hydrodynamic friction conditions, friction decreased with roughness. Correspondingly, in the present study on the oscillating tribometer (hydrodynamic friction conditions), friction decreased with the roughness of the steel sliders.

Table 3. Comparison of test parameters of the inclined ice track tribometer and the oscillating tribometer.

Test Parameter	Inclined Ice Track Tribometer	Oscillating Tribometer
Ice temperature	−2 and −7 °C	−8 °C
Ambient temperature/ relative humidity	0 °C and −4 °C/60%–80%	4 °C/30%
Sliding contact	Steel sample slides over a fresh ice surface	Steel sample slides over a run-in ice surface
Sliding distance	40 tests × 3300 mm per test	6912 mm (before that up to 47,280 mm for ice smoothening)
Ratio ice track length:sample length	84	1.7
Motion dynamics	Unidirectional, accelerating/decelerating	Oscillating, sinusoidal
Contact pressure	0.001 N/mm ²	0.08 N/mm ²
Sliding velocity	From 0 up to ~3.5 m/s	From 0 up to 0.60 m/s

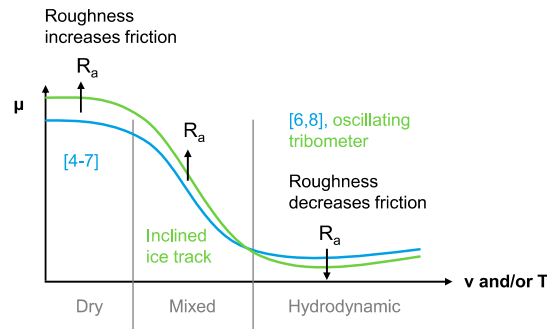


Figure 9. Schematic representation of the hypothetical influence of surface roughness on the shape of the Stribeck curve for ice friction based on results from different studies.

Another possible explanation for the inversely different results of coefficients of friction and sliding velocity is that under the applied testing conditions, samples with higher friction achieved higher velocities due to the more efficient formation of the liquid-like layer as a consequence of higher frictional heating. From friction between snow and waxed ski bases it is known that at low temperatures, harder waxes which prevent from snow crystal penetration (and produce more frictional heat) are needed for the enhancement of the liquid-like layer formation and the corresponding achievement of higher sliding velocities, while at higher temperatures, softer hydrophobic waxes which prevent from excessive viscous friction are used [13].

However, the hypotheses described above must still be examined in further investigations in order to be able to explain the observed effects with greater certainty.

Due to a myriad of influencing parameters, the unstable nature of ice and the still relatively vaguely understood properties of the interface that enables its low friction properties, ice friction is probably one of the most complex tribological systems with ambiguities in the understanding of the basic mechanisms. In the last decade new theoretical and experimental findings have challenged the existing theories and postulated a need for complete reformulation of the frameworks describing ice friction. As far as the authors are aware of, the present study is one of the first to compare steel sliders on ice using different experimental setups. The obtained results indicate that extreme caution is required when comparing results from different experimental setups and to some extent explains why for ice friction so many contradicting results can be found in the literature.

It should also be pointed out the nature of the liquid-like layer is much more complex than that of the Newtonian liquids considered in general lubrication theories. In recent years, novel findings contradicting the assumption that this slippery layer is a liquid are continuously being reported. The research group who made the first direct observations of this layer, prefer to call it a quasi-liquid as it represents a transitional stage between solid and liquid as the temperature increases [14]. Their observations were confirmed by complex mechanical behavior of the interstitial meltwater, which exhibits the rheology of a complex yielding material: its large viscosity, coupled to an elastic response, yields an excellent hydrodynamic lubricant behavior, leading to low friction [15]. In another study, ice slipperiness was attributed to highly mobile DA water molecules (molecules donating and accepting one hydrogen bond) that diffuse over the ice surface: in this case, a layer of mobile ice at the surface makes the surface smooth and lubricates the contact [16]. Elsewhere, authors claim that this layer should be called a “supersolid skin” because the weak bonds between H₂O molecules at the surface are stretched but unlike in liquid water none of them are broken [17,18]. They also argue that this elongation of bonds ultimately produces a repulsive electrostatic force between the surface layer and anything it comes into contact with – similarly to a levitating effect.

In order to gain deeper understanding of the ice friction effects—especially in relation to the surface properties of the sliders as well as their geometry/form—further investigations are planned.

5. Conclusions

In the present study, analyses of sliding velocity and coefficient of friction of stainless steel samples having different isotropic surface roughness were conducted for ice contact on two different experimental setups and test parameter sets. It was observed that:

1. On the inclined ice track tribometer, the samples with higher roughness reached lower velocities than the samples with lower roughness, while on the oscillating tribometer samples with higher roughness provided lower friction than the samples with lower roughness.
2. Assuming that lower friction leads to a higher velocity, the results from the oscillating tribometer show a reverse tendency compared to the results from the inclined ice track tribometer.
3. In the available literature, increase of friction with increased surface roughness was typically observed for dry/mixed friction conditions due to increased deformative friction, while decrease of friction with increased surface roughness was typically observed for hydrodynamic friction conditions due to decreased adhesion and lower friction in the liquid-like layer.
4. It is possible that due to different test conditions, different friction regimes were established on both experimental setups.
5. Since the relationship between the friction and the sliding velocity is also unknown for the system under consideration, further investigations will be carried out in order to further analyze the influence of the surface roughness on ice friction in different friction regimes.
6. The presented findings indicate that due to the highly sensitive nature of ice, extreme caution is required when interpreting the results obtained under laboratory or real scale conditions in scientific research as well as in industrial practice. Conduction of comparative measurements using different experimental setups has shown to be very useful in providing a wider frame for the analysis of the ice friction mechanisms.

Author Contributions: Conceptualization, I.V. and J.L.; investigation, I.V., J.L. and E.J.; methodology, analysis and validation, I.V., J.L., E.J., S.K., J.V. and F.A.; writing—original draft preparation, I.V., J.L. and E.J.; writing—review and editing, S.K., J.V. and F.A.

Funding: Parts of this work were funded by the Austrian COMET Programme (Project XTribology, no. 849109) and carried out at the “Excellence Centre of Tribology” (AC2T research GmbH) in cooperation with V-Research GmbH and Riga Technical University. Parts of this work were also funded by the ERDF project “The quest for disclosing how surface characteristics affect slideability” (No.1.1.1.16/A/129) which is being implemented in Riga Technical University. Financial support of Austrian Cooperative Research (ACR) is gratefully acknowledged.

Acknowledgments: The authors would like to thank the Latvian bobsled and skeleton technical crew for sharing their practical observations and providing useful additional information.

Conflicts of Interest: The authors declare no conflict of interest.

References

1. Kietzig, A.-M.; Hatzikiriakos, S.G.; Englezos, P. Physics of ice friction. *J. Appl. Phys.* **2010**, *107*, 081101. [[CrossRef](#)]
2. Marmo, B.A.; Blackford, J.R.; Jeffree, C.E. Ice friction, wear features and their dependence on sliding velocity and temperature. *J. Glaciol.* **2005**, *51*, 391–398. [[CrossRef](#)]
3. Rosenberg, R. Why Is Ice Slippery? *Phys. Today* **2005**, *58*, 50–55. [[CrossRef](#)]
4. Ducret, S.; Zahouani, H.; Midol, A.; Lanteri, P.; Mathia, T.G. Friction and abrasive wear of UHMWPE sliding on ice. *Wear* **2005**, *258*, 26–31. [[CrossRef](#)]
5. Calabrese, S.J.; Buxton, R.; Marsh, G. Friction Characteristics of Materials Sliding Against Ice. *Lubr. Eng.* **1980**, *36*, 283–289.
6. Kietzig, A.-M.; Hatzikiriakos, S.G.; Englezos, P. Ice friction: The effects of surface roughness, structure, and hydrophobicity. *J. Appl. Phys.* **2009**, *106*, 024303. [[CrossRef](#)]

7. Spagni, A.; Berardo, A.; Marchetto, D.; Gualtieri, E.; Pugno, N.M.; Valeri, S. Friction of rough surfaces on ice: Experiments and modeling. *Wear* **2016**, *368–369*, 258–266. [[CrossRef](#)]
8. Rohm, S.; Hasler, M.; Knoflach, C.; van Putten, J.; Unterberger, S.H.; Schindelwig, K.; Lackner, R.; Nachbauer, W. Friction Between Steel and Snow in Dependence of the Steel Roughness. *Tribol. Lett.* **2015**, *59*, 27. [[CrossRef](#)]
9. Itagaki, K.; Lemieux, G.E.; Huber, N.P. Preliminary study of friction between ice and sled runners. *J. Phys. Colloq.* **1987**, *48*, C1–C297. [[CrossRef](#)]
10. Dong, W.P.; Sullivan, P.J.; Stout, K.J. Comprehensive study of parameters for characterising three-dimensional surface topography III: Parameters for characterising amplitude and some functional properties. *Wear* **1994**, *178*, 29–43. [[CrossRef](#)]
11. Jansons, E.; Lungevics, J.; Stiprais, K.; Pluduma, L.; Gross, K.A. Measurement of sliding velocity on ice, as a function of temperature, runner load and roughness, in a skeleton push-start facility. *Cold Reg. Sci. Technol.* **2018**, *151*, 260–266. [[CrossRef](#)]
12. Lungevics, J.; Jansons, E.; Gross, K.A. An Ice Track Equipped with Optical Sensors for Determining the Influence of Experimental Conditions on the Sliding Velocity. *Latv. J. Phys. Tech. Sci.* **2018**, *55*, 64–75. [[CrossRef](#)]
13. Rogowski, I.; Leonard, D.; Gauvrit, J.-Y.; Lanteri, P. Influence of fluorine-based additive content on the physical and physicochemical properties of ski gliding wax. *Cold Reg. Sci. Technol.* **2007**, *49*, 145–150. [[CrossRef](#)]
14. Sazaki, G.; Zepeda, S.; Nakatsubo, S.; Yokomine, M.; Furukawa, Y. Quasi-liquid layers on ice crystal surfaces are made up of two different phases. *Proc. Natl. Acad. Sci. USA* **2012**, *109*, 1052–1055. [[CrossRef](#)] [[PubMed](#)]
15. Canale, L.; Comtet, J.; Niguès, A.; Cohen, C.; Clanet, C.; Siria, A.; Bocquet, L. Nanorheology of interfacial water during ice gliding. *Phys. Rev. X* **2019**, *9*, 041025. [[CrossRef](#)]
16. Weber, B.; Nagata, Y.; Ketzetzi, S.; Tang, F.; Smit, W.J.; Bakker, H.J.; Backus, E.H.G.; Bonn, M.; Bonn, D. Molecular Insight into the Slipperiness of Ice. *J. Phys. Chem. Lett.* **2018**, *9*, 2838–2842. [[CrossRef](#)] [[PubMed](#)]
17. Zhang, X.; Sun, C.Q.; Zhang, X.; Huang, Y.; Ma, Z.; Zhou, Y.; Sun, C.Q. Skin supersolidity slipperizing ice. *arXiv* **2013**, arXiv:1310.08889.
18. Sun, C.Q.; Sun, Y. Superlubricity of ice. In *The Attribute of Water, Springer Series in Chemical Physics*; Springer: Berlin/Heidelberg, Germany, 2016; pp. 203–243.



© 2019 by the authors. Licensee MDPI, Basel, Switzerland. This article is an open access article distributed under the terms and conditions of the Creative Commons Attribution (CC BY) license (<http://creativecommons.org/licenses/by/4.0/>).

APPENDIX 4
PUBLICATION 4

Velkavrh I., Voyer J., Wright T., Lungevics J., Jansons E., Boiko, I. *Variations of ice friction regimes in relation to surface topography and applied operating parameters*, IOP Conf. Ser. Mater. Sci. Eng. 1140 (2021) 012033

Available: <https://doi.org/10.1088/1757-899X/1140/1/012033>

Open access

© Content from this work may be used under the terms of the Creative Commons Attribution 3.0 licence. Any further distribution of this work must maintain attribution to the author(s) and the title of the work, journal citation, and DOI.

PAPER • OPEN ACCESS

Variations of ice friction regimes in relation to surface topography and applied operating parameters

To cite this article: Igor Velkavrh *et al* 2021 *IOP Conf. Ser.: Mater. Sci. Eng.* **1140** 012033

View the [article online](#) for updates and enhancements.

You may also like

- [Roles of charged particles and reactive species on cell membrane permeabilization induced by atmospheric-pressure plasma irradiation](#)
Shota Sasaki, Makoto Kanzaki, Yutaro Hokari *et al.*
- [Successive H-atom Addition to Solid OCS on Compact Amorphous Solid Water](#)
Thanh Nguyen, Yasuhiro Oba, W. M. C. Sameera *et al.*
- [Instrumented figure skating blade for measuring on-ice skating forces](#)
S A Acuña, D M Smith, J M Robinson *et al.*



The Electrochemical Society
Advancing solid state & electrochemical science & technology

242nd ECS Meeting

Oct 9 – 13, 2022 • Atlanta, GA, US

Abstract submission deadline: **April 8, 2022**

Connect. Engage. Champion. Empower. Accelerate.

MOVE SCIENCE FORWARD



Submit your abstract



Variations of ice friction regimes in relation to surface topography and applied operating parameters

Igor Velkavrh^{1*}, Joël Voyer¹, Thomas Wright¹, Jānis Lungevičs²,
Ernests Jansons², Irina Boiko²

¹V-Research GmbH, Stadtstrasse 33, 6850 Dornbirn, Austria

²Riga Technical University, Department of Mechanical Engineering and Mechatronic,
Kipsalas str. 6b, Riga, 1048, Latvia

* igor.velkavrh@v-research.at

Abstract. To evaluate the effects of surface topography, ice and ambient conditions on the sliding behaviour of steel samples on ice, in the present study friction and velocity measurements were performed with steel samples having different surface roughness values and distinct surface structures. It was shown that the influence of surface roughness on friction and sliding velocity is strongly dependant on ice conditions and the applied experimental parameters due to the formation of different friction regimes.

1. Introduction

In ice friction, depending on the contact conditions and operating parameters such as temperature, sliding velocity and contact pressure, different processes and mechanisms prevail, which define different friction regimes: boundary, mixed or hydrodynamic friction [1]. One of the main parameters defining the ice friction regimes is the thickness of the lubricating liquid-like layer (LLL) on ice with respect to the roughness of the ice and the slider [2,3]. Generally, in different friction regimes different friction levels prevail, thus understanding of boundaries and transitions between different friction regimes is essential for the control of ice friction.

In winter sports, high velocities are desired and therefore the drag between the slider and the ice/snow surface should be minimal. Minimal drag can typically be correlated with the optimal LLL thickness which is dependent on a myriad of parameters and boundary conditions and is anything but straightforward. In a previous study [4], it was shown that depending on the tribometer type, different effects of surface roughness on the coefficient of friction and sliding velocity were observed. On an inclined ice track tribometer, the samples with higher roughness reached lower velocities than the samples with lower roughness, while on oscillating tribometer samples with higher roughness provided lower friction than the samples with lower roughness.

To further evaluate the observed effects, in this study, ice friction measurements were performed with steel samples having different surface roughness values and distinct surface structures. An oscillating tribometer measuring the coefficient of friction and an inclined ice plane measuring the sliding velocity of the steel samples were used to determine the sliding ability.

2. Experimental

2.1. Samples

All samples were manufactured from the Uddeholm Ramax HH steel, which is a chromium alloyed, corrosion-resistant holder steel supplied in a high pre-hardened condition. All samples were cut to



dimensions of 35 mm x 18 mm x 14 mm and polished to mirror polish ($R_a < 0.01 \mu\text{m}$). Steel samples having two distinct surface textures were prepared: one by polishing and abrading the samples in sliding direction and another one by sandblasting and polishing [5]. In Figure 1, sample topographies and roughness values R_a of the tested samples are presented. For sample denotation, G stands for “grooved samples”, while SP stands for “sandblasted and polished samples”. Sample G1 is the control sample, while samples G2 and G3 were further treated by roughening with different grade sandpapers to achieve parallel grooves in the direction of sliding, having two different depths respectively. Samples SP240, SP150 and SP30 were sandblasted and polished to achieve different surface structures and roughness values.

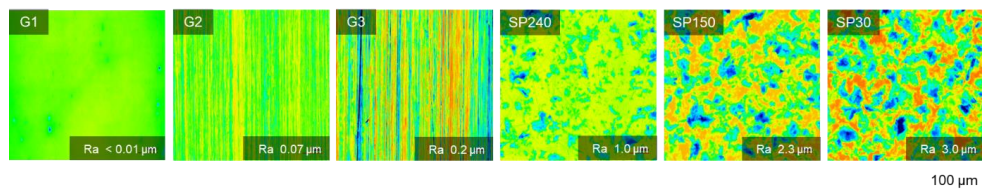


Figure 1. Surface topographies and roughness values R_a of the tested samples.

2.2. Ice preparation

In tribological tests on the oscillating tribometer, four different test conditions were applied within 2 different test series (Table 1). As can be seen from Table 1, the main difference between the test series 1 and 2 lies in the steel sample temperature: in the test series 1, before the test, the steel sample was kept in a freezer at around -18°C , while in the test series 2, the steel sample was kept in the cooling chamber and had a temperature close to that of the ambient atmosphere (around 5°C).

Before each test series, a new ice surface was prepared. The ice rink was 20 mm wide, 80 mm long and 5 mm deep. For ice formation, 18 ml of distilled water was used to which 0.5 ml of tap water was added to accelerate ice crystallization. To achieve a homogeneous temperature and crystallization rate within the ice volume, the sample was cooled for 40 min. Due to the expansion of the water volume under sub-zero temperatures, when ice was formed, it had a curved surface, therefore, the surface was smoothed with an aluminium plate having surface dimensions of 45 mm x 28 mm. The smoothing of the ice surface was performed at a normal load of 692 N at a sliding velocity of 0.08 m/s until the height difference between the left and the right side of the ice track was lower than $100 \mu\text{m}$. Usually, this was achieved within 10-20 min of sliding the aluminium plate back and forth.

Table 1: Ambient and ice conditions for different test setups on the oscillating tribometer.

Test series	Test setup	Ambient temperature ($^\circ\text{C}$)	Ambient RH (%)	Ice surface temperature ($^\circ\text{C}$)	Ice bulk temperature ($^\circ\text{C}$)	Sample temperature ($^\circ\text{C}$)
1	1-1A	7.7 ± 0.8	42 ± 7	ca. -8.0	ca. -9.0	ca. -18.0
2	2-1A	2.7 ± 0.3	15 ± 1	-8.6 ± 0.5	-9.1 ± 0.0	ca. 5.0
	2-2A	3.0 ± 0.5	20 ± 3	-8.7 ± 0.3	-8.7 ± 0.3	ca. 5.0
	2-2B	6.7 ± 0.3	53 ± 4	-8.3 ± 0.4	-8.7 ± 0.2	ca. 5.0

Tests on the inclined plane tribometer were conducted at different ice and air temperatures to see how ambient conditions influence the results. All known ambient conditions for inclined plane tests are summarized in Table 2. Test 1 was conducted at lower ambient temperatures than Test 2. The ice was frozen identically for all the test setups. The temperature was -10°C while the ice was frozen layer by layer (5 layers in total). Each new layer was poured on the previous one and warm water was used to ensure a better mixture of the layers. Before experiments, the ice surface was levelled with a specifically developed planer that also creates a small groove on the ice surface. The groove guides freely sliding

samples in a straight line while they are sliding down the inclined plane. Small ice debris was removed from the planed ice with a moist sponge to ensure a smooth ice surface. The same ice was used in all experiments which were conducted on the same experiment day. The sample groups were tested on different days (two experiment days in total).

Table 2: Ambient and ice conditions for different tests on the inclined plane tribometer.

Samples	Test setup	Ambient temperature (°C)	Ambient RH (%)	Ice surface temperature (°C)	Sample temperature
G	1	-1.6±0.2	63±2	-9.1±0.2	ca. -1.6°C
	2	-0.8±0.3	64±3	-9.0±0.2	ca. -0.8°C
SP	1	-3.5±0.5	64±3	-7.0±0.2	ca. -3.5°C
	2	-0.4±0.3	75±3	-2.0±0.3	ca. -0.4°C

2.3. Friction measurements

A universal modular designed tribometer (RVM1000, Werner Stehr Tribologie GmbH, Germany) was used in oscillating mode. Tests were performed at a constant normal load of 52 N. In each friction test, initially, a running-in phase was employed for 60 s at 0.1 m/s resulting in 120 cycles. Afterwards, 7 increasing velocity steps (0.02, 0.05, 0.10, 0.14, 0.19, 0.29 and 0.38 m/s) were employed. In each velocity step at least 10 cycles were performed and at the same time, for each velocity step, a minimum of 3 s duration was employed. Further details on the experimental setup can be found elsewhere [4].

2.4. Velocity measurements

Steel samples were slid down a 3 m long ice path tilted at an angle of $16 \pm 0.5^\circ$, which was sufficient to promote sliding of steel samples without stacking in the start position. Samples always started the movement from a steady-state (using a start gate) and accelerated freely sliding down the ice surface. To measure the sliding time, optical sensors allowing time measurements with 0.01 s resolution were used. From the time measurements, the average sliding speed of the samples was calculated. The total distance between the first and the last optical sensor was 2850 mm. Each sample was tested 40 times. From 40 measurements, 3 fastest and 3 slowest results were eliminated. The results shown in the graphs herein represent the average of the selected 34 measurements. Further details on the experimental setup (inclined plane tribometer) can be found elsewhere [4].

3. Results

In Figure 2, the coefficient of friction of sandblasted and polished samples at two different ice and atmospheric conditions are presented. From Figure 2a it can be seen that for test setup 1-1A coefficient of friction decreased with sliding velocity and slightly increased with decreasing surface roughness. Higher friction of the smoother samples could be correlated with their large contact area which resulted in higher adhesive forces than for the rougher samples with a smaller contact area. From Figure 2b, for test setup 2-2A, coefficients of friction significantly decreased as compared to test setup 1-1A. This is most probably correlated with a higher sample temperature resulting in the formation of a LLL. At the same time, in Figure 2b the influence of surface roughness is not as pronounced; however, it can be observed that it has an inverse effect on friction as in test setup 1-1A. Namely, for test setup 2-2A, coefficient of friction with rougher samples was higher than for the smoother samples, which was especially pronounced at low velocities.

In Figure 3, results with grooved samples are presented for different ice and atmosphere conditions. From Figure 3a, it can be observed that the coefficient of friction increased with sliding velocity and at the same time, the coefficient of friction increased with surface roughness. From Figure 3b, at higher ambient temperature and humidity and/or on a run-in ice surface (in test 2B, ice surface was additionally run-in) coefficient of friction decreased, the influence of roughness remained unchanged, while the influence of velocity was less pronounced than in test setup 2-1A.

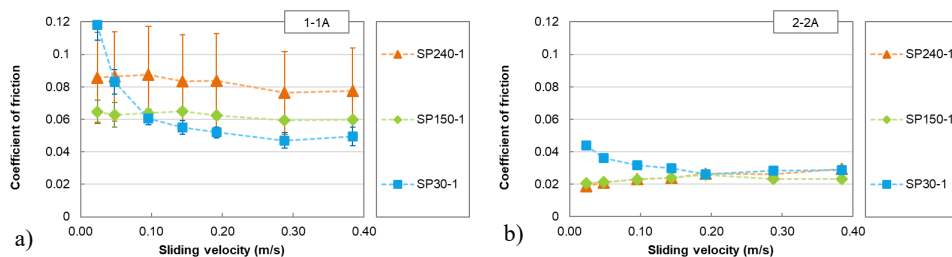


Figure 2. Coefficient of friction of sandblasted and polished samples at two different ice and atmosphere conditions: (a) test setup 1-1A, (b) test setup 2-2A.

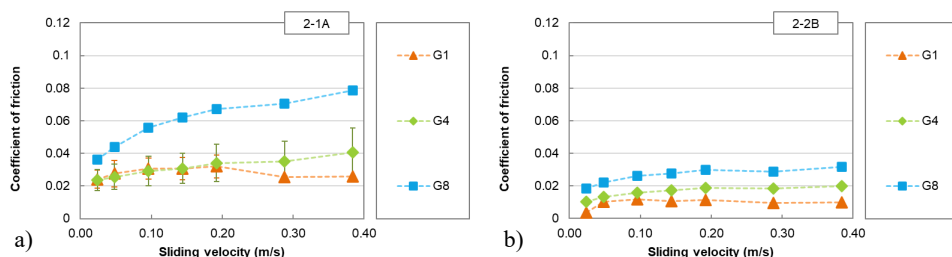


Figure 3. Coefficient of friction of grooved samples at different ice and atmosphere conditions: (a) test setup 2-1A (b) test setup 2-2B.

In Figure 4, test results from the inclined plane tribometer are shown. As shown in Table 2, test 1 was conducted at lower ambient temperatures thus providing a “drier” ice surface while test 2 provided a “wetter” ice surface. For both sample types, a trend of decreased sliding velocity for rougher surfaces can be observed. With grooved samples, at higher ambient temperature (test 2) higher sliding velocities were achieved, while with sandblasted and polished samples an opposite trend was observed. The decrease of sliding velocity at higher temperatures could be caused by a thicker LLL resulting in increased hydrodynamic drag for such isotropic surfaces at low normal loads. Figure 4 indicates a pronounced influence of the ambient conditions on the sliding velocity and suggests that changes in the ambient conditions might have a larger effect on sliding performance of the steel samples than their surface texture modifications.

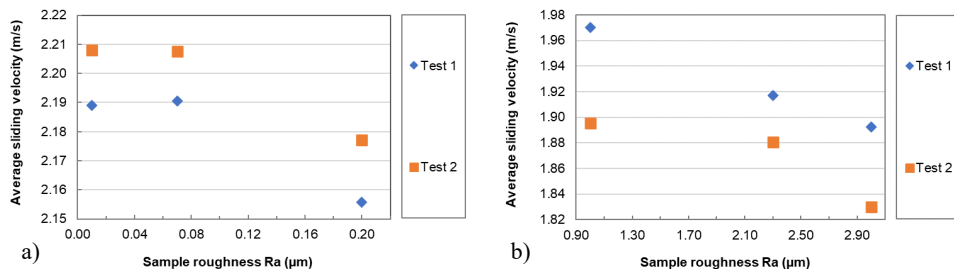


Figure 4. Average sliding velocity on the inclined plane tribometer for (a) grooved and (b) sandblasted and polished samples. Test 1 was performed at lower air and ice temperatures than test 2. Each sample group was tested on a different day.

4. Discussion

In the present study, an inverse roughness-friction correlation was observed for the sandblasted and polished samples tested at different boundary conditions on an oscillating tribometer. Most probably, the inverse roughness-friction correlation occurred due to the difference in the steel sample temperature. In the test 1-1A, where samples with higher roughness provided lower friction values, the initial sample temperature was approximately -18°C , thus in the contact areas between the steel sample and ice, LLL viscosity was lower or even freezing of the LLL could have occurred on a small scale. Since the smoother samples have a larger contact area with the ice surface, more “freezing” points could have formed which resulted in higher friction values. In test series 2, where warmer samples were used, freezing of the LLL did not occur. On the contrary, steel samples melted the ice surface due to heat transfer from the relatively warm samples. Due to a larger contact area with the smoother samples, LLL formed more effectively, resulting in lower friction values. For the grooved samples, the influence of surface roughness on friction was similar as for the sandblasted and polished samples in test series 2, which most probably is correlated with the similar sample temperature in both tests and thus more efficient LLL formation for the smoother steel samples.

Inclined ice plane tests showed a deteriorated sliding ability at higher ambient temperatures for the sandblasted and polished samples, while for the grooved samples an opposite effect was observed. Different influence of the ambient temperature indicates that with different surface structures, thickness of the LLL and the corresponding hydrodynamic drag can vary significantly.

5. Conclusions

In the present study it was observed that:

1. At very low sample temperature, the influence of surface roughness had an inversely different effect on friction compared to tests which were performed with higher sample temperatures. This effect was correlated with different heat transfer effects between the sample and the ice for different sample temperatures.
2. In the inclined ice plane tests sliding velocity decreased with the roughness of the steel samples regardless of their texture type.
3. For similar sample conditions, results on the oscillating tribometer and the inclined ice plane are in good correlation.

Acknowledgements

Parts of this work were funded by the Austrian COMET Program (Project InTribology, no. 872176) and carried out at the “Excellence Centre of Tribology” (AC2T research GmbH) in cooperation with V-Research GmbH and Riga Technical University. Financial support of Austrian Cooperative Research (ACR) is gratefully acknowledged.

References

- [1] Kietzig A-M, Hatzikiriakos S G and Englezos P 2010 Physics of ice friction *Journal of Applied Physics* **107** 081101
- [2] Kietzig A-M, Hatzikiriakos S G and Englezos P 2009 Ice friction: The effects of surface roughness, structure, and hydrophobicity *Journal of Applied Physics* **106** 024303
- [3] Marmo B A, Blackford J R and Jeffree C E 2005 Ice friction, wear features and their dependence on sliding velocity and temperature *J. Glaciol.* **51** 391–8
- [4] Velkavrh I, Lungevičs J, Jansons E, Klien S, Voyer J and Ausserer F 2019 The Influence of Isotropic Surface Roughness of Steel Sliders on Ice Friction Under Different Testing Conditions *Lubricants* **7** 106
- [5] Jansons E, Lungevičs J and Gross K A 2016 Surface roughness measure that best correlates to ease of sliding *Proceedings of 15th International Scientific Conference Engineering for Rural Development* Engineering for Rural Development (Jegava, Latvia: Latvia University of Agriculture, Latvia) pp 687–95

APPENDIX 5
PUBLICATION 5

Jansons E., Lungevics J., Jerane I., Gross K. *A Smaller Bearing Ratio, as a Surface Texture Measure, Promotes Faster Sliding on Ice*. Journal of Tribology, 2021, Vol. 143, No. 11, Article number 111801. ISSN 0742-4787. e-ISSN 1528-8897

Available: doi.org/10.1115/1.4049704

ASME copyrights the full text of Publication 5 in electronic format. The first page of the Publication 5 is available on the next page.

The full text of the Publication 5 is available on request for Doctoral Thesis defense purposes only. ASME kindly granted permission.

© 2021 by ASME

Ernests Jansons¹

Biomaterials Research Laboratory,
Faculty of Materials Science and
Applied Chemistry,
Riga Technical University,
3 Paula Valdeņa Street,
Riga LV-1048, Latvia;
Department of Mechanical Engineering and
Mechatronics,
Faculty of Mechanical Engineering,
Transport and Aeronautics,
Riga Technical University,
6B Kipsalas Street,
Riga LV-1048, Latvia
e-mail: Ernests.Jansons_1@rtu.lv

Jānis Lungevičs

Department of Mechanical Engineering and
Mechatronics,
Faculty of Mechanical Engineering,
Transport and Aeronautics,
Riga Technical University,
6B Kipsalas Street,
Riga LV-1048, Latvia
e-mail: Janis.Lungevics@rtu.lv

Ilze Jerāne

Biomaterials Research Laboratory,
Faculty of Materials Science and
Applied Chemistry,
Riga Technical University,
3 Paula Valdeņa Street,
Riga LV-1048, Latvia
e-mail: Ilze.Jerane@rtu.lv

Kārlis Agris Gross

Biomaterials Research Laboratory,
Faculty of Materials Science and
Applied Chemistry,
Riga Technical University,
3 Paula Valdeņa Street,
Riga LV-1048, Latvia
e-mail: kgross@rtu.lv

A Smaller Bearing Ratio, as a Surface Texture Measure, Promotes Faster Sliding on Ice

Surfaces only characterized by a roughness Ra or Sa may have a totally different surface texture and include complex patterns such as grooves, dimples, or a mirror-polish. Here, the bearing ratio is proposed as an additional characterization measure to determine the sliding performance of a steel–ice friction pair. Different steel surfaces were produced by milling, shot blasting, and scratching, followed by texture assessment with a stylus type three-dimensional (3D) profilometer. The bearing ratio and other 3D roughness parameters were determined. Tribology experiments involved a 3 m long inclined plane tribometer and the speed measured at four points during the sliding experiment. Correlation between the steel sliding speed and the bearing ratio was observed under two different regimes: at warmer conditions and at colder conditions. Experiment 1 depicting warmer conditions exhibited a relative humidity of 64%, an air temperature of -2°C , and an ice temperature of -9°C . Experiment 2 for colder conditions showed a relative humidity of 78%, an air temperature of 1°C , and an ice temperature of -4°C . The sliding speed correlated with the bearing ratio in these two conditions showing -0.91 and -0.96 , respectively. A strong correlation between the sliding speed and the bearing ratio shows the value of the bearing ratio as an additional surface characteristic for considering larger surface features.
[DOI: 10.1115/1.4049704]

Keywords: ice, tribology, friction, texture, bearing ratio, surface characterization, hydrodynamic lubrication, mixed lubrication, scratching, sliding, surface properties and characterization, surface treatments, tribological systems

1 Introduction

Various surface technologies—milling, turning, polishing, sandblasting, and laser texturing—have generated distinctly different surface textures for ice friction studies [1–4]. Each surfacing process imparts individual texture characteristics that are unlike and so require a means and measure to detect these differences. The most common report of the surface texture to report the surface is limited to the surface roughness [2–5]. For distinctly different surfaces, where a comparison of the performance is required, it is difficult to find a surface characteristic that measures the surface texture and provides a correlation with the sliding speed on the ice.

Previously authors have made experimental samples with isotropic and anisotropic surfaces using surface roughness Ra (arithmetic mean height of the profile) as surface describing parameter. Spagni et al. [4] used stainless steel pins treated with sandblasting, providing isotropic surface textures with different Ra values 0.11,

1.4, and $2.6\ \mu\text{m}$. Jansons et al. [5] produced anisotropic surface textures with different surface roughness using scratching and polishing (Ra 0.01, 0.02, 0.08, and $0.18\ \mu\text{m}$) and emphasized the fact that only Ra as a surface characterization parameter might be not enough if surfaces are treated using different technologies. In both cases separately, Ra can describe the surface texture, and results correlate with a coefficient of friction or sliding speed. However, if both surface treatment techniques are used in one experiment, the surface characterization using Ra might not be enough due to significant differences in surface textures.

The direction of the sample's treatment can have a significant effect on sliding properties retaining the same surface roughness. Kietzig et al. [2] used polished and laser-irradiated metal samples and compared friction coefficient under three different temperatures. Kietzig used Ra as a surface characterization parameter, informing that Ra for a polished sample was about $0.6\ \mu\text{m}$ and for laser-irradiated samples $1.12\ \mu\text{m}$. In the process of experiment development, Kietzig noted that polishing direction influences sliding ability. Thus, two samples with different polishing directions—randomly oriented and with concentric grooves in the sliding direction—were produced with the same surface roughness (Ra of $0.6\ \mu\text{m}$). Samples with grooves in the sliding direction

¹Corresponding author.

Contributed by the Tribology Division of ASME for publication in the JOURNAL OF TRIBOLOGY. Manuscript received September 10, 2020; final manuscript received January 4, 2021; published online February 12, 2021. Assoc. Editor: Yong Hoon Jang.

APPENDIX 6
PUBLICATION 6

Lungevics J., Jansons E., Boiko I., Velkavrh I., Voyer J., Wright T. *A Holistic Approach towards Surface Topography Analyses for Ice Tribology Applications*. *Frontiers in Mechanical Engineering*, 2021, Vol. 7, No. 1, pages 42-56. ISSN 2297-3079.

Available: [10.3389/fmech.2021.691485](https://doi.org/10.3389/fmech.2021.691485)

Open access

© 2021 Lungevics, Jansons, Boiko, Velkavrh, Voyer and Wright. This is an open-access article distributed under the terms of the Creative Commons Attribution License (CC BY)



A Holistic Approach Towards Surface Topography Analyses for Ice Tribology Applications

Janis Lungevics^{1*}, Ernests Jansons¹, Irina Boiko¹, Igor Velkavrh², Joël Voyer² and Thomas Wright²

¹Department of Mechanical Engineering and Mechatronic, Riga Technical University, Riga, Latvia, ²V-Research GmbH, Dornbirn, Austria

A surface texture can be subdivided into three categories based on the magnitude of its wavelengths, i.e., macro-geometrical form, waviness, and roughness (from largest to smallest). Together, these components define how a surface will interact with the opposing surface. In most ice tribology studies, <2% of the entire sample surface is topographically analyzed. Although such a small percentage of the entire surface area generally provides statistically relevant information, the missing information about the texture complexity on a larger scale might reduce the possibility of accurately explaining the resulting tribological behavior. The purpose of this study was to review the existing surface measurement methods related to ice tribology and to present a holistic approach towards surface topography measurements for ice tribology applications. With the holistic surface measurement approach, the entire sample surfaces are scanned, and the measured data is analyzed on different magnitude levels. The discussed approach was applied to sandblasted steel samples which were afterward tested on two different ice tribometers. The experimental results showed that additional information about the sample surface topography enabled a better understanding of the ice friction mechanisms and allowed for a more straightforward correlation between the sample surface topography and its ice friction response.

Keywords: ice friction, surface topography, contact area, contact pressure, friction regimes, coefficient of friction, sliding velocity

OPEN ACCESS

Edited by:

Emile Van Der Heide,
University of Twente, Netherlands

Reviewed by:

Aydar Akchurin,
SKF, Netherlands
Árpád Czifra,
Óbuda University, Hungary

*Correspondence:

Janis Lungevics
janis.lungevics@rtu.lv

Specialty section:

This article was submitted to
Tribology,
a section of the journal
Frontiers in Mechanical Engineering

Received: 06 April 2021

Accepted: 26 May 2021

Published: 09 June 2021

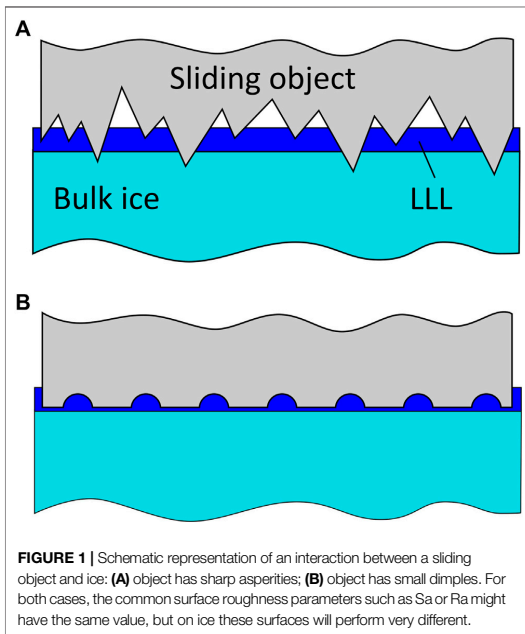
Citation:

Lungevics J, Jansons E, Boiko I,
Velkavrh I, Voyer J and Wright T (2021)
A Holistic Approach Towards Surface
Topography Analyses for Ice
Tribology Applications.
Front. Mech. Eng 7:691485.
doi: 10.3389/fmech.2021.691485

INTRODUCTION

Motion between solid objects and ice is one of the most complex tribological systems. This is due to the many influencing factors, which define the properties of the liquid-like layer (LLL) on ice such as ambient temperature and humidity, sliding velocity, the contact area between the sliding object and ice, the roughness and wettability of the sliding object, the texture, and hardness of ice, etc. Scientists are continuously seeking a better understanding of this highly unstable process, but the various mutually related variables and demanding experimental execution make it a very challenging task.

Among the most influencing and at the same time least understood factors are the properties of the LLL. Its thickness is still largely unknown even for static systems, while for dynamic systems it is additionally influenced by the motion dynamics and sliding surface texture and thus even more difficult to estimate. Despite the mentioned obstacles, effective experimental work with various types of laboratory equipment has already been performed over a wide range of sliding velocities (Bäurle



et al., 2007; Rohm et al., 2015; Hasler et al., 2016; Scherge et al., 2018; Ripamonti et al., 2020; Lieferrink et al., 2021), as well as variations applied loads (Scherge et al., 2013).

To improve our understanding of ice friction, reliable information about the interactions between the sample, ice and LLL are necessary. There is a general agreement among scientists that the topography of sliding body and ice play a significant role in the ice friction process (Ducret et al., 2005; Bäurle et al., 2007; Kietzig et al., 2009; Kietzig et al., 2010b; Sukhorukov and Marchenko, 2014; Rohm et al., 2015; Spagni et al., 2016; Lieferrink et al., 2021). This was already described in different experimental studies (Ducret et al., 2005; Rohm et al., 2015; Jansons et al., 2016; Spagni et al., 2016; Jansons et al., 2018; Lieferrink et al., 2021). However, it is still not clear how the surface topography influences the ice friction process, especially if different loads are applied. In some studies, for simplification purposes, the surface is considered perfectly smooth, which distracts from the true process essence. In some cases, the surface topography is analyzed using a measurement from a tiny fraction (<1%) of the whole sample surface. Typically, surface topography measurements are followed by several filtration operations that extract roughness components from the primarily measured texture. Of course, even the measurement of a small fraction of the entire surface provides valuable information, but the whole texture complexity cannot be evaluated if not measured correspondingly. To analyze the interactions between object surfaces and ice in more detail, the geometrical form and waviness of the sliding object should be considered as well, because only a combination of these three

components can provide reliable information about the true contact area.

Another issue in topography analysis is the selection of the most appropriate topography parameters. For example, it can be easily pictured how the surface asperities will penetrate the ice surface (Figure 1A) if a rough surface is put on ice or that small dimples on a flat surface might work as reservoirs for melted water (Figure 1B). Such principally different surfaces might have the same Arithmetical mean height parameter values (Sa or Ra), although the actual texture and its functionality are significantly different. This means that additional information is necessary to explain how such textures will perform in tribological contacts.

The purpose of this paper is to review the existing surface characterization methods, analyzed parameters, and equipment, used in the field of ice tribology. Along with this review, the authors provide some ideas on how ice tribology surfaces could be characterized in further research for more detailed information about surface topography and texture. The proposed measurement approach could help towards a better understanding of the complex ice friction process—not only in the specific experimental setups used in the present study but also in other applications related to ice and snow tribology.

LITERATURE REVIEW

Previously Used Surface Texture Measurement Methods in the Field of Ice Tribology

The existing ice and snow friction studies provide different approaches to surface texture measurements and analyses. The most common are non-contact profilometry (Bäurle et al., 2007; Kietzig et al., 2009; Kietzig et al., 2010b; Rohm et al., 2015; Scherge et al., 2018; Ripamonti et al., 2020; Lieferrink et al., 2021), contact profilometry (Sukhorukov and Marchenko, 2014; Jansons et al., 2016; Spagni et al., 2016), scanning electron microscopy, SEM (Ducret et al., 2005; Bäurle et al., 2007; Kietzig et al., 2009; Kietzig et al., 2011; Ling et al., 2016; Ripamonti et al., 2020), optical microscopy (Rohm et al., 2015; Ling et al., 2016) and atomic force microscopy, AFM (Scherge et al., 2013). All these methods provide useful information about the surface topography, for example, SEM provides a high depth-of-field image of small surface details, such as asperity tips, scratch mark pileups, laser-texturing quality, surface polishing, etc. Optical images offer a time-efficient overview of the surface quality, while non-contact profilometry provides detailed 3D information, but at the same time has its limitations, for example with reflective surfaces or sharp-angled asperities due to the artefacts produced by such surfaces. Contact type profilometry does not possess the limitations of non-contact profilometry but is on the other hand limited by the size of the profilometer tip—e.g., for measurements on a submicron scale. Hybrid type contact profilometer (contour measurement + roughness) can be used for measurements of macro geometry and topography on the same device, i.e., without relocating the analyzed part. Besides the mentioned methods, coordinate measurement machines (CMM) can be used for the

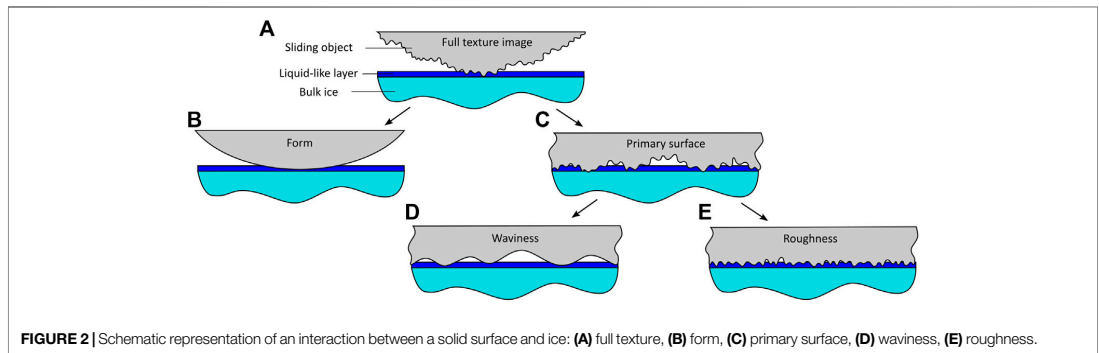


TABLE 1 | Limitations of the common surface topography measurement tools.

	Form > 1 mm	Waviness > 10 μm	Roughness < 10 μm	Limitations	Typical measurement limits
2D measurements					
Profilometer-contact	+	+	+	Stylus tip diameter > 4 μm	Profile length: 50 mm Height: 2 mm
Optical microscope	X	?	+	Surface reflection contrast	Area: 200 \times 200 mm
SEM	X	?	+	Sample preparation	Area: 5 \times 5 mm
3D measurements					
Coordinate measurement machine	+	?	X	Stylus tip diameter > 300 μm	Produced in small and large sizes
Contour measurement machine	+	+	?	Stylus tip diameter > 4 μm	Profile length: 100 mm Height: 60 mm
Non-contact profilometer	+	+	+	Light absorption Reflection Steep asperity slopes	Area: 150 mm \times 200 mm Height: 2 mm
Contact profilometer	+	+	+	Stylus tip diameter > 4 μm	Area: 50 mm \times 100 mm Height: 2 mm
AFM	X	?	+	Limited sample size	Area: 200 μm \times 200 μm Height: 50 μm

Symbols "+", "?" and "X" stand for "measurement is possible", "measurement is potentially possible", and "measurement is not possible", respectively.

measurement of sample macro geometry and X-ray computer tomography for the determination of contact area of various materials, e.g., snow and polymer (Bäurle et al., 2007). All measuring methods have their advantages and disadvantages (Gross et al., 2018), and the limitations of the common surface topography measurement tools are summarized in Table 1.

Examined Surface Areas in the Existing Literature

Depending on the used instrument and data post-processing method, examined sample surface areas can be widely different, from 50 μm \times 50 μm (Scherge et al., 2013) and up to 11 mm \times 11 mm (Rohm et al., 2015). The sample sizes and geometries vary in a broad range as well: from pins, rings, rectangular blocks, to sledges, spheres, etc. Typically, in the studies, some information about the sample texture and/or macro geometry is given, but

information about the full surface geometry and topography is rarely provided. In computational studies, the sample macro geometry is considered, and for simplicity reasons roughness is ignored, while in experimental studies roughness is typically measured, and the macro geometry is only roughly described.

Roughness Analysis of Previous Studies

In some studies, only 2D profile data are used (Kietzig et al., 2010a; Sukhorukov and Marchenko, 2014; Scherge et al., 2018), but in most of the research 3D surface measurements or combination of both are considered (Bäurle et al., 2007; Rohm et al., 2015; Jansons et al., 2016; Spagni et al., 2016; Lungevics et al., 2018; Scherge et al., 2018; Ripamonti et al., 2020; Liefferink et al., 2021). The problem with 2D profile measurements is that 2D profiles often provide misleading information about the surface texture, especially when anisotropic surfaces are used. For example (Rohm et al., 2015),

TABLE 2 | Texture parameters used in the existing ice tribology studies.

2D parameters	
Ra	Arithmetical mean deviation of the assessed profile. Defines surface asperity average height Kietzig et al. (2009); Sukhorukov and Marchenko (2014); Jansons et al. (2016); Scherge et al. (2018)
Rdq	Root mean square (RMS) slope of profile. Defines the steepness of the asperities Spagni et al. (2016)
Rsm	Mean width of the roughness profile elements Sukhorukov and Marchenko (2014); Jansons et al. (2016); Lungevics et al. (2018). Defines how densely packed or stretched are roughness asperities
3D parameters	
Sa	Arithmetical mean deviation of the assessed surface Jansons et al. (2016), Jansons et al. (2018); Gross et al. (2018); Lungevics et al. (2018)
Sq	RMS roughness Lieferink et al. (2021)
Ssk	The skewness of the surface. Characterizes whether a sample has asperities on top of the flat surface or dimples/scratches below the flat surface Rohm et al. (2015); Spagni et al. (2016)
Sku	Kurtosis of the surface. The measure of the asymmetry of the probability distribution of a real-valued random variable about its mean Rohm et al. (2015); Spagni et al. (2016)
S10z	Ten-point height. Indicates surface height calculated using only 5 highest asperities and 5 lowest valleys. It gives better insight into texture asperity actual amplitude. Due to the involvement of the 5 highest asperities, this parameter might change rapidly if the sample starts to wear Rohm et al. (2015)
Sz	The maximum amplitude of the surface texture. Indicates height between surface highest asperity and deepest valley. As far as only the highest and lowest points are used, this parameter will start to change rapidly if sample starts to wear Scherge et al. (2013)
Sfd	Fractal dimension. Characterizes the complicity of the texture. If the parameter value aspires to number 2 surface is smooth and "simple", if the parameter aspires to number 3 surface is more complex thus has a larger theoretical contact surface Spagni et al. (2016)
Non-standardized parameters	
B	Attack angle. The angle between sample surface which is considered as flat, and snow (ice) roughness asperity slope Ducret et al. (2005)
KK	The criterion of contact. It is calculated as Rsm/Sa ratio. Indicates the steepness of asperities, i.e., larger ratio represents smoother surfaces with low and wide asperities, but a smaller ratio represents high and densely packed asperities Jansons et al. (2016)

TABLE 3 | Examples of ice friction research texture measurements.

Sample type and dimensions (mm)	Measured lengths/ areas (mm)	Equipment	Calculated parameters	Ref
Pin: Diameter = 3	0.4 × 2.8	Confocal microscopy	Ra, Rq, Rsk, Rku	Scherge et al. (2018)
Pin, dimensions: n/s	0.5 × 0.5	Stylus 3D profilometer	Ra, Rdq, Ssk, Sku, Sfd (D)	Spagni et al. (2016)
Ring type slider: Outer diameter = 25.4; inner diameter = 23.4; H = 1	Profiler: n/s AFM: n/s SEM: 0.2 × 0.2	Noncontact profilometer, AFM, SEM	Ra, Microscale bump diameter	Kietzig et al. (2009)
Steel ski: L = 487.5; W = 30; H = 30	1.7 × 1.8 3.3 × 3.3 8.2 × 7.8 11.3 × 11.3	Focus variation microscope	Sa, Sz, Ssk, Sku	Rohm et al. (2015)
Steel runner: L = 150; W = 8; H = 20; Runner transverse radius = 4	0.05 × 0.05	AFM	Sa, St	Scherge et al. (2013)
UHMWPE polymer samples: n/s	0.4 × 0.5	Interferometer, SEM	Attack angle	Ducret et al. (2005)
UHMWPE ski sole on aluminum body: L = 65; W = 40; H = n/s	0.5 × 1	Confocal microscopy	Width of the ridges	Böttcher et al. (2017)
Laser textured skis with attachable metallic base plate: L = 200; W = 20; H = 0.5	0.6 × 0.6	SEM, optical profilometer	Dimple diameter and depth	Ripamonti et al. (2020)
Silicon carbide spheres: R = 0.75; 6.00	0.2 × 0.2	Laser-scanning confocal microscopy	Sq	Lieverink et al. (2021)
Soda-lime glass spheres: R = 1.84				
Sapphire sphere: R = 1.59				
Model ice skate: R ≈ 22				
Steel block: L = 35; W = 18; H = 14	2 × 2 20 × 10 32 × 16	Interferometer, contact type profilometer	Ra, Rsm, Rz, Rpk, Sa, KK, Sdq, Ssk, Sku	Jansons et al. (2016), Jansons et al. (2021); Velkavrh et al. (2019)

Abbreviations: n/s, not stated; L, length; W, width; H, height; R, radius.

reported that for the same sample the value of the Ra parameter could change up to six times if a different measurement trajectory is used on anisotropic surfaces.

ISO 2D and 3D texture standards contain more than 30 different parameters from which only a few are ever used ice friction research (see **Table 2**).

Besides the described parameters in **Table 2**, the bearing ratio curve is used in ice tribology as well (Bäurle et al., 2007; Scherge et al., 2018; Jansons et al., 2021). It describes the cumulative probability density function of the surface profile height. It is useful for surface lubrication possibility analysis and can provide information about the sample contact with the opposing surface as well.

The final issue related to surface roughness measurements is texture filtration. In most studies, approaches described in ISO 4287 and ISO 2517 standards are used for the roughness measurements and post-processing. This leads to the filtration/neglect of the geometrical form and waviness from the measured surface profiles, thus changing the texture appearance and the calculated parameter values. For the calculation of the actual contact area, this approach might not be the most reliable since the filtered roughness profiles only provide a part of the information about the contact (Lou et al., 2013a; Lou et al., 2013b), see **Figure 2**.

Table 3 summarizes some examples of previously used samples, their surface measurement approach, and considered texture parameters.

In the existing literature on ice friction, very different topography measurement methods and approaches have been applied, and no standard methodology exists yet. The common trend is to analyze a small fraction of the full surface and neglect the waviness and geometrical form of the sliding surfaces. One might ask why a larger surface area should be measured at all. For example, let us imagine that a cylindrical pin with a flat tip is used on a tribometer test rig similarly as in studies (Spagni et al., 2016; Scherge et al., 2018). The pin tip is first polished and afterward post-processed to achieve the desired surface texture/roughness. After polishing and post-processing, the pin tip is most likely no longer flat but slightly cambered. In **Figure 2** a schematic representation of the influence of the macro geometry and waviness on the contact area between the pin tip and the ice is presented. In such a case, the macro geometry of the sample has a more significant effect on the contact area than the surface roughness. However, in the existing studies, typically, only a tiny fraction of the sample surface is measured (the waviness is filtered out) and used as a measure for the contact area, while the macro geometry of the contact surface is neglected. By neglecting the macro geometry and waviness, the real contact pressures between the sample and ice can be misjudged. To avoid this, a simple and practical method for obtaining information about the sample micro-, and macro-geometrical properties should be developed.

In the present research, the authors investigate how full surface measurements of sliding samples can benefit the understanding of experimental data in the field of ice tribology. For this, samples with anisotropic surfaces were prepared and analyzed by using non-contact and contact 3D surface measurement equipment. The measured topography values were compared, and a method for sample contact area measurements was proposed.

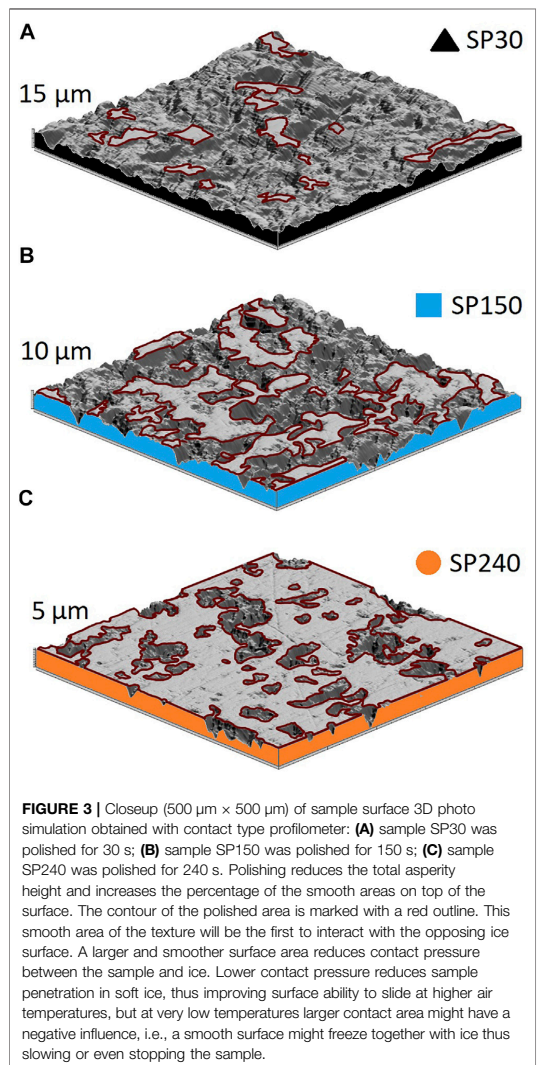


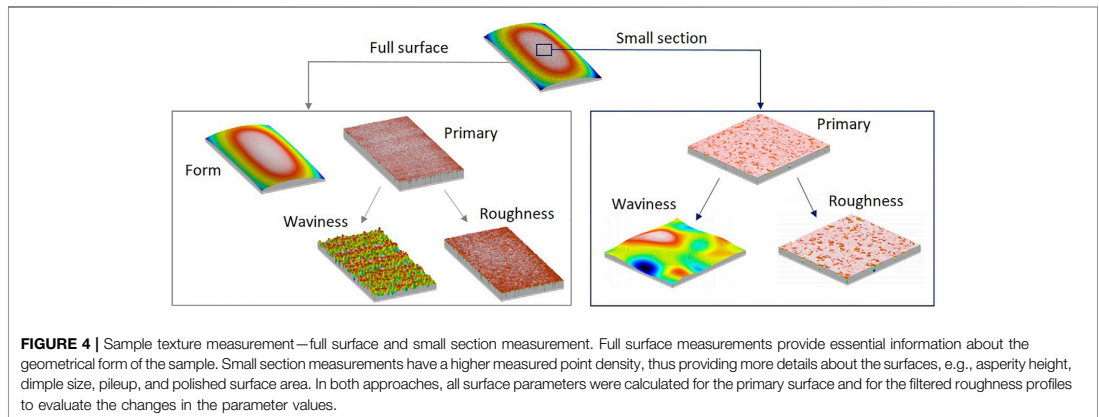
FIGURE 3 | Closeup (500 $\mu\text{m} \times 500 \mu\text{m}$) of sample surface 3D photo simulation obtained with contact type profilometer: **(A)** sample SP30 was polished for 30 s; **(B)** sample SP150 was polished for 150 s; **(C)** sample SP240 was polished for 240 s. Polishing reduces the total asperity height and increases the percentage of the smooth areas on top of the surface. The contour of the polished area is marked with a red outline. This smooth area of the texture will be the first to interact with the opposing ice surface. A larger and smoother surface area reduces contact pressure between the sample and ice. Lower contact pressure reduces sample penetration in soft ice, thus improving surface ability to slide at higher air temperatures, but at very low temperatures larger contact area might have a negative influence, i.e., a smooth surface might freeze together with ice thus slowing or even stopping the sample.

Furthermore, surface measurement data are compared to tribological results obtained on two different test rigs to verify whether more detailed topographical data can provide a better understanding of the ice friction process.

MATERIALS AND METHODS

Experimental Sample Preparation

All samples were manufactured from the Uddeholm Ramax HH steel, which is a chromium alloyed, corrosion-resistant steel supplied in a high pre-hardened condition. Samples were cut



as rectangular blocks with dimensions of 35 mm × 18 mm × 14 mm. All sides of the blocks were grounded simultaneously side by side in one batch to obtain as similar initial geometry as possible. Afterward, sample test surfaces were sandblasted to get isotropic texture. Sandblasting was followed by polishing to achieve three different surface roughness levels. Polishing times were set to 30, 150, and 240 s. **Figure 3** shows a small section (500 μm × 500 μm) of the sample surfaces. In **Figure 3**, polishing reduced the height of the asperities, which formed during sandblasting. The height of asperities was initially around 20 μm, after polishing for 30 s it reduced to 15 μm, after polishing for 150–10 μm, and after polishing for 240–5 μm. Furthermore, with the reduction of asperity height, polishing increased the smooth surface area on the sample surfaces. The smooth area defines the contact surface with ice because it is the first to interact with the ice. A larger smooth area reduces the contact pressure between the sample and ice. On the other hand, the texture valleys that remained unpolished can act as reservoirs for the LLL and thus provide improved lubrication of the ice surface, which also is the reason for the selection of this specific surface preparation procedure.

Sample Texture Measurements

Contact Profilometry

Form Talysurf Intra 50 profilometer with 112/2009 stylus (Taylor Hobson, United Kingdom) was used to measure 84% of the full sample surface, covering 32 mm × 16.5 mm area. This measurement includes information about sample form, waviness, and roughness. The profilometer was set to measure 600 profiles parallel to the shorter sample side, resulting in 10,000 measuring points per profile. In total, 6 million measuring points were taken on the surface, which results in 11363 points/mm². Due to low point density, this can be considered a low resolution (LR) measurement. Afterward, 2 mm × 2 mm area was measured in the center of the same sample, using the same number of parallel profiles and points per profile, resulting in 1.5 million points/mm². This is considered a high-resolution (HR) measurement. The measurement of the 2 mm × 2 mm area

provided a 136-times higher measured point density compared to the 32 mm × 16.5 mm area, thus providing smaller details about the sample surfaces. All noise filters were neglected for the measurements to avoid any texture measurement manipulations. An example of full surface and small section measurement is shown in **Figure 4**.

Non-contact Profilometry

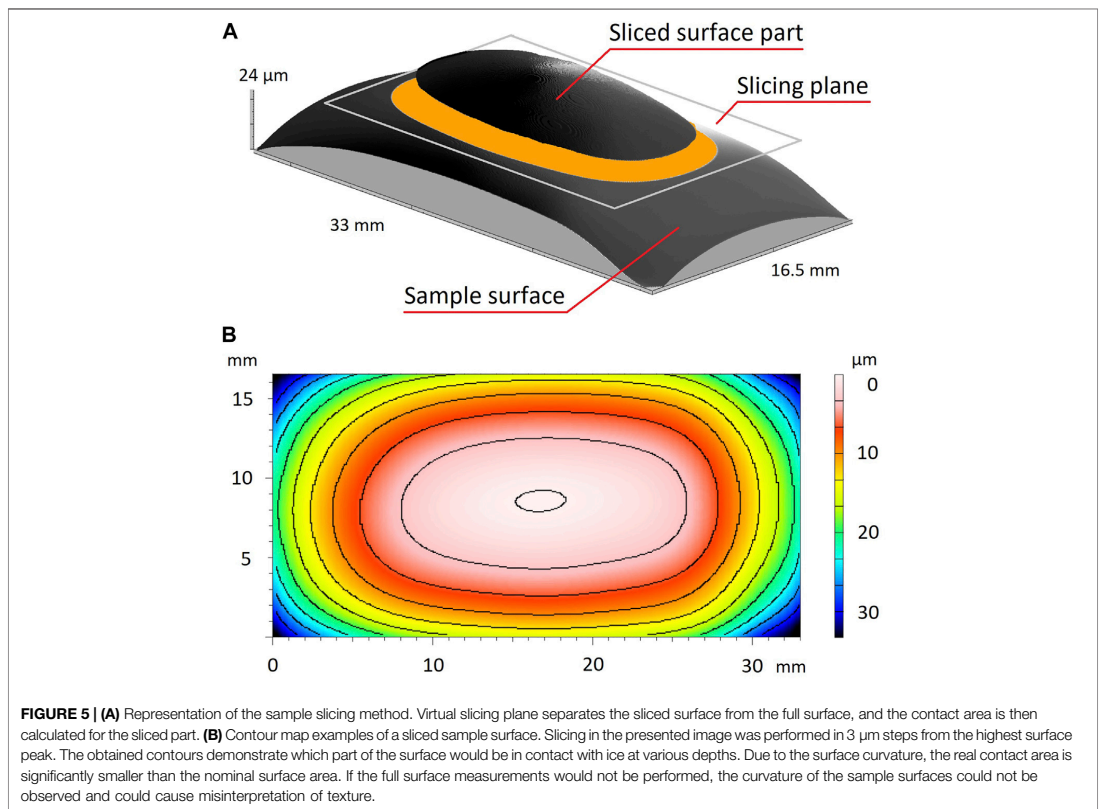
To compare contact and non-contact profilometry data, surface topography measurements were performed using a laser confocal microscope (VK-X250/260, Keyence International NV/SA, Belgium). Measurements were performed in the center of the sample surfaces, identically as in contact type small section measurements. The laser confocal microscope works on the principle of combined laser light and white light microscopy using a violet semiconductor laser with a 408 nm wavelength. It contains a 16-bit PMT (photomultiplier tube) color CCD (charge-coupled device) image sensor, the recording resolution is 3,072 × 2,304 pixels, i.e., there are more than 3 million measuring points in each scanning plane. Due to the high measurement point density, these measurements are also considered as high resolution (HR) measurements.

Post-Processing of Topography Data

Contact type profilometry measurement post-processing was performed in *TalyMap Expert* software. The obtained surface texture data were analyzed in three ways:

- Only roughness was considered for full surface and small section measurements.
- The primary surface (roughness and waviness) was considered for full surface and small section measurements.
- All surface levels (geometrical form, waviness, and roughness) were considered. Only full surface measurement was used without any applied filters.

During the first approach, geometrical form and waviness were filtered out according to ISO 2517 requirements for surface



roughness characterization. This included the use of Gaussian filter, cut-off, and low pass filter according to Taylor Hobson Form Talysurf Intra 50 user manual and ISO 2517 guidelines. During the second approach, only the geometrical form was filtered out, while waviness was left unfiltered. In the third approach, no information was filtered out, i.e., the sample geometrical form, waviness, and roughness were left unmodified after the measurement.

For the evaluation of the influence of contact area between the sample and ice, a virtual sample slicing method was applied. Here, the highest peak on the surface was used as a reference point from which the sample surface was sliced with a virtual slicing plane at various depths between 1 and 12 μm below the highest peak. **Figure 5A** shows the principle of sample surface slicing, and in **Figure 5B**, contours of sliced surface areas are presented for different slicing depths. At a certain slicing depth, the whole curvature of the surface would be virtually sliced off, resulting in the nominal contact area of the sample.

The samples used in the present study have a noticeably curved shape, thus the contact area with ice will depend on how deep the curved surface will penetrate the ice during sliding. **Figure 6** shows the surfaces of test samples sliced at 4 μm depth

under the highest surface peak. On the left side, 3D representations of the sliced surfaces are shown, and for comparison, on the right-side top view of the contact area, images at the same slicing-depth are shown.

Contact areas of the sliced surfaces were calculated using *TalyMap Expert* software built-in functions and were used for calculations of the contact pressures in tribological tests. The measurement topography parameters were then compared with the results from tribological tests by evaluating the correlation between the surface parameters and the tribological values (coefficient of friction and achieved sliding velocity of the samples), and by calculating the proportion of variance between the mentioned parameters.

Tribological Tests

Two different tribological test setups were used for the testing of the same samples. A schematic representation of both test setups is shown in **Figure 7**: inclined ice surface where the sliding velocity of the steel sample blocks were determined (**Figure 7A**); oscillating tribometer where the coefficient of friction was assessed for the same samples (**Figure 7B**). In the first test setup, no additional normal force was applied to the steel

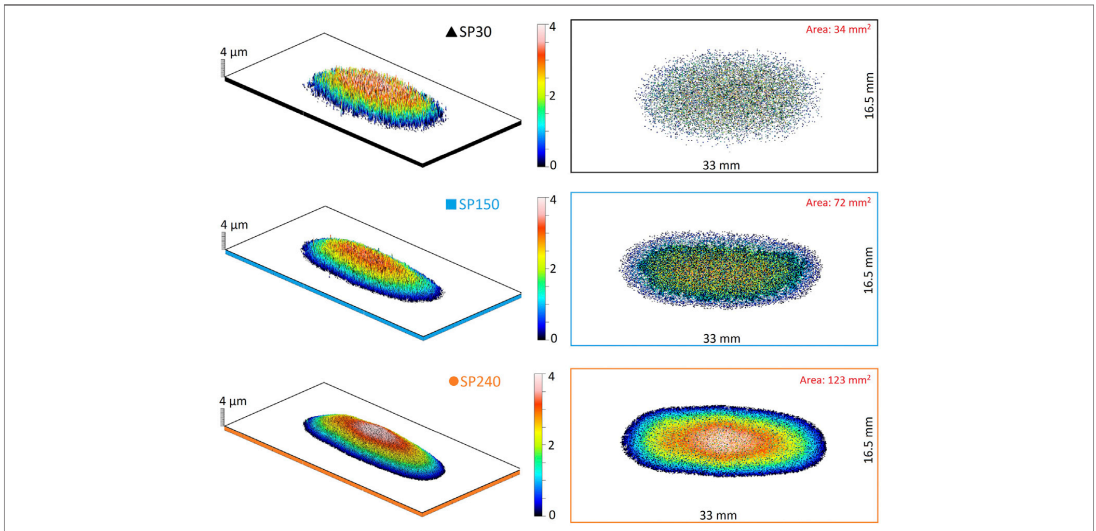


FIGURE 6 | Surfaces of test samples sliced at 4 μm depth under the highest surface peak. On the left side, 3D representations of the sliced surfaces are shown, and for comparison, on the right-side top view of contact area, images at the same slicing-depth are shown. Sample with the highest surface roughness (SP30) has the smallest contact area, which consists of fewer asperities than for other samples. Under loading conditions, fewer asperities can more easily penetrate the ice surface. Generally, the contact area of samples increased with polishing time since during polishing surfaces become smoother, and at the same time, the height of asperities is reduced.

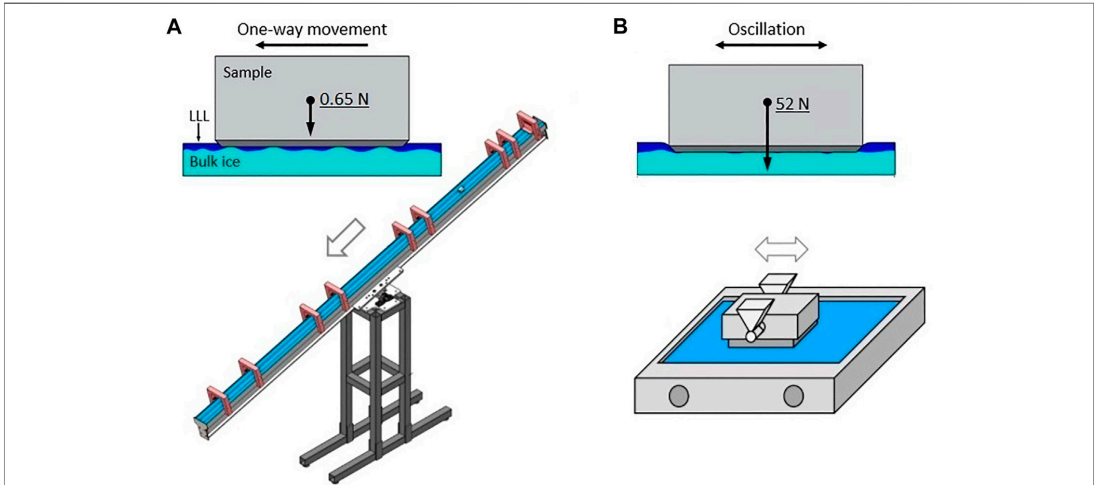


FIGURE 7 | A schematic representation of the test setups used: **(A)** inclined plane tribometer that ensures sample sliding in one direction down the plane without any additional load on the samples. The velocity of freely sliding samples was measured using eight optical sensors. Higher measured sample velocity indicates better sliding ability, **(B)** oscillating tribometer. The sample oscillates on the ice surface with an additional applied normal load of 52 N. Since the sample oscillates with high frequency on the same ice surface, the ice surface is slightly melted, allowing the sample to penetrate deeper into the ice surface. Additionally, the melted ice may work as a lubricant. More information about the test setups can be found elsewhere (Velkavrh et al., 2019).

samples (weighing 68 g); while in the second test setup an additional normal force of 52 N was applied to the steel samples. The test setups are described in more detail elsewhere (Velkavrh et al., 2019).

Velocity Measurements on the Inclined Plane Tribometer

For velocity measurements, a 3 m long inclined plane tribometer was used (Figure 7A). The plane was tilted at $16 \pm 0.5^\circ$. The start gate ensures that the experimental samples start the movement from the same position and in a steady state. The sliding velocity was measured using eight optical sensors at defined positions resulting in four velocities sections: V_1 , V_2 , V_3 , and V_4 . Additionally, average sliding velocity V_{avg} was calculated for the sliding distance between the first and the last optical sensor. Sliding velocity was used to describe the sliding ability: the faster the sample accelerates, the better its sliding performance. No additional weight was placed on the samples during the tests; thus, the contact pressure between the sample and the ice was relatively low, ca. 0.001 N/mm^2 of nominal contact pressure, i.e., assuming that the sample surface is perfectly flat and in full contact with ice.

The tribometer was located in a climate simulation chamber, which enables ambient temperature regulation in the range of $+30^\circ\text{C}$ down to -20°C and is equipped with an ice plane cooling system, allowing precise regulation of the ice temperature. Humidity and air temperature in the climate simulation chamber were measured using a P330 Temp thermometer (Dostmann electronic, Germany), while the ice temperature was measured with thermocouple TP-122-100-MT-K (Czaki, Poland) plugged into infrared thermometer Proscan 520 (Dostmann, Germany). Temperature and relative humidity measurements were documented after every 10th sliding test, and the final value was calculated as the average of all measurements of a single experimental session.

Before the sliding tests, the ice surface was leveled flat, and a small groove was embedded in ice in the movement direction to keep the samples in a straight trajectory during sliding. During the tests, the samples were slid down the ice track in a random order to prevent the eventual influence of fluctuation of ambient conditions on the experimental results of specific samples. The average sliding velocity for each sample was calculated from 40 individual sliding velocity measurements. During data post-processing five fastest and five slowest measurements were excluded from the calculation.

Tests on an Oscillating Tribometer

In oscillating tribometer tests, an ice rink with dimensions of 20 mm width, 80 mm length, and 5 mm depth was used. Before each test series, a new ice surface was prepared. For ice formation, 18 ml of distilled water was used to which 0.5 ml of tap water was added to accelerate the ice crystallization. In all tests, the ice temperature at the bottom of the ice bath was -10°C (at the surface, it was estimated to around -8°C under the applied ambient conditions).

Before tribology tests specially developed aluminum leveling tool with a contact area of $45 \text{ mm} \times 28 \text{ mm}$ was inserted in the

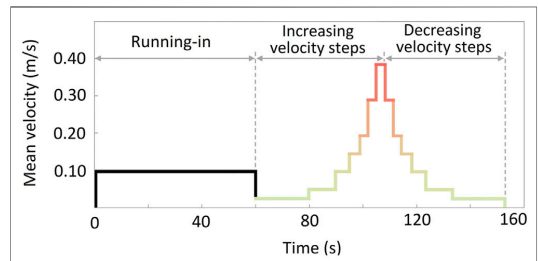


FIGURE 8 | Change of sliding velocities during each experiment performed on the oscillating tribometer. Tests were carried out at different velocities, first at increasing and afterward at decreasing velocity, to analyze the influence of both types of motion dynamics.

sample holder and rubbed against the ice surface to create an ice surface as flat and smooth as possible. The smoothing was performed at a normal force of 692 N and an average sliding velocity of 0.08 m/s until the height difference between the left and right sides of the ice surface was lower than $100 \mu\text{m}$. The flatness of the ice surface was measured with a built-in tribometer dial gauge. After leveling, the leveling tool was replaced by an experimental sample, and the tribological test was conducted.

Experiments were carried out at a constant normal load of 52 N and a stroke of 24 mm. The contact pressure between the sample and the ice was ca. 0.084 N/mm^2 if it assumed that the sample surface is perfectly flat and in full contact with ice. For each test, a run-in period of 60 s at 0.10 m/s was first performed to adjust the sample temperature to the ice temperature. Afterwards, experiments were carried out at 7 velocity levels (average sliding velocities of 0.02, 0.05, 0.10, 0.14, 0.19, 0.29, and 0.38 m/s). During each experiment, friction measurements at all velocity levels were performed twice—once at increasing and once at decreasing velocity. The change of sliding velocities during each experiment performed on the oscillating tribometer is shown in Figure 8.

RESULTS

Surface Texture Measurements

In Table 4 values measured using contact and non-contact profilometer and post-processed according to the procedure described in section of post-processing of topography data. are listed. In Table 4, other roughness parameters are not included because they showed similar relative trends as the parameter Sa.

The comparison of the Sa parameter shows that a higher measured point density on the surface (HR measurements) results in a higher Sa value. The highest Sa values were obtained with the non-contact laser confocal microscope, followed by small surface measurements with the contact type profilometer, while the lowest Sa values were obtained in large area roughness measurements with the contact type profilometer. Higher Sa values obtained with the non-contact method can be explained by its ability to measure deeper and narrower surface

TABLE 4 | Surface roughness parameter Sa [μm] measured using contact and non-contact profilometers and processed according to the procedure described in Section of non-contact profilometry.

	Non-contact measurement		Contact measurement			
	(HR)		(HR)		(LR)	
	Roughness		Primary	Roughness	Primary	Roughness
SP30	3.15	2.99	2.91	1.70	1.13	
SP150	2.44	2.02	1.97	1.10	0.75	
SP240	0.98	0.81	0.79	0.45	0.31	

Abbreviations “HR” and “LR” stand for “High resolution” and “Low resolution” measurements, respectively.

valleys than the contact type profilometer. This is because the 2 μm tip radius of the contact profilometer cannot reach small dimples or bores. It should also be pointed out that the cone-shaped profilometer tip tends to describe narrow and/or sharp edges as rounded ones.

Also, it was noticed that the unfiltered primary surface has a higher Sa value than the filtered roughness profile, which is because waviness enhances the overall amplitude, thus increasing the Sa value. Typically, in ice tribology studies, waviness is not considered, but it might play an important role. Therefore, for analyses of sample interactions with ice, the authors propose the use of the unfiltered primary surface instead of filtered roughness profiles.

The observations about the influence of point density and waviness on the measured Sa values are logical and do not provide any groundbreaking discoveries, but do provide a useful guideline: the question of which method for measurement and calculation of roughness parameters is the best and/or more accurate is very complex and difficult to answer, however, the roughness parameter values of different surfaces can be effectively compared as long as they are measured in the same way and by using the same device. This conclusion is supported by the data in **Table 4**: regardless of the profilometer used or the measuring area size, the relative proportion between the roughness parameters was very similar—only the absolute values of the roughness parameters are different.

Contact Area and Contact Pressure

Virtual slicing of the sample surfaces was performed in 1 μm steps from the highest surface peak to 12 μm below it, as explained in “Non-contact Profilometry” section. The contact area values for sliced surfaces of all samples are shown in **Figure 9A**.

In **Figure 9**, the contact area increases with increasing slicing depth for all samples. The smallest contact area was observed for sample SP30, which after sandblasting was polished for the shortest time and has the highest roughness, while the largest contact area was observed for sample SP240, which after sandblasting was polished for the longest time and had the lowest roughness. At the virtual slicing depth of 12 μm , the size of contact surfaces of samples SP240 and SP150 become similar. By increasing the slicing depth further, samples reach the nominal contact area, i.e., the actual curvature of the sample is fully sliced off, and the ideal flat surface remains, which is same for all samples.

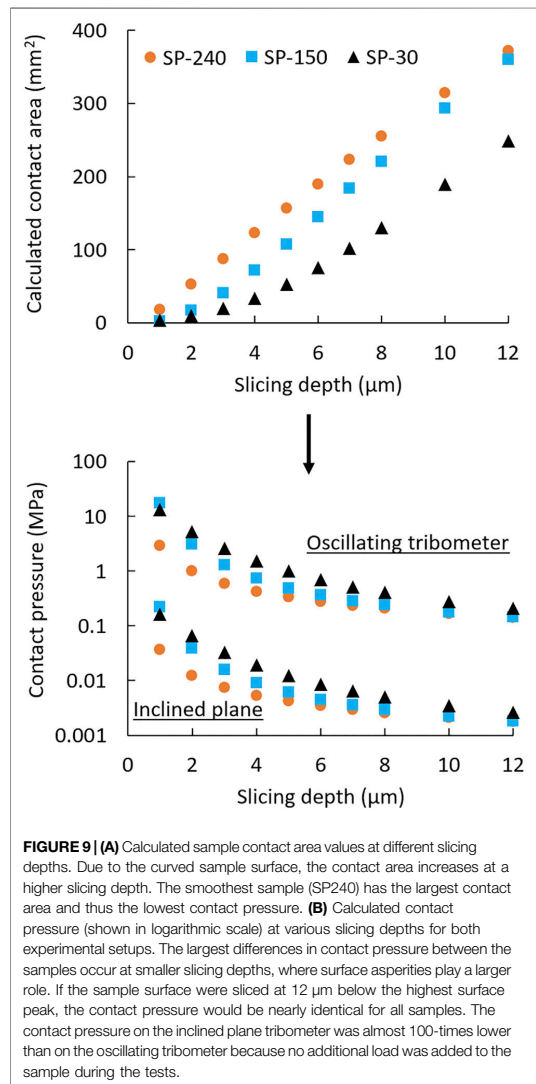


FIGURE 9 | (A) Calculated sample contact area values at different slicing depths. Due to the curved sample surface, the contact area increases at a higher slicing depth. The smoothest sample (SP240) has the largest contact area and thus the lowest contact pressure. (B) Calculated contact pressure (shown in logarithmic scale) at various slicing depths for both experimental setups. The largest differences in contact pressure between the samples occur at smaller slicing depths, where surface asperities play a larger role. If the sample surface were sliced at 12 μm below the highest surface peak, the contact pressure would be nearly identical for all samples. The contact pressure on the inclined plane tribometer was almost 100-times lower than on the oscillating tribometer because no additional load was added to the sample during the tests.

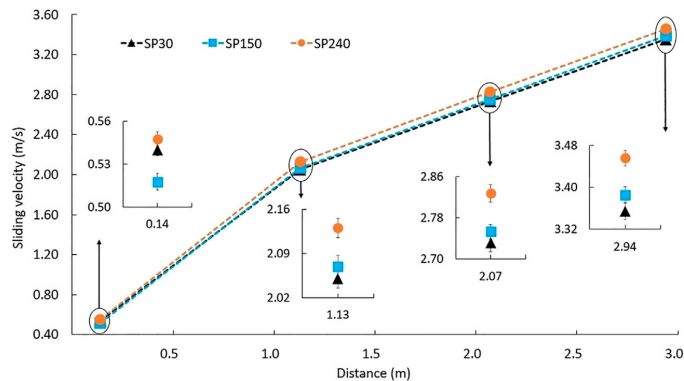


FIGURE 10 | Sliding velocities measured on the inclined plane tribometer. Sample velocity increases due to accelerated movement down the inclined plane. In the magnified closeups, the smoothest sample SP240 is faster than samples SP30 and SP150, which show similar velocities. Slightly different behavior between the latter is observed only in the first measurement point, where the roughest sample SP30 is faster than the intermediately rough sample SP150.

Considering the calculated contact areas at the respective slicing depths, in **Figure 9B**, the contact pressure for each sample was calculated for both experimental setups—oscillating tribometer and inclined plane tribometer. The contact pressure values of the oscillating tribometer experiments are noticeably higher due to the additional applied force (52 N) in these tests. The relationships in both cases are practically identical, only the absolute values change. As the slicing depth increases, the contact pressure decreases for all samples, since if the sample is sliced at a lower depth (0–3 μm), only a portion of the surface asperities is in contact resulting in higher contact pressure, but as the sample is sliced at higher slicing depths, the contact area increases, thus decreasing the contact pressure. The highest contact pressure was obtained for sample SP30 (the roughest surface), and the lowest for sample SP240 (the smoothest surface).

Inclined Plane Tests

Inclined plane tests were conducted under the following conditions: ice temperature $-7 \pm 0.5^\circ$; air temperature $-4 \pm 0.5^\circ$ and relative humidity $60 \pm 3\%$. Sliding velocities were obtained at 4 different positions, and the final values shown in **Figure 10** were calculated from 40 individual measurements for each sample. The magnifications for each measurement section were made to better highlight differences between samples. In all cases, Y-axis represents the sliding velocity while X-axis represents the distance from the movement starting position.

In **Figure 10**, sample SP240 (the lowest contact pressure) reached the highest sliding velocity in all four measurement positions. On the other hand, sample SP30 (the highest contact pressure) is the slowest one.

In measuring position V_1 , the sample behavior appears to be random, which is most likely because the samples start their movement from a steady state where an eventual stick-slip movement may randomly affect the samples' ability to start sliding. In the steady state, the rougher sample has the advantage of a smaller contact area on which adhesive forces

can work, possibly resulting in lower static friction. However, under higher applied loads this effect might not be observed because the asperities of the rough surface would penetrate the ice resulting in higher deformative friction, ploughing and/or mechanically interlocking with the ice surface.

As the samples move down the inclined plane, their velocity increases. When the samples have gained some inertia, i.e., in measuring positions V_2 , V_3 , and V_4 , the difference between the velocities of samples SP30 and SP150 decreased to approximately 1%, while the difference between the velocities of the slowest and the fastest sample, SP30 and SP240, respectively, were around 3–4%. Such difference may not seem much, but for winter sport athletes it could provide a major benefit.

Oscillating Tribometer Tests

Oscillating tribometer tests were conducted under the following conditions: ice temperature $-8 \pm 0.5^\circ$; air temperature $7 \pm 1^\circ$ and relative humidity $55 \pm 2\%$. The measurements were conducted at various velocities as shown in **Figure 8**. In **Figure 11**, the coefficient of friction values measured on the oscillating tribometer are presented.

In **Figure 11**, the lowest coefficient of friction (0.015) was observed for sample SP240. A slightly higher coefficient of friction was obtained for sample SP150 (0.025). For both samples, the effect of velocity on the coefficient of friction in the observed range was negligible. The roughest sample SP30 showed the highest coefficient of friction values, which varied in the range from 0.04 to 0.08 depending on velocity. As velocity increased, the coefficient of friction reduced by a factor of 2, and at the same time, the coefficient of friction values during the decreasing velocity steps was slightly lower compared to the increasing velocity steps. This could be due to the LLL which formed during the test as the sample was oscillating over the same ice surface. It is presumed that the thickness of LLL increased during the test, thus reducing the coefficient of friction in the second part of the test, i.e., during the decreasing velocity steps.

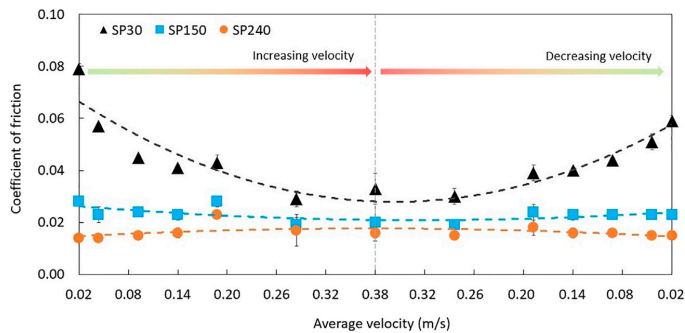


FIGURE 11 | Coefficients of friction measured on the oscillating tribometer. The obtained friction curves show that samples with higher contact area (smoother ones) yield lower coefficient of friction values. At the same time, the influence of velocity on the coefficient of friction is noticeably higher for the roughest sample SP30 than for the smoother samples SP150 and SP240.

The obtained coefficient of friction values and the general sample behavior correlate well with the data reported by (Spagni et al., 2016). In the mentioned study, sandblasted surfaces were used but having different magnitudes of asperities, and the asperity tips were not polished as in the present study. In the mentioned study, a pin-on-disc type tribometer was used, and the samples were prepared as pins. Similarities in the results from different test setups indicate that the observed trends are representative and can be used as a reference for future studies with similar surface textures.

Texture Parameter Correlation With Tribology Experiments

In **Supplementary Figures 1 and 2**, correlation analysis for the contact pressures and roughness parameters of specific samples and their velocities and coefficients of friction from tribometer tests is presented. Values in colored fields show the calculated proportion of variance (RSQ) between the measured roughness parameters and the results from tribological tests. The closer the value gets to number 1, the higher the correlation between the compared parameters is. For a graphic representation, RSQ values are colored in a color scale, reaching from red (value 0) to yellow (value 0.5) and green (value 1). Red shades represent areas with low correlation, while green shades represent areas with high correlation.

In **Supplementary Figure 1**, contact pressure/surface roughness show and good correlation with sliding velocity for all measuring positions except for the first one. This is because on the inclined plane tribometer the initial velocity V_1 is highly influenced by static friction, as explained in section of inclined plane tests.

The highest correlation between the contact pressure and the sliding velocity was observed at a slicing depth of 1–3 μm . This is because, at low contact pressure applied in the inclined plane tribometer tests (only sample's weight), the samples did not penetrate deeply into the ice surface.

All analyzed surface texture parameters show a very high correlation (above 0.8) with the sliding velocity and indicate they can be used for the evaluation of sliding ability in ice tribology studies. The high correlation between the surface texture parameters and the sliding velocity may also be due to the low contact pressure applied in these tests. Since only the tip of the curved sample surface is in contact with the ice surface, texture roughness on the tip has a stronger influence on its sliding ability than at high contact pressures, where a higher proportion of the sample surface is in contact with ice and, therefore, the waviness and the geometrical form of the sample additionally influence its sliding ability.

For the oscillating tribometer setup where higher contact pressure was applied, the correlation results (**Supplementary Figure 2**) are quite different from the inclined plane tribometer (**Supplementary Figure 1**).

In **Supplementary Figure 2** the highest correlation between the contact pressure and coefficient of friction is observed at a slicing depth of 4–6 μm . This is due to the higher contact pressure and oscillating movement on the same ice surface, where the sample surface asperities penetrate deeper into the ice surface than in the inclined plane tests. Consequently, the waviness and the geometrical form (curvature) of the sample play a more significant role. Therefore, the correlation between the surface roughness parameters and the coefficient of friction values is lower than for sliding velocity; however, the S_a parameter of the unfiltered primary surface shows a better correlation with the coefficient of friction values than the S_a parameter of the filtered roughness profile—due to the included waviness of the sample. It is also interesting to note that for lower velocities better correlation between the contact pressure and coefficient of friction was observed at higher slicing depths (6–8 μm), while for higher velocities, a better correlation was observed at lower slicing depths (4–6 μm)—possibly due to the hydrodynamic effects at the higher velocities which separate the sample from the ice surface more efficiently at higher velocities than at the lower ones.

DISCUSSION

The present study shows that currently, researchers in the field of ice tribology measure surfaces in very different ways: by using different surface roughness parameters to describe the surfaces and post-processing the data differently. All these methods are efficient and provide a lot of useful information; however, for a better understanding of interactions between solid surfaces and ice, a unified surface measurement methodology is recommended so that in terms of surface characterization, all researchers in the field would “speak the same language.”

This specific study was conducted to highlight the importance of understanding the full surface geometry instead of focusing only on the micro- or nanoscale of the surface texture. The proposed surface analysis method is not in its final stage yet, however, it will be further developed and validated using different sample textures in future research. Since for theoretical calculations of coefficient of friction, information about the contact area is required as well, possible collaborations in this regard will be established to see if the proposed methodology can enable a more accurate match between experiments and theory. In this sense, applying data science and data mining methodologies (Bitrus et al., 2021) will be considered as well.

CONCLUSION

The present research brings out several conclusions:

- A. The current surface measurement trends in ice tribology are focused on small surface area investigation, while the information about the sample macro geometry is rarely considered. This indicates that researchers may lack crucial information that could help them understand the sample behavior in contact with ice.
- B. The proposed surface measurement and contact area analysis approach using the virtual surface slicing technique provided important information about the sample macro geometry that helped understanding sample behavior under different measuring conditions applied in different experimental setups. The surface measurement approaches found in the available literature typically neglect the information about the sample form and waviness, providing only the roughness component of the surface. Such deficient information about the sample surfaces prevents from wholesome analyses and comparison of results from different studies. If the overall (primary) information about the test surface is presented, understanding of the sample behavior under different measuring conditions can be improved. Afterwards, additional filtering can be applied, and the obtained results analyzed in the context of roughness or waviness. The proposed surface analysis approach can be helpful not only

for ice tribology but for other tribology studies, where two surfaces are in contact as well.

- C. A similar influence of surface texture and/or roughness on the coefficient of friction and sliding velocity (decrease with decreased surface roughness) was observed in different experimental setups (inclined plane tribometer and oscillating tribometer). The observed results correlate with observations reported by other scientists for similar experimental conditions.

DATA AVAILABILITY STATEMENT

The raw data supporting the conclusions of this article will be made available by the authors, without undue reservation.

AUTHOR CONTRIBUTIONS

Conceptualization, JL, EJ, and IV; investigation, JL, EJ, and IV; methodology, analysis and validation, JL, EJ, IV, IB, JV, TW; writing—original draft preparation, JL, EJ, and IV; writing—review and editing, IV, JV, TW, IB.

FUNDING

Parts of this work were funded by the Austrian COMET Program (Project InTribology, No. 872176) and carried out at the “Excellence Centre of Tribology” (AC2T research GmbH) in cooperation with V-Research GmbH and Riga Technical University. Financial support of Austrian Cooperative Research (ACR) is gratefully acknowledged. Parts of this work were also funded by the ERDF project “The quest for disclosing how surface characteristics affect slideability” (No. 1.1.1.1/16/A/129), which is being implemented in Riga Technical University. This research was partly supported by the Doctoral Grant Program of Riga Technical University. Riga Technical University Research Support Fund has supported the costs for open-access publishing of this article.

SUPPLEMENTARY MATERIAL

The Supplementary Material for this article can be found online at: <https://www.frontiersin.org/articles/10.3389/fmech.2021.691485/full#supplementary-material>

SUPPLEMENTARY FIGURE 1 | The proportion of variance (RSQ) between surface roughness/contact pressure and the measured sliding velocities on the inclined plane tribometer.

SUPPLEMENTARY FIGURE 2 | The proportion of variance (RSQ) between surface roughness/contact pressure and the measured coefficients of friction (COF) on the oscillating tribometer.

REFERENCES

- Bäurle, L., Kaempfer, T. U., Szabó, D., and Spencer, N. D. (2007). Sliding Friction of Polyethylene on Snow and Ice: Contact Area and Modeling. *Cold Regions Sci. Techn.* 47, 276–289. doi:10.1016/j.coldregions.2006.10.005
- Bitrus, S., Velkavrh, I., and Rigger, E. (2021). “Applying an Adapted Data Mining Methodology (DMME) to a Tribological Optimisation Problem,” in *In Data Science – Analytics And Applications*. Editors P. Haber, T. Lampoltshammer, M. Mayr, and K. Plankensteiner (Wiesbaden: Springer Vieweg), 38–43. doi:10.1007/978-3-658-32182-6_7
- Böttcher, R., Seidelmann, M., and Scherge, M. (2017). Sliding of UHMWPE on Ice: Experiment vs. Modeling. *Cold Regions Sci. Techn.* 141, 171–180. doi:10.1016/j.coldregions.2017.06.010
- Ducret, S., Zahouani, H., Midol, A., Lanteri, P., and Mathia, T. G. (2005). Friction and Abrasive Wear of UHMWPE Sliding on Ice. *Wear* 258, 26–31. doi:10.1016/j.wear.2004.09.026
- Gross, K. A., Lungevics, J., Zavicki, J., and Pluduma, L. (2018). A Comparison of Quality Control Methods for Scratch Detection on Polished Metal Surfaces. *Measurement* 117, 397–402. doi:10.1016/j.measurement.2017.12.022
- Hasler, M., Schindelwig, K., Mayr, B., Knoflach, C., Rohm, S., van Putten, J., et al. (2016). A Novel Ski-Snow Tribometer and its Precision. *Tribol Lett.* 63, 12552. doi:10.1007/s11249-016-0719-2
- Jansons, E., Lungevics, J., and Gross, K. A. (2016). “Surface Roughness Measure that Best Correlates to Ease of Sliding,” in *Proceedings of 15th International Scientific Conference Engineering for Rural Development* (Jegava: Latvia University of Agriculture), 687–695. Available at: <http://www.tf.llu.lv/conference/proceedings2016/Papers/N127.pdf>
- Jansons, E., Lungevičs, J., Jerāne, I., and Gross, K. A. (2021). A Smaller Bearing Ratio, as a Surface Texture Measure, Promotes Faster Sliding on Ice. *J. Tribology* 143 (8), 111801. doi:10.1115/1.4049704
- Jansons, E., Lungevics, J., Stiprais, K., Pluduma, L., and Gross, K. A. (2018). Measurement of Sliding Velocity on Ice, as a Function of Temperature, Runner Load and Roughness, in a Skeleton Push-Start Facility. *Cold Regions Sci. Techn.* 151, 260–266. doi:10.1016/j.coldregions.2018.03.015
- Kietzig, A.-M., Hatzikiriakos, S. G., and Englezos, P. (2010a). Ice Friction: the Effect of thermal Conductivity. *J. Glaciol.* 56, 473–479. doi:10.3189/002214310792447752
- Kietzig, A.-M., Hatzikiriakos, S. G., and Englezos, P. (2009). Ice Friction: The Effects of Surface Roughness, Structure, and Hydrophobicity. *J. Appl. Phys.* 106, 024303. doi:10.1063/1.3173346
- Kietzig, A.-M., Hatzikiriakos, S. G., and Englezos, P. (2010b). Physics of Ice Friction. *J. Appl. Phys.* 107, 081101. doi:10.1063/1.3340792
- Kietzig, A.-M., Mirvakili, M. N., Kamal, S., Englezos, P., and Hatzikiriakos, S. G. (2011). Nanopatterned Metallic Surfaces: Their Wettability and Impact on Ice Friction. *J. Adhes. Sci. Techn.* 25, 1293–1303. doi:10.1163/016942411X55587210.1163/016942410x549988
- Liefferink, R. W., Hsia, F.-C., Weber, B., and Bonn, D. (2021). Friction on Ice: How Temperature, Pressure, and Speed Control the Slipperiness of Ice. *Phys. Rev. X* 11, 011025. doi:10.1103/PhysRevX.11.011025
- Ling, E. J. Y., Uong, V., Renault-Crispo, J.-S., Kietzig, A.-M., and Servio, P. (2016). Reducing Ice Adhesion on Nonsmooth Metallic Surfaces: Wettability and Topography Effects. *ACS Appl. Mater. Inter.* 8, 8789–8800. doi:10.1021/acsami.6b00187
- Lou, S., Jiang, X., and Scott, P. J. (2013a). Correlating Motif Analysis and Morphological Filters for Surface Texture Analysis. *Measurement* 46, 993–1001. doi:10.1016/j.measurement.2012.10.001
- Lou, S., Zeng, W.-H., Jiang, X.-Q., and Scott, P. J. (2013b). Robust Filtration Techniques in Geometrical Metrology and Their Comparison. *Int. J. Autom. Comput.* 10, 1–8. doi:10.1007/s11633-013-0690-4
- Lungevics, J., Jansons, E., and Gross, K. A. (2018). An Ice Track Equipped with Optical Sensors for Determining the Influence of Experimental Conditions on the Sliding Velocity. *Latvian J. Phys. Tech. Sci.* 55, 64–75. doi:10.2478/lpts-2018-0007
- Ripamonti, F., Furlan, V., Savio, A., Demir, A. G., Cheli, F., Ossi, P., et al. (2020). Dynamic Behaviour of Miniature Laser Textured Skis. *Surf. Eng.* 36, 1250–1260. doi:10.1080/02670844.2018.1512730
- Rohm, S., Hasler, M., Knoflach, C., van Putten, J., Unterberger, S. H., Schindelwig, K., et al. (2015). Friction Between Steel and Snow in Dependence of the Steel Roughness. *Tribol Lett.* 59, 12552. doi:10.1007/s11249-015-0554-x
- Scherge, M., Böttcher, R., Richter, M., and Gurgel, U. (2013). High-Speed Ice Friction Experiments under Lab Conditions: On the Influence of Speed and Normal Force. *ISRN Tribology* 2013, 1–6. doi:10.5402/2013/703202
- Scherge, M., Böttcher, R., Spagni, A., and Marchetto, D. (2018). High-Speed Measurements of Steel-Ice Friction: Experiment vs. Calculation. *Lubricants* 6, 26. doi:10.3390/lubricants6010026
- Spagni, A., Berardo, A., Marchetto, D., Gualtieri, E., Pugno, N. M., and Valeri, S. (2016). Friction of Rough Surfaces on Ice: Experiments and Modeling. *Wear* 368–369, 258–266. doi:10.1016/j.wear.2016.10.001
- Sukhorukov, S., and Marchenko, A. (2014). Geometrical Stick-Slip between Ice and Steel. *Cold Regions Sci. Techn.* 100, 8–19. doi:10.1016/j.coldregions.2013.12.007
- Velkavrh, I., Lungevičs, J., Jansons, E., Klien, S., Voyer, J., and Ausserer, F. (2019). The Influence of Isotropic Surface Roughness of Steel Sliders on Ice Friction Under Different Testing Conditions. *Lubricants* 7, 106. doi:10.3390/lubricants7120106

Conflict of Interest: Authors IV, JV, and TW were employed by the company “VResearch GmbH”

The remaining authors declare that the research was conducted in the absence of any commercial or financial relationships that could be construed as a potential conflict of interest.

Copyright © 2021 Lungevics, Jansons, Boiko, Velkavrh, Voyer and Wright. This is an open-access article distributed under the terms of the Creative Commons Attribution License (CC BY). The use, distribution or reproduction in other forums is permitted, provided the original author(s) and the copyright owner(s) are credited and that the original publication in this journal is cited, in accordance with accepted academic practice. No use, distribution or reproduction is permitted which does not comply with these terms.

Information about sample surface																
Contact Pressure, [MPa]	Slicing depth, [µm]	SP30	SP150	SP240												
	1	0.164	0.219	0.037	■											
	2	0.066	0.039	0.012		■										
	3	0.033	0.016	0.007			■									
	4	0.019	0.009	0.005				■								
	5	0.012	0.006	0.004					■							
	6	0.009	0.005	0.003						■						
	7	0.006	0.004	0.003							■					
	8	0.005	0.003	0.003								■				
	10	0.003	0.002	0.002									■			
	12	0.003	0.002	0.002										■		
	Texture parameters	Sa (R), µm	3.2	2.4	1.0											
Sa (P), µm		1.7	1.1	0.4												
Ssk (P)		-0.6	-1.2	-2.9												
Sku (P)		3.0	3.8	12.0												
Sds (P), pks/mm2		4272	5622	10881												
Inclined plane tests																
Measurement position	Velocity, m/s	Contact Pressure VS velocity, [RSQ]										Texture VS velocity, [RSQ]				
V1	0.540 0.518 0.548	0.77	0.06	0.00	0.00	0.00	0.01	0.01	0.02	0.03	0.05	0.18	0.07	0.23	0.41	0.30
V2	2.050 2.069 2.130	0.75	0.91	0.79	0.73	0.69	0.66	0.64	0.62	0.57	0.53	0.99	0.93	1.00	0.98	1.00
V3	2.731 2.754 2.828	0.75	0.91	0.78	0.72	0.68	0.66	0.63	0.61	0.56	0.52	0.99	0.93	1.00	0.98	1.00
V4	3.354 3.386 3.456	0.67	0.95	0.85	0.79	0.76	0.74	0.71	0.69	0.65	0.61	1.00	0.96	1.00	0.95	0.99
Vavg	1.895 1.902 1.967	0.86	0.82	0.66	0.59	0.55	0.52	0.49	0.48	0.43	0.39	0.94	0.84	0.97	1.00	0.99

Information about sample surface																		
Contact Pressure, [MPa]	Slicing depth, [µm]	SP30	SP150	SP240														
	1	13.18	17.57	2.93	■													
	2	5.27	3.10	0.99		■												
	3	2.64	1.29	0.60			■											
	4	1.55	0.73	0.43				■										
	5	0.99	0.49	0.34					■									
	6	0.69	0.36	0.28						■								
	7	0.52	0.29	0.24							■							
	8	0.41	0.24	0.21								■						
	10	0.28	0.18	0.17									■					
	12	0.21	0.15	0.14										■				
	Texture parameters	Sa (R), µm	3.2	2.4	1.0													
Sa (P), µm		1.7	1.1	0.4														
Ssk (P)		-0.6	-1.2	-2.9														
Sku (P)		3.0	3.8	12.0														
Sds (P), pks/mm2		4272	5622	10881														
Oscillating tribometer tests																		
Velocity, [m/s]	incr./decr.	COF values			Contact Pressure VS COF, [RSQ]							Texture VS COF, [RSQ]						
0.02	Increase	0.079	0.028	0.014	0.18	0.91	0.98	1.00	1.00	1.00	1.00	0.99	0.98	0.76	0.89	0.70	0.52	0.64
0.04		0.057	0.023	0.014	0.17	0.90	0.98	1.00	1.00	1.00	1.00	0.99	0.98	0.75	0.88	0.70	0.52	0.63
0.10		0.045	0.024	0.015	0.25	0.95	1.00	0.99	0.99	0.98	0.98	0.96	0.95	0.83	0.94	0.78	0.61	0.72
0.15		0.041	0.023	0.016	0.23	0.94	1.00	1.00	0.99	0.99	0.98	0.97	0.95	0.81	0.93	0.76	0.59	0.70
0.19		0.043	0.028	0.023	0.20	0.93	0.99	1.00	1.00	1.00	0.99	0.98	0.97	0.79	0.91	0.74	0.56	0.67
0.29	Decrease	0.029	0.019	0.017	0.14	0.88	0.97	0.99	1.00	1.00	1.00	1.00	0.99	0.71	0.85	0.66	0.47	0.59
0.39		0.033	0.020	0.016	0.19	0.92	0.99	1.00	1.00	1.00	1.00	0.99	0.98	0.78	0.90	0.72	0.54	0.66
0.29		0.030	0.019	0.015	0.18	0.94	0.99	1.00	1.00	0.99	0.99	0.97	0.96	0.80	0.92	0.75	0.58	0.69
0.19		0.039	0.024	0.018	0.24	0.95	1.00	1.00	1.00	0.99	0.99	0.98	0.97	0.82	0.93	0.77	0.60	0.71
0.15		0.040	0.023	0.016	0.24	0.95	1.00	1.00	1.00	0.99	0.99	0.98	0.96	0.82	0.93	0.78	0.60	0.71
0.10		0.044	0.023	0.016	0.20	0.93	0.99	1.00	1.00	1.00	0.99	0.99	0.98	0.97	0.91	0.74	0.56	0.67
0.04		0.051	0.023	0.015	0.18	0.91	0.98	1.00	1.00	1.00	1.00	0.99	0.98	0.76	0.89	0.71	0.53	0.64
0.02	0.059	0.023	0.015	0.15	0.89	0.99	0.99	1.00	1.00	1.00	1.00	0.99	0.99	0.73	0.86	0.67	0.49	0.60

APPENDIX 7
PUBLICATION 7

Gross K., Lungevics J., Jansons E., Jerane I., Wood M., Kietzig A. *Surface Hierarchy: Macroscopic and Microscopic Design Elements for Improved Sliding on Ice. Lubricants*, 2021, Vol. 9, No. 103, Article 103. ISSN 2075-4442.

Available: [10.3390/lubricants9100103](https://doi.org/10.3390/lubricants9100103)

Open access

© 2021 by the authors. Licensee MDPI, Basel, Switzerland. This article is an open access article distributed under the terms and conditions of the Creative Commons Attribution (CC BY) license



Article

Surface Hierarchy: Macroscopic and Microscopic Design Elements for Improved Sliding on Ice

Karlis Agris Gross ^{1,*}, Janis Lungevics ², Ernests Jansons ², Ilze Jerane ¹, Michael J. Wood ³ and Anne-Marie Kietzig ³

¹ Faculty of Materials Science and Applied Chemistry, Institute of Materials and Surface Engineering, Riga Technical University, LV-1048 Riga, Latvia; ilze.jerane@rtu.lv

² Department of Mechanical Engineering and Mechatronics, Faculty of Mechanical Engineering, Transport and Aeronautics, Riga Technical University, LV-1048 Riga, Latvia; janis.lungevics@rtu.lv (J.L.); ernests.jansons_1@rtu.lv (E.J.)

³ Department of Chemical Engineering, McGill University, Montreal, QC H3A 0C5, Canada; michael.wood3@mail.mcgill.ca (M.J.W.); anne.kietzig@mcgill.ca (A.-M.K.)

* Correspondence: kgross@rtu.lv

Abstract: Frictional interaction with a surface will depend on the features and topography within the contact zone. Describing this interaction is particularly complex when considering ice friction, which needs to look at both the macroscopic and microscopic levels. Since Leonardo da Vinci shared his findings that roughness increases friction, emphasis has been placed on measuring surface coarseness, neglecting the contact area. Here, a profilometer was used to measure the contact area at different slicing depths and identify contact points. Metal blocks were polished to a curved surface to reduce the contact area; further reduced by milling 400 μm grooves or laser-micromachining grooves with widths of 50 μm , 100 μm , and 150 μm . Sliding speed was measured on an inclined ice track. Asperities from pileup reduced sliding speed, but a smaller contact area from grooves and a curved sliding surface increased sliding speed. An analysis of sliding speed versus contact area from incremental slicing depths showed that a larger asperity contact surface pointed to faster sliding, but an increase in the polished surface area reduced sliding. As such, analysis of the surface at different length scales has revealed different design elements—asperities, grooves, curved zones—to alter the sliding speed on ice.

Keywords: ice friction; topography; texture; contact area



Citation: Gross, K.A.; Lungevics, J.; Jansons, E.; Jerane, I.; Wood, M.J.; Kietzig, A.-M. Surface Hierarchy: Macroscopic and Microscopic Design Elements for Improved Sliding on Ice. *Lubricants* **2021**, *9*, 103. <https://doi.org/10.3390/lubricants9100103>

Received: 18 June 2021

Accepted: 22 September 2021

Published: 12 October 2021

Publisher's Note: MDPI stays neutral with regard to jurisdictional claims in published maps and institutional affiliations.



Copyright: © 2021 by the authors. Licensee MDPI, Basel, Switzerland. This article is an open access article distributed under the terms and conditions of the Creative Commons Attribution (CC BY) license (<https://creativecommons.org/licenses/by/4.0/>).

1. Introduction

Ice friction draws on the initial finding by Leonardo di Vinci, that friction between two surfaces varies linearly with the force applied to a surface, acting through the contact area. Recent explanations of ice friction have been interpreted through lower friction from a lubricant film [1] or by considering the thermodynamics at the sliding interface [2]. Contact area from the application of a load has only been approximated, emphasizing the need for renewed efforts to quantify the actual surface contact. The goal of this work was to evaluate the contact area at the macro-scale and the micro-scale to see the effect of sliding over ice and then propose further characterization at the nanoscale.

Few ice-friction studies have investigated the effect of the contact area. Initial experiments from 1939—in a cave dug out from ice at Jungfrauoch in the Swiss Alps—showed a slight increase in the friction coefficient with contact area, where the contact area varied from 2 to 300 mm^2 [3]. Experiments on a larger tribometer with a more pliable polyethylene slider (contact area: 200–1000 mm^2) on ice displayed a larger change in friction [4]. Recent experiments on contact area have shown that the increase in contact area of an ice-hemisphere loaded onto a quartz base correlates well with the friction force [5]. On a larger scale—such as with the skeleton—the contact area reduced by bending the runner

showed faster sliding [6]. These experiments have emphasized the importance of contact area, also recognized by Makkonen [2] and Lozowski [7], but only the macroscopic contact area was considered and not the microscopic and nanoscopic contacts.

Contact Area and Surface Topography

Contact mechanics introduced by Hertz [8]—some 400 years after Leonardo da Vinci—showed that the contact area increases with applied force, suggesting increased friction force from the more influential effect of asperities ploughing into the opposing surface. As a result, roughness as a statistical assessment of surface height variations has been commonly used to describe surfaces. A range of characterization methods provide different quantitative results with AFM most accurately measuring the total variation in the height, but is limited to a low vertical range and small analysis area. Profilometers (contact and optical) provide a more practical approach for larger areas. Many studies have insufficiently reported the roughness with a line scan—as opposed to a surface scan—to give a bearing ratio, the percentage of actual surface contact [9–11]. This “bearing ratio” or “bearing area”—coined by Abbot and Firestone [12]—as a means to more finely define the interaction surface between sliding bodies provides the basis for greater insight into physical surface features that support easier sliding.

The true contact area has been referred to in models of friction, but a report of this contact in ice friction studies remains to be seen. Baurle [4] referred to “contact spots”, Bowden and Hughes [3] suggested “minute adhesions acting across the real area of contact”, but Makkonen [2] outlined “contacts” at the interface over which a thermodynamic model was established. In the discussion, Makkonen suggested that an inadequate measure of the contact area increased the error. Contact area, contact points, and their location and distribution need further consideration. Measurement of the contact surface and the design of the contact surface are equally important.

Descriptive characterization of the surface has been more common, with reference to micro-sized morphologies in nature. The most functionality-inducing surfaces relevant to ice friction have been the tree frog’s toe pad [13] and shark skin [14]. Focus on the contact surface shows that the arrangement and gaps between the tree frog’s toe pads allow it to climb and adhere to extremely wet and slippery surfaces as interfacial water is squeezed and channeled out between the toe pads. In relation to the shark, fast swimming sharks benefit from a specific texture on their scales that suppresses drag at the interface: longitudinal microscopic grooves on small raised convex features [15,16]. Such grooves have a depth of 4–90 μm , width of 15–98 μm and spacing of 34–83 μm with a placement that may vary [15–19]. Micro-sized features also influence ice friction with spot contacts recently addressed for winter tires [20], but the micro-sized contacts for sliding on ice require more attention.

It is common practice in competitive ice sports to abrade blade and runner surfaces longitudinally before competing; such grooves can affect the sliding performance. If there are changes in the surface, what are the most decisive features that govern sliding over ice? This general enquiry is a question, lurking in the background, for athletes wanting to slide faster over ice. The technology versus skill level is an aspect always tested by all national teams at World Cup and Olympic events. The first step involves creating a surface that leads to faster sliding, but equally important is the characterization of the surface to determine how the contact surface structure influences sliding speed.

Attention must be focused on the total contact area: the macroscopic and the microscopic views with further consideration of the nanoscopic dimension. Previous work typically only reported roughness as an indicator of asperities on smaller areas—50 \times 50 μm [21], 500 \times 500 μm [9], 3 \times 3 mm [10]; Rohm et al. [22] showed the importance of reporting roughness anisotropy on a larger 11 \times 11 mm area, but restricted the scope of investigation to the less-sensitive focus-variation microscope.

The objective of this work was to characterize a slider’s contact area and then assess its influence on sliding over ice. This involved a grooved block made by milling and by

laser machining. Attention will be directed to the macroscopic domain—contact provided from the overall shape including the laser-machined grooves (Figure 1, left)—and the microscopic domain, pointing to anisotropy adjacent to the laser-machined grooves (Figure 1, center). This study will step out from the small analysis area—previously accepted as the norm—to include an analysis of the total area. Surface features that will be addressed include the dome-like surface at the macroscale (Feature 1), together with grooves (Feature 2) and asperities at the microscale (Feature 3), as seen in Figure 1.

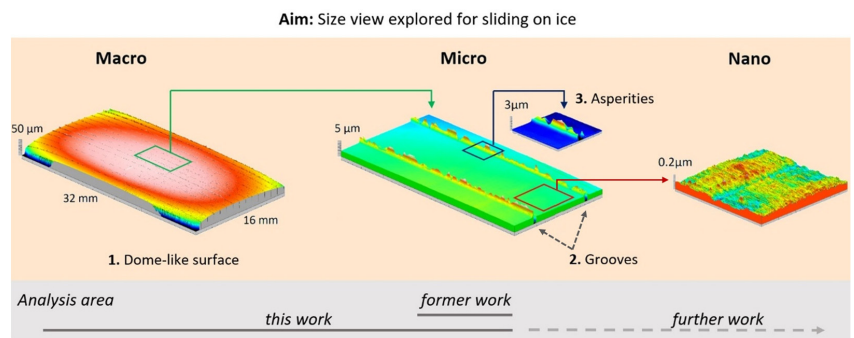


Figure 1. The different length scales of surface texture on the block showing the full texture, peaks/valleys, and roughness. The three features addressed in this work include (1) the dome-like surface also referred to as a curved surface; (2) grooves and the ledges that separate the flat regions; and (3) asperities on the pileup. This map of surveyable items—created from profilometer data—will be investigated in detail.

Characterization was restricted to a contact profilometer, the standard method in metrology, over the entire surface to determine the contact area at different slicing depths as a basis for seeking the influence on sliding. The hypothesis is that reduction in the contact surface from narrow grooves will lead to faster sliding.

2. Materials and Methods

A closer analysis of sliding on ice required a careful preparation of the sliding block surface, a detailed characterization of the sliding surface and strict control of the environmental conditions.

An array of more stringent test conditions for better experimental conditions (a) employed a test setting representative of free sliding, (b) used tight control of the environmental conditions, and (c) introduced a flattened dome-like surface on the steel block to facilitate sliding. In contrast to seeking the friction coefficient and an extrapolation to predict sliding speed, the sliding speed was directly measured for a steel block sliding down an ice-track equipped with timing sensors [23]. The variation of environmental conditions was lowered by placing an enclosure over the ice track to lower the sliding speed error. Finally, better sliding was promoted by curvature on the underside of the block, representative for many sliders in ice sports; achieved here by a more elaborate autopolishing procedure (detailed below). The collective use of these conditions facilitated easier sliding and reduced the measurement error.

2.1. Preparation of the Sliding Block

Ferritic stainless-steel blocks (82% Fe, 13.25% Cr, 1.75% Ni, 1.49% Mn, 0.56% Mo, 0.46% C, 0.23% V, 0.2% Al, 0.11% S) were milled to a size of $35 \times 18 \times 14 \pm 0.1$ mm and a weight of 68 ± 0.5 g. The blocks were initially polished before adding grooves to the underside.

2.1.1. Polishing for a Curved Sliding Base

The underside of the block was prepared with a raised central area by a modified polishing procedure; the intention was to prevent ploughing of the block into the ice while sliding. This central raised section was created from rocking of the block, in all directions, over the abrading/polishing surface. The slight rocking motion of the block under the push-rod was facilitated by the 0.5 mm gap in the rectangular cavity located in the support disc, Figure 2 (center, above).

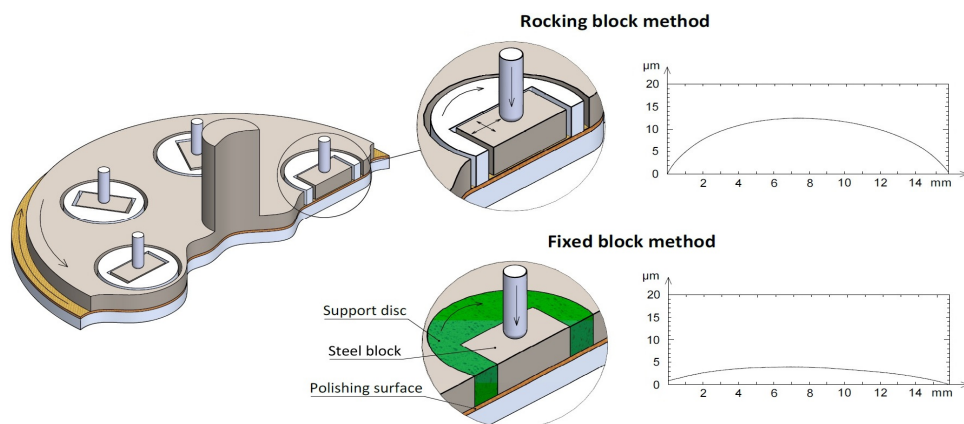


Figure 2. The block fixture in the moving plate of the automated polisher showing rotation from the free space around the block led to a rounded central region (top case) as opposed to a fixed block in a mount that created a flat surface.

To show that the magnitude of the central section was higher from the rocking motion during polishing, another block was fixed within the cylindrical mount and then polished—as per the right-most mounted block in Figure 2 (center, below). The fixed block was subjected to the same polishing procedure and then broken-out of the mount. The surface profile across the width through the center of the block showed that rocking created a 4-fold higher central section, Figure 2 (right, top).

Automatic polishing was conducted on an abrasive hard surface for initial leveling followed by polishing on a more elastic surface with an incremental step toward smaller diamond sizes from 9 μm , 3 μm to 1 μm ; more detail is available elsewhere [24].

For a rigid surface, grooves can be extended over the entire sliding surface. This work will consider 120 μm wide milled grooves in addition to laser machined parallel grooves of three different widths: 50 μm , 100 μm , and 150 μm .

2.1.2. Milling and Final Polishing

Parallel grooves were milled into the polished block surface to a width of 0.4 mm, a depth of 120 μm , and 0.6 mm between groove centers. Previous work has shown that the decrease in surface area is the first means of decreasing the area upon which friction occurs, and that any depression is more favorably oriented parallel to the sliding direction [11]. Grooves were milled with a Mazak Vertical Center Smart 530C milling machine. Given the limitation in the smallest groove width by milling, narrower grooves were introduced by laser machining.

2.1.3. Laser Machining

A Coherent Libra Ti:sapphire femtosecond laser system (Coherent, Inc., Santa Clara, CA, USA) was used to micromachine deep grooves into mirror-polished stainless-steel blocks. This laser system has an inherent wavelength of 800 nm, pulse duration <100 fs, repetition rate of 1 kHz, and a maximal output power of 4 W. A half-wave plate and a polar-

izing beam splitter reduced the output power to the desired processing power of 200 mW. The stainless-steel substrates were mounted onto a computer-controlled 3D translation stage (Newport, Corp, Deere Avenue Irvine, CA, USA). The linear scanning velocity was set at 5 mm/s for all micromachining routines used. The laser beam was focused onto the stainless-steel substrates using a plano-convex lens (Thorlabs, Inc., Newton, NJ, USA) with a 50 mm focal length.

Three distinct inscribed geometries were designed for machining with the laser system: 50 μm wide \times 50 μm deep grooves, 100 μm wide \times 100 μm deep grooves, and 150 μm wide \times 150 μm deep grooves, spanning the entire length of the polished stainless-steel block. In all cases, the edge-to-edge distance between consecutive grooves was held constant at 1 mm. The pristine polished stainless-steel blocks were ultrasonically cleaned in acetone for 15 min prior to irradiation and again after micromachining for 15 min to remove any non-sintered nanoparticles.

2.2. Measurement of Texture

The surface texture was measured by a contact stylus profilometer (Taylor Hobson Form Talysurf Intra 50) with a 2 μm tip (112/2009 stylus). An area of 32 \times 16 mm was measured, representing 81% of the surface. The very edge was not included in the measured zone to prevent exceeding the limit of measurement in the z-direction, leaving the outer 1 mm unmeasured around the perimeter of the block. Texture was measured from 600 profiles: each line scan contained 6000 points to give 3,600,000 points with a point density of 7031 points/ mm^2 . Data processing was made with the Talymap Gold analysis software and initially involved levelling. Roughness (Sa), skewness (Ssk), kurtosis (Sku), peak density (Spd), and peak curvative (Spc) were calculated on the pile-up and polished sections.

The contact surface was determined by slicing at a predetermined distance from the highest asperity—digitally extracting data from the outermost layer. Slicing the top 1 μm , 2 μm , and 4 μm layers allowed visualization of the contact areas at different depths; the contact surfaces at each depth were associated with contour maps to show the microscopic contact region size and location (Figure 3). Detail on the microscopic contact area was quantified at submicron depth increments from the top-most surface to obtain a contact area profile versus the slicing depth requiring slicing up to 18 μm from the top of the surface. Slicing together with detailed reporting enabled microscopic reporting of the contact area in contrast to the previously accepted macroscopic report from the bearing ratio (compared in Figure 3).

Contact area at a given slicing depth collected incremental contributions up to the stated depth—taking input from asperities with vertical/angled walls and more gradual changes. Contact area at the slicing depth was expected to provide the best view (Figure 3).

The zoom function magnified the view of selected locations. An area of 4 \times 2 mm was selected to view the smoothness of the polished area (nanoscopic view), and pileups on the edges of laser-machined grooves (microscopic view). Roughness of the polished area between the grooves (2 \times 1 mm) was calculated according to ISO 25178 [25] after removing the form, the waviness, and then using a cut-off of 0.08 mm for the measurement. The profile extraction function was applied to obtain additional surface views; for example, determining the shape of the corners.

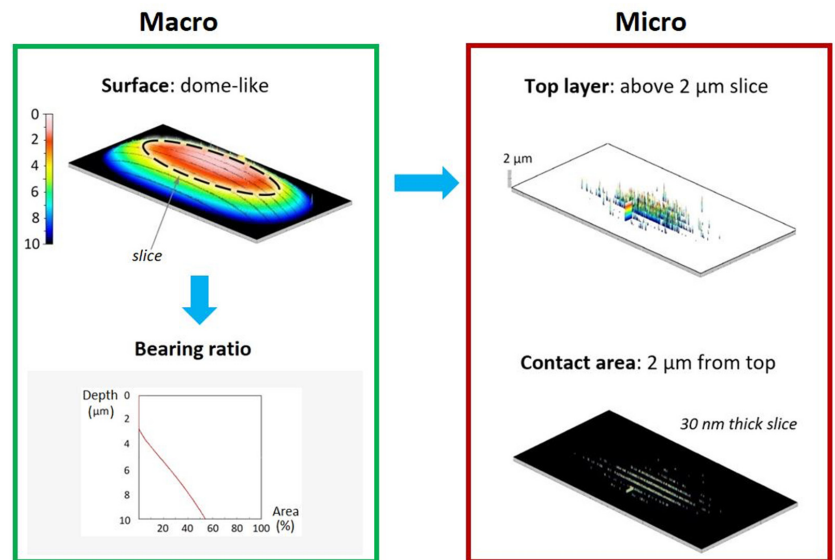


Figure 3. “Slicing depth” at 2 μm from the surface (left) shows the microscopic view of the contact area when the object sinks 2 μm deep into the ice surface (right). This contact area from digitally “slicing” (right) is contrasted with the 2 μm top layer (right) that shows incremental features in the surface.

2.3. Sliding Speed

Two types of grooved blocks were tested for sliding speed: blocks grooved by milling and by laser machining. The milled blocks were slid 20 times on ice after milling, repolished, and slid another 20 times to determine the effect of repolishing. Laser machined blocks (with 50 μm, 100 μm, and 150 μm grooves) were slid only after laser machining and were slid 20 times.

The time for sliding blocks down a 2.74 m ice track (inclined at $16 \pm 0.5^\circ$) was measured by timing sensors. Briefly outlining the ice preparation, tap water was frozen overnight in the rectangular section, levelled by planing, and made smooth by applying a thin layer of warm water, thereby creating a pore-free top layer. Reference blocks were slid on the ice track as controls.

The temperature and humidity were maintained constant in an enclosure placed around the ice track to further reduce any departure from the conditions set in the climate simulation chamber. The ice temperature was measured with a thermocouple TP-122-100-MT-K (Czaki, Rybie, Poland) connected to a Proscan520 (Dostmann electronic GmbH, Wertheim-Reiholzheim Germany). More details on this approach for directly measuring the ease-of-sliding, as opposed to the ice friction, is detailed in Jansons et al. (2021) [11]. The improved stability of the air humidity, air temperature, and ice temperature are shown by smaller error bars with the enclosure (termed “closed”) when compared to without the enclosure (labelled “open”), as seen in Figure 4.

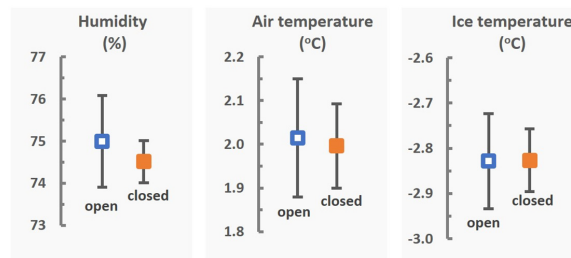


Figure 4. The enclosure (labelled “closed”) reduced air and ice condition variability.

Two air/ice conditions were chosen to represent two different ice conditions that are the most reported and vary with respect to the water layer thicknesses on the ice. The colder ice temperature is representative of the mixed friction/boundary lubrication regime (thinner water-like layer), while the warmer ice temperature is more characteristic of hydrodynamic lubrication (thicker water-like layer), as seen in Table 1. Within this work, we did not relate the conditions to a water film thickness due to the inability to report a numerical value. Sliding speed experiments on a skeleton in a bobsled push-start facility have, however, shown a significant influence of the air humidity [26], and so humidity, air, and ice temperature were selected to match colder conditions as closely as possible in our experimental setup.

Table 1. Air and ice conditions for the sliding blocks (milled, laser-machined).

Conditions	Milled Block		Laser-Machined Blocks	
	Milled	Repolished	Ice1	Ice2
Air humidity	65%	63%	68%	63%
Air temperature	−1.0 °C	−3.0 °C	−1.2 °C	−4.3 °C
Ice temperature	−4.0 °C	−8.0 °C	−2.2 °C	−7.8 °C

A correlation was sought between the sliding speed and the contact area (calculated at different slicing depths) at increasing slicing depths. The contact area was matched to the average sliding speed for the block in question, giving three data pairs that were plotted and the correlation coefficient was calculated. The correlation coefficient was determined over a range of slicing depths.

3. Results and Discussion

Aspects of contact area and asperities will first be addressed on a block with wider grooves, followed by a new “contact area at slice-depth” measurement method to assess contributions from asperities and a curved surface, and then we finally used this new measurement method to show the contribution of micro-sized and macro-sized contact on a laser-grooved block with narrower grooves on sliding speed.

3.1. Milled Surface Grooves Influence Sliding Speed

Milling of the polished block introduced 0.175 mm wide ridges, separated by 0.4 mm wide grooves. Mechanical cutting introduced an angle in the groove wall. Unintended pileups of deformed metal—resulting from cutting by the milling tool—remained on both sides of the ridge. The pileups varied in height and were unsymmetrical on each ridge, extending 8 μm to 20 μm from the top surface, as seen in Figure 5 (top, left). In some instances, even a double-peaked pileup was observed.

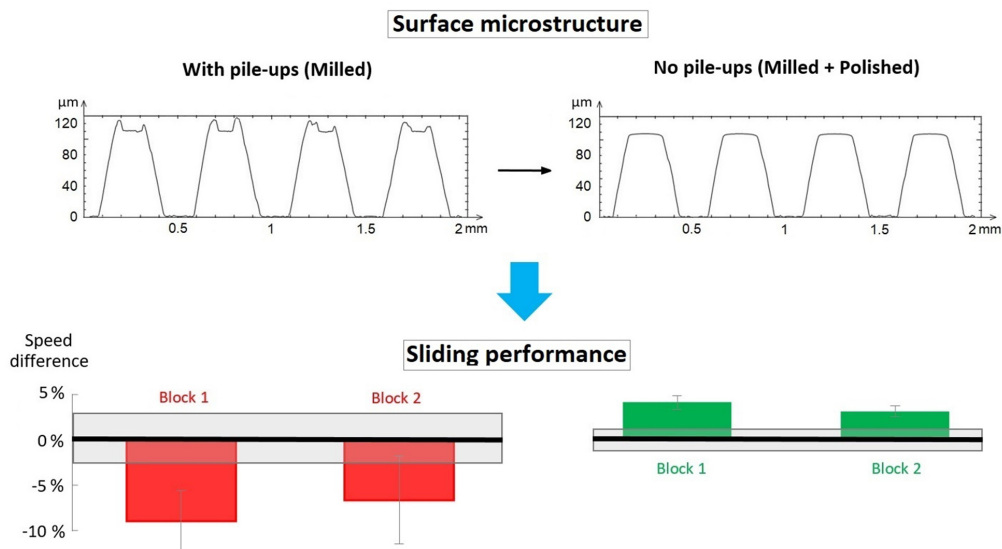


Figure 5. The grooved block exhibited asperities from pileups after milling (left) and flat ridges after repolishing (right). The sliding speed of blocks with pileups was slower relative to the flat surface, but faster when the pileup was removed by polishing.

Polishing the grooved block removed the pile-up, flattened, and rounded the ridges. The ridge width increased from about 0.175 mm to 0.190 mm, introducing a gentle rounding at the edge of each ridge, as seen in Figure 5 (top, right). Pileup was removed with a marginal reduction in the groove depth. Polishing-out the pileup removed the microscopic aspect and returned a nanoscopic roughness on the ridge surface to 13 nm.

Sliding speed was influenced by the reduced contact area introduced by grooving and the pileup remaining after machining. A comparison was established to an ungrooved reference block—shown as a black reference box in Figure 5. Sliding speed was slower with pileup on the grooved block when compared to the ungrooved flat block, Figure 5 (lower figure). With the pileup removed, the sliding speed was faster than the ungrooved block. This collective information shows the larger influence of surface roughness from asperities, possibly explaining the easier detection by Leonardo da Vinci. With surface roughness removed, a smaller contact area on the grooved block aided faster sliding on ice. This emphasized the influence of both microsized contacts and macroscale contact area on the sliding speed.

The pileup also increased the sliding speed error. The difference in temperature between the two testing days increased the error by 50% for the polished reference block, but the error was twofold to threefold higher for the blocks with pileup. Sliding speed for the blocks were as follows: sliding speed for milled Block 1 was 1.552 ± 0.053 m/s and 1.592 ± 0.077 m/s for milled Block 2, compared to 1.705 ± 0.058 m/s for the polished block to which the results were compared. An increase in sliding speed after removing ridges with polishing was clear, showing a sliding speed of 1.898 ± 0.024 m/s for Block 1 and 1.868 ± 0.025 m/s for Block 2 when compared to 1.812 ± 0.045 m/s for the ungrooved polished reference block.

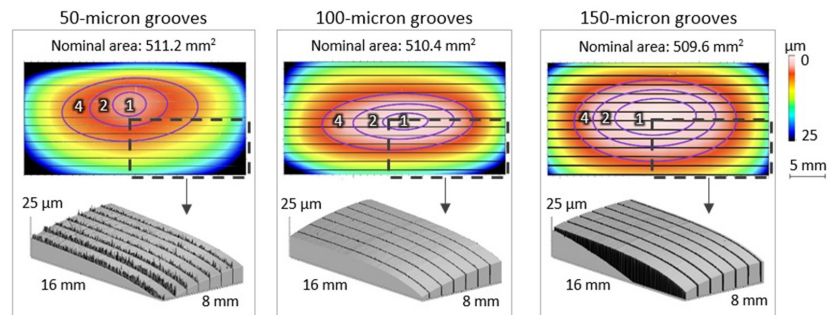
Sliding for the milling-grooved blocks was improved by the absence of asperities and a smaller contact area imparted by grooves.

3.2. Characterization of Laser-Grooved Blocks

The contour maps of Figure 6 represent three laser-engraved blocks with grooves as black lines and rounded corners from the rocking-block polishing method. The size of

the central plateau from the rocking-block polishing method varied amongst the blocks (Figure 6a). The smallest plateau was found on the 50 μm laser-grooved block, as seen by the smallest encompassing ellipse that shows the 1 μm top-layer; the 100 μm wide grooved block exhibited a more elongated 1 μm top-layer, but the block with 150 μm grooves showed the largest top 1 μm contact footprint. Since larger contact areas are associated with more friction [21,27,28], then the initial intuition could be that the last block would have the slowest sliding speed. Reports on the sliding speed, however, indicated the opposite trend.

a) Contour plots and corner views - larger vertical scale



b) Contact area – smaller vertical scale

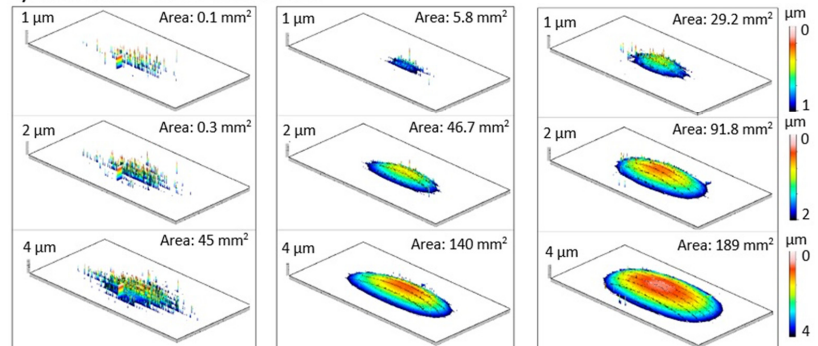


Figure 6. (a) Contour plots with a larger vertical scale show a central raised section and laser-machined grooves. The contours display the location and placement of the upper 1 μm , 2 μm , and 4 μm layers on the overall surface form. Photo-simulated corner views show rounding from the rocking-block polishing method and pileup adjacent to the grooves. (b) Contact area was considerably smaller than the footprint area for the 50 μm grooved surface in the 1 μm , 2 μm , and 4 μm top layers with more pronounced asperities.

The contours do not represent the contact area, but the footprint that encloses the highest points. The actual contact area at the three different depths (1 μm , 2 μm , and 4 μm) was significantly smaller than the footprint area; the contact area at a depth of 1 μm for the 50 μm , 100 μm , and 150 μm grooved blocks was 0.11, 5.77, and 29.2 μm^2 , respectively. Contact area at 1 μm from the top surface differed by as much as about 300 times between the 50 μm grooved block and the 150 μm grooved block.

Digital slicing of the grooved blocks shows points of contact—a useful addition to contour maps. The color gradation within each slice, provided by the analysis software, aids in the interpretation of the height (Figure 6b). The small 0.11 μm^2 true contact area in the 1 μm slice of the 50 μm grooved block can be attributed to sparsely populated pileup within the larger footprint. Contact points on the 100 μm grooved and the 150 μm grooved

blocks were less associated with asperities, but more with the rounded surface (Figure 6a). This closer view at the microscopic level provided closer examination of the contact area than the contour plot.

A close-up examination revealed that asperities adjacent to the grooves appeared as long narrow sawtooths (Figure 1—microscopic view). Pileups from the line scan were 1.2 μm high for the 50 μm grooved surface, and between 2 μm and 3 μm for the other two laser engraved surfaces (see Supplementary Figure S1).

The photosimulated view of the corner area (at 2 mm from the edge) provided more detail on the shape and asperities (Figure 6a). Rounding at block corners created a 20 μm height difference with the center of the block (Figure 6). Such rounding from the rocking-block polishing method presents an advantage for better sliding on ice.

Contact area visualization on the total block revealed three topographical features: (1) a central plateau, (2) ridges, and (3) asperities from laser-machining. Primary attention was given to roughness, as initially pointed out by Leonardo da Vinci [29], and often shown by ice-friction researchers. Roughness along the saw-toothed microscopic pileup was largest on the 50 μm laser-grooved block with S_a at 0.58 μm (Table 2). Roughness on the surrounding polished ridges exhibited nanoscopic roughness—between 6 and 8 nm for all blocks. This information announces the possible dominating role of roughness, but a larger number of contact points per unit area and the associated contact area needs to be evaluated. The contact points (Spd) were not resolvable on the pile-up due to filters in the analysis software.

Table 2. Roughness characteristics of the laser-grooved and milling-grooved blocks.

	Texture Parameters				
	S_a Nm	Ssk	Sku	Spd pks/mm ²	Spc 1/m
Laser-grooved block, along pileups					
50 μm	581.1	1.04	3.53	-	-
100 μm	65.3	0.15	5.03	-	-
150 μm	49.4	1.23	8.51	-	-
Laser-grooved block, polished zone					
50 μm	7.7	-0.02	3.09	7971	0.029
100 μm	6.3	-0.09	2.97	5440	0.026
150 μm	6.4	0.02	2.89	3823	0.021
Milling-grooved block					
polished	13.4	-0.96	10.7	20654	0.126

As expected, the SEM micrographs did not detect a curved surface, and little signs of a ridge or asperities (see Supplementary Figure S2) when compared to the information generated from profilometry. It is noteworthy that laser-machined grooves show distinct, and for laser machining at the respective fluence, characteristic hole structures. These microfeatures are typically superhydrophobic [28] and can serve as traps for wear debris [30,31].

- S_a —the arithmetic mean height of asperities.
- Ssk—skewness to indicate peaks or holes above the mean plane.
- Sku—kurtosis to represent the sharpness of peaks.
- Spd—density of peaks per unit area.
- Spc—the arithmetic mean peak curvature shows whether the asperity is pointed or rounded.

Grooving was conducted on stainless-steel blocks (82.00% Fe, 13.25% Cr, 1.75% Ni, 1.49% Mn, 0.56% Mo, 0.46% C, 0.23% V, 0.20% Al, 0.11% S).

3.3. Quantification of Contact Area

The expected contact area was determined from the analysis of contacts on the sliding surface with reference to hierarchical features—asperities, grooves, and the curved surface. Contact area at different slice depths parallel to the surface at submicron increments first showed the initial contact made with asperities, followed by further contact from the curved block surface. This situation is based on the penetration of asperities into ice and the increase in contact area arising from the larger asperity base, new asperities, and contact on the macroscopic curved surface. Further discussion will be directed to the “contact area vs. slice-depth” curve (Figure 7).

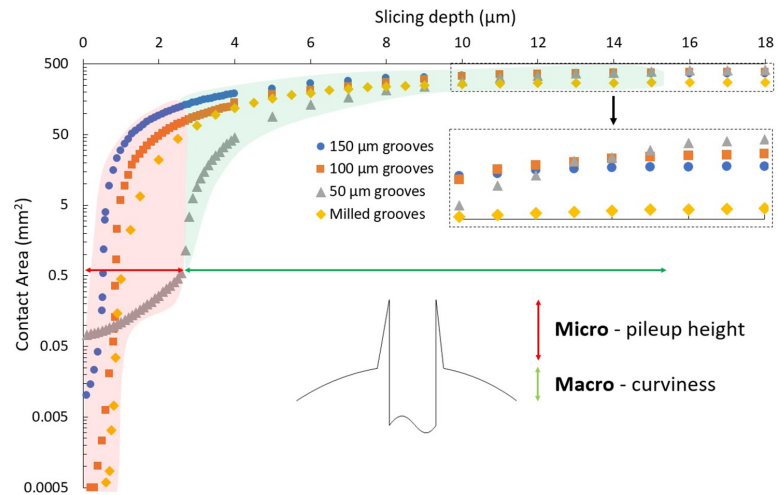


Figure 7. Contact area with slice depth shows minimal pileup for the 100 μm and 150 μm laser-grooved blocks, as shown by the rapidly rising contact area with slice depth, but a larger contact from numerous asperities on the 50 μm laser grooved block. The case for the 50 μm laser grooved block is accented with the red shading, showing the asperities, and the green shading shows the main contribution from the curved surface. The larger contact area for the 50 μm laser-grooved block becomes evident at a 16 μm slice depth from the highest asperity. The repolished block with milled grooves is shown for comparison.

The contact area with the slice-depth curve showed more micro-contact characteristics, an aspect that was not evident in the bearing-ratio representing the percentage of surface contact. Two aspects are noteworthy: the initial contact area and the change in contact area with slice depth. The smallest initial contact was noted for the 100 μm laser-grooved block. This suggests that few peaks, small in size, established the first contact. The same small initial contact was observed for the milled-grooved block, but from rounded peak contact (formed during the polishing process). The first contact is a feature unique to the “contact area vs. slice-depth” curve.

The change in contact area with depth was seen in more detail in the slice-depth curve as opposed to the bearing-ratio curve. A logarithmic gradation measure of contact area allowed the feature height to be determined: asperities on the 50 μm laser-grooved block were the highest amongst all blocks, as seen in the relatively constant contact area with slice-depth (shown by the red horizontal arrow in Figure 7, indicating the microscopic dimension). A similar, nearly undetectable, trend was recognized for the milled-grooved block at the initial contact, suggesting a very small asperity height. In Figure 7, this micro-hierarchical feature for the 50 μm grooved surface—highlighted in the red-shaded region—allows for the estimation of the asperity height. More detailed information of the microscopic contact builds on the feature height seen as the initial step in the bearing-ratio

curve, as confirmed by the more-constant initial contact area for the taller asperities on the 50 μm grooved surface (Figure 8).

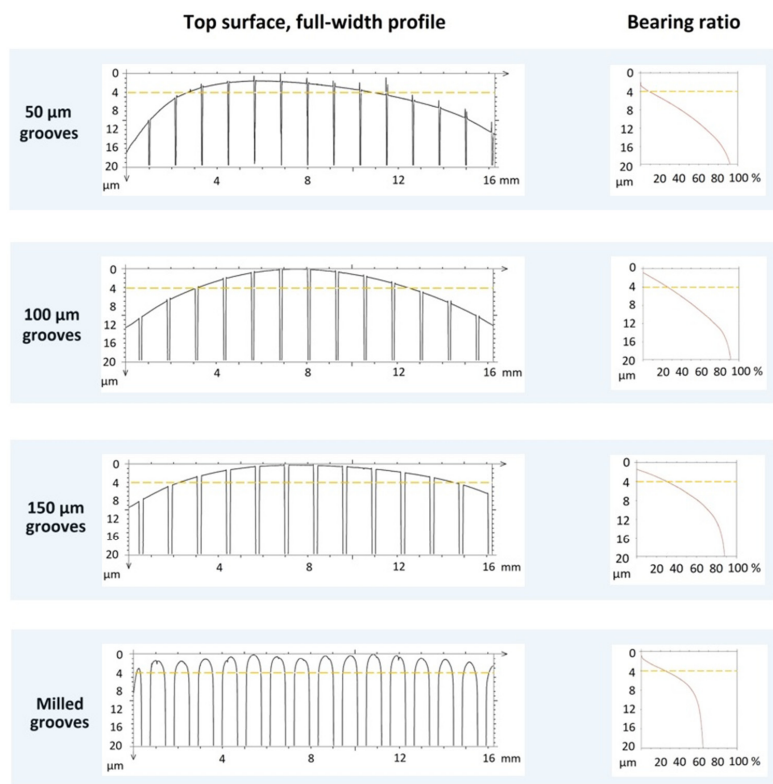


Figure 8. The profile of grooved blocks at a vertical magnification shows the straight edges after laser-grooving (50 μm , 100 μm , and 150 μm grooves) and the rounded edges on the milled and polished blocks. The bearing ratio curve shows the asperity height at the start with the initial vertical displacement, indicating a larger step with the 50 μm grooved block.

The added benefit of the slice–depth curve (Figure 7) is the potential to measure the steepness of the microsized features. Sloped asperities in the case of the 50 μm grooved block appear as a sloped line in the “contact area versus slice depth” curve representing the micro-zone (see Figure 7); asperities with a vertical wall would appear as a horizontal flat line, but less-steep asperities would exhibit a more rapidly rising line in the micro-zone. This explanation holds true for simpler situations for asperities in the top layer followed by a flat or curved base underneath. Therefore, the “contact area with slice–depth” curve holds more information than the conventionally used texture parameter Sdq (root mean square gradient). A complete picture of the viewed area is recommended to confirm the interpretation of the asperity shape. Herein lies an opportunity for more detailed characterization of asperity size and shape to more accurately interpret the asperities that interact with opposing surfaces.

Slicing at different depths allows the texture to be evaluated in a subsurface layer to observe the finer asperities and larger more continuous surface contribution to the contact area. This analysis could prove useful to predict the interaction of the surface under heavier loading conditions, where the surface further sinks into and further interacts with the opposing surface. For ice, this increasing contact area situation will arise at warmer ice

conditions where the slicing surface can slide into the softer ice surface. The additional interaction could then be individually assessed. This supplementary contact area from a deeper layer could be visually assessed after compiling the contact area from the different slices. Along with the need for a more detailed examination of texture within each slice will be the need for higher resolution measurement from profilometer systems: this greater resolution may result from combining results from different measurement systems such as the profilometer with atomic force microscopy data, or the continual development of profilometer measurement systems.

3.4. Sliding Speed of Laser-Grooved Blocks

Repeatability in the sliding speed was improved from a number of factors. The error in the sliding speed was significantly reduced with the enclosure placed around the ice track (giving as much as a three-fold smaller error), increasing the sensitivity to discern difference (Table 3). On Ice1 at $-2.2\text{ }^{\circ}\text{C}$, the sliding speed of the $50\text{ }\mu\text{m}$ grooved block was $2.101 \pm 0.007\text{ m/s}$; for the $100\text{ }\mu\text{m}$ grooved block $2.139 \pm 0.015\text{ m/s}$; for the $150\text{ }\mu\text{m}$ grooved block $2.187 \pm 0.008\text{ m/s}$; and 2.177 ± 0.020 for the milling-grooved reference block. On Ice2 at $-8.8\text{ }^{\circ}\text{C}$, the sliding speeds were $2.159 \pm 0.012\text{ m/s}$, $2.181 \pm 0.011\text{ m/s}$, $2.220 \pm 0.005\text{ m/s}$, and $2.216 \pm 0.019\text{ m/s}$ for the same blocks.

Table 3. Contribution of enclosure conditions, ice temperature, and block surface to the sliding speed error, with reference to the sliding speed. Grey shading denotes similar settings for an easier comparison.

Environmental Conditions		Sliding Block Surface			Sliding	Error
Control	T_{ice} ($^{\circ}\text{C}$)	Preparation (Groove Width)	Form (mm)	S_a (mm)	Speed (m/s)	(%)
w/o enclosure	-4.0	milled 400 mm	2	-	-	0.96
“	-8.0	milled 400 mm, polished	2	13	2.216	0.80
enclosure	-2.2	polished, laser 50 mm	16	581	2.101	0.33
“	-2.2	100 mm	12	65	2.139	0.70
“	-2.2	150 mm	10	49	2.187	0.36
“	-7.8	50 mm	16	581	2.159	0.55
“	-7.8	100 mm	12	65	2.181	0.50
“	-7.8	150 mm	10	49	2.220	0.22

T_{ice} —temperature of ice; Form—total vertical displacement of the curved surface (left visual in Figure 8 for more detail); S_a —average roughness over entire surface.

Smaller errors in sliding speed appeared at colder temperatures, and on blocks with less curvature on the sliding surface (Table 3). We hypothesized that a larger error arises from the larger interaction volume between the sliding surface and the ice at temperatures closer to the melting of ice; testing at warmer temperatures therefore requires even higher accuracy in the different measures to discern the most influential factor. Again, we considered that a larger curvature on a freely sliding body will add to a greater degree of freedom

and more interactions with the sides of the ice track that would increase the contact area during sliding, and hence lower the sliding speed.

Sliding speed was slowest for the 50 μm grooved block, intermediate for the 100 μm grooved block, and fastest for the 150 μm grooved surface. Reference was made to the fastest sliding milling-grooved-polished block, as reported numerically above (Table 3).

Since the milling-grooved block was made with the smallest contact area, it was expected to have a faster sliding speed. The sliding speed for the 150 μm wide laser-grooved block showed a slightly higher speed than the 400 μm wide milling-grooved-polished block, accenting the contact surface at the macroscale.

Differences in sliding speed needed consideration of the surface area (after compounded effects from “rocking-block polish” and laser-grooving) and asperities remaining from laser machining. By determining the correlation of sliding speed with contact area, it was conjectured that a high correlation would be found to indicate the depth of asperity penetration into the ice surface, the results, however, showed a positive correlation with slice depths up to about 8 μm and a negative correlation at depths greater than 14 μm (Figure 9). The positive correlation from an increased contact area suggested that sliding was dictated by an effect from asperities; a larger contact area possibly distributed the load amongst more contact points, causing less asperity penetration into ice, and less resistance to sliding. The negative correlation agreed well with expectations from previous work, in that a higher contact area increases interaction/friction between surfaces [11]. The overall effect resulted in slower sliding for the 50 μm laser-grooved block.

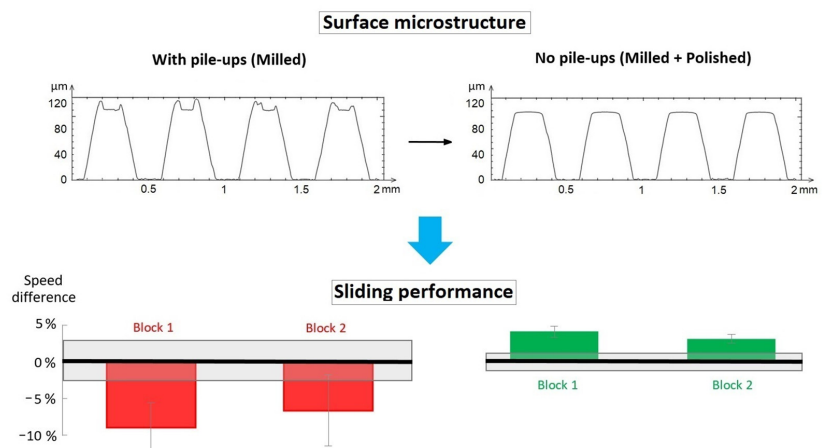


Figure 9. Sliding speed of laser machined blocks on ice (Ice1: $-2.2\text{ }^{\circ}\text{C}$ and Ice2: $-8.8\text{ }^{\circ}\text{C}$) relative to grooved and polished block. The initial positive correlation suggests a faster speed from an increasing contact area from more contact point up to a slice depth of about 7 μm , followed by a negative correlation at slice depths more than 14 μm where an increase in contact area reduces sliding speed. The fastest sliding speed was 2.23 m/s.

The contact area of the 50 μm grooved surface, at slice depths showing good correlation with sliding speed—at 2 μm , 7 μm , and 15 μm —showed asperities at each slice depth (Figure 10). Such slice views are valuable to interpret the effective contact area upon penetration into ice, and discontinuous areas on the sliding surface. The resistance to sliding from asperities appeared both at the center and on the curved corners. Therefore, during stable sliding, the asperities in the center were active (see Figure 6), and if there was any rocking, then the asperities on the curved corners would also delay sliding (Figures 6 and 9).

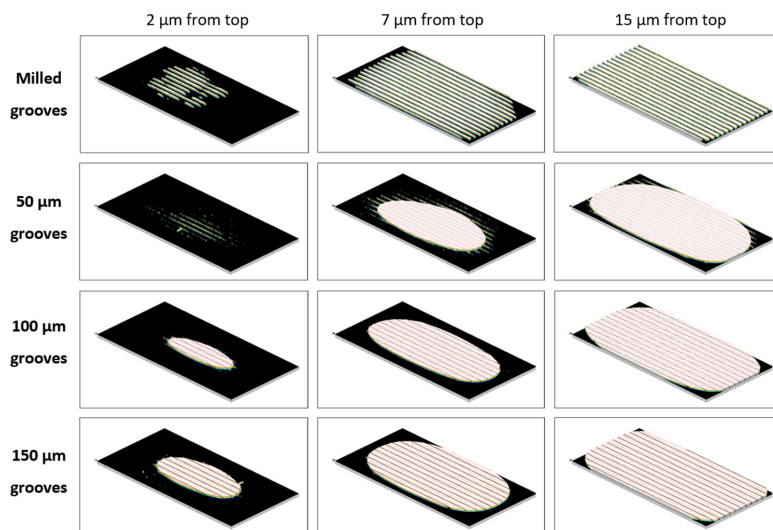


Figure 10. The contact area at 2 μm , 7 μm , and 15 μm slices (0.1 μm thick layer) showing the contact location on the milling-grooved block, and the laser-grooved blocks with 50 μm , 100 μm , and 150 μm grooves.

A comparison of the milling-grooved block and the faster sliding 150 μm laser-grooved block showed that the rounded macroscopic shape contact area would have been more favorable for sliding. The larger error in the sliding speed for the milling-grooved block could have arisen from the more rectangular contact area shape (Figure 10). The size, shape, and location of the contact areas will individually impact the ease of sliding—a contribution that is yet to be determined.

The effect of faster sliding by the 150 μm laser-grooved block was slightly more discernable on ice closer to the melting temperature at $-2.2\text{ }^{\circ}\text{C}$. At $-8.8\text{ }^{\circ}\text{C}$, the 150 μm laser-grooved slider was only slightly faster than the grooved and polished reference slider, possibly due to larger resistance-to-sliding from roughness on colder ice [32]. It is interesting that larger differences in the sliding speed were observed on warmer ice, despite overall slower sliding. The larger difference in sliding speed at warmer temperatures could arise from more interaction of asperities with softer ice—ploughing has a bigger effect on warmer (and softer) ice.

Since each block has a different curved surface, number, and size of asperities, then the penetration into ice and the resulting contact area will be different for each block. The contact area during sliding could be defined by the area required to establish an applied stress equal to ice hardness. The area at each slice will allow the effective stress to be determined. For shallow slices, the area will be smaller and the effective stress will be greater than the hardness. Slices deeper into the block will increase the area and lower the effective stress until the effective stress reaches the ice hardness. At that point—where the effective stress and the hardness are equal—no more penetration occurs into ice, thereby defining the contact area. Therefore, the determination of sliding contact area first requires information on the ice hardness, which may change due to frictional heating at the front-end block contact to the trailing edge while sliding on ice.

More detail needs to be directed to the combined view of roughness (S_a) and peak sharpness (S_{ku}) (Table 2) to see how the peak curvature would influence the sliding speed. There is a growing need to use texture parameters, “contact area at slice depth”, distribution of contact points, and mapping of the surface for showing topography to determine the source of friction.

The analysis showed the dominating role of asperities and so further work could consider how asperity nanotopography interacts with ice to influence the sliding speed. Nanoscale roughness is starting to be more actively investigated in friction studies [33]. In past studies, the interacting ice surface has been either modeled as a solid surface with mobile water molecules [34–36] or interpreted by others as a liquid—termed the “liquid-like layer” [1]. Further studies need more detail and further characterization of the sliding surface and the underlying ice surface. While previous studies have considered that water evolved from friction or from the less influential pressure melting when addressing the thermodynamics at the sliding interface [2], the extension of the model to include the influence of asperities on ice-friction would make an important contribution.

3.5. Further Considerations on the Contact Area

This work has presented an approach to determine the contact area over a larger area of engineering significance: the location of the contacts and the total contact area at deeper slicing depths. These two new aspects were introduced to continue from Makkonen’s thermodynamic model [2], which showed greater friction from a longer ridge-like asperity. This highlights the importance for the 3-D characterization of asperities.

A further development could make a 3D model of the surface texture and model the increase in surface area under changing loading conditions. Initial studies on contact areas have been measured by conductivity on a very small scale using a contact-AFM [37]. Larger contact areas have been visualized using an optical microscope through molecules that fluoresce under load [38]—a forerunner to a contact microscope [39]. Both methods characterize at a smaller scale than the profilometry that has been used here. These concurrent activities highlight active research on more precise measurements of contact between two bodies.

Ice as the sliding surface has been assumed as stable with defined properties, but recent work has revealed changes with temperature and sliding speed. A decrease in ice hardness with temperature [2,40] lowers the resistance for penetration into the ice. Presence of asperities on a slider such as with the 50 μm laser-grooved block would make penetration into ice even more pronounced from the higher contact stress. The slider contact area with slicing depth would allow a closer insight into the possible asperity penetration depth and the resulting sliding resistance. Asperity penetration depth may factor in the increase in ice hardness with sliding speed, previously noted during slow sliding speeds [41]; the change in hardness at higher speeds remains to be asserted and quantified. Finally, mechanically disturbed ice will change to heal previously made scratches [42], and in real-life conditions, will need to consider continuous changes to the ice surface from the pounding of runners during sliding over ice [26].

Previous studies have shown that a lower bearing ratio (% of slider contact) aids in a faster sliding speed [11], but like roughness, it is a statistical measure of the surface; without information on the microtopographic features and for practical use, there is an assumption of the asperity penetration depth. The bearing ratio measures the macroscopic aspect (initially proposed by Abbot and Firestone [12]), however, the “contact area versus slice depth” curve and maps of contact area at different depths show the microscopic and macroscopic contributions. Recent experiments from our group have given insights into slicing from a polishing process [43], but polishing additionally introduces rounding of the contact area. Slicing, as shown in this work, showed that the contact area locations could aid the prediction of balanced sliding or veering to one side of the ice track. The 50 μm grooved block showed an off-center central plateau (Figures 6 and 8), which would have caused erratic sliding movement from continuous impact to one side of the ice track. Assessment of contact points, contact area, and contact location will assist in the design of experiments on sliding.

Surface design elements could be implemented on a smaller scale and extended to the nanoscale. More regular contact points have a lower contact area than a flat surface and is promising in stabilizing sliding on ice. The high correlation between sliding speed

and the pileup contact area from Figure 9 suggests that smaller dome-like features, akin to those on sharkskin scales, could distribute the applied load to lower penetration into ice, leaving the question of the ideal size and spacing between contact points. Grooving on raised sections provide considerations for designing surfaces with faster sliding on ice.

Sliding resistance in real-life sees contributions from ice-friction and physical barriers: ice friction from slider asperities penetrating ice to spot contacts that adhere opposing faces and physical barriers that impede motion from both surfaces (Figure 11). Surface characterization can further include the contact area with slice depth, and the shape of asperities from both surfaces. This necessitates the importance of characterizing surface topography at the macroscale, microscale, and nanoscale and a consideration of measurement from the outermost surface to provide the contact area. All these contributing factors will influence the initial stick-slip phenomena at the initial stage of sliding and determine the speed at which ice-friction is reduced to the smallest value [44].

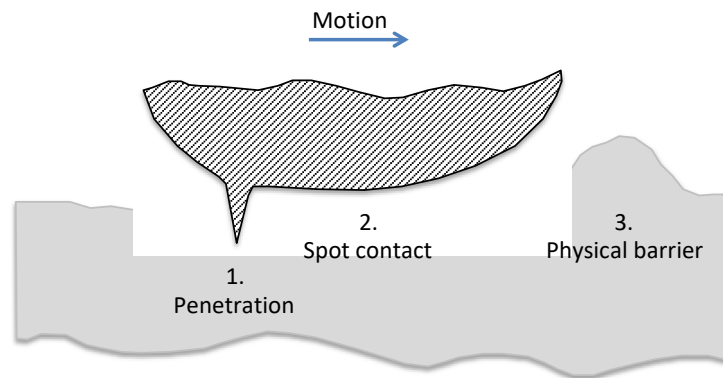


Figure 11. A sketch of three factors contributing to the sliding resistance: penetration of asperities, spot adhesive contacts, and physical barriers.

Further developments will benefit from providing a series of roughness parameter values, the contact area with slice depth, and a map of topographical features with more detailed characterization of the contact points. The roughness gives insight into asperity penetration into the opposing ice surface. Values of roughness (S_a), skewness (R_{sk}), kurtosis, and more detail on the contact point population (S_{sd}) and contact point geometry (S_{pc}) will be more informative of the surface. This broadens the previous report of the surface by Scherge [10] to include information about contact points for a detailed analysis of the contact area. Measurement of these texture parameters from measurements on the more sensitive 3D laser microscope ($0.2\ \mu\text{m}$ probe compared with a $2\ \mu\text{m}$ probe on the contact profilometer) will provide more accurate reports of the surface texture.

The hierarchical assessment of topography (specifically contact points and roughness) will be relevant to other lubricating applications such as pistons in pursuit of the lowest friction most commonly referenced to cartilage [45].

4. Conclusions

Sliding on ice depends on both the macroscopic and microscopic surface details of the contact area with contributions from the curved underside, grooves, and asperities over the entire surface. Microsized metal pileup decreased the sliding speed by supposedly penetrating the ice, while grooves and the domed surface jointly lowered the contact area to increase the sliding speed.

Correlation was found between the sliding speed and the pileup contact area at different slice depths, explained by more asperities lowering the contact stress and reducing

the penetration in ice. The effect of asperities was more pronounced closer to the melting point of ice, indicating deeper asperity penetration and a greater sliding contact area.

A new “rocking-block” polishing method where the block slightly rocked during polishing showed a means of introducing a curved sliding surface to lower the contact area for easier sliding over ice.

Recommendations are given to characterize the entire surface and a method suggested to measure the contact area at increasing slicing depth to provide foresight into the expected contact area at greater loading. A list of texture parameters is given to more completely describe asperities located on the sliding surface. This detailed surface characterization will find use beyond ice friction to any situation involving interactions with the surface.

Supplementary Materials: The following are available online at <https://www.mdpi.com/article/10.3390/lubricants9100103/s1>, Figure S1: An enlarged view of the grooved blocks and the associated profile for the 50 µm grooved block (upper), 100 µm grooved block (middle), and 150 µm grooved block (lower). The pileup can be seen at the edge of the grooves. Figure S2: SEM micrographs showing the grooves seen at lower magnification, the holes in the grooves at the intermediate magnification, and the pileup at higher magnification.

Author Contributions: Conceptualization, surface preparation—K.A.G., M.J.W., Polishing—K.A.G., Hierarchy—K.A.G. and J.L.; Investigation—E.J., I.J. and A.-M.K.; Analysis—K.A.G., E.J., I.J. and A.-M.K.; Visualization—K.A.G., J.L., E.J. and I.J.; Writing—K.A.G.; Storyline development with visuals and text—K.A.G., E.J., J.L. and I.J.; Revisions—K.A.G. and A.-M.K.; Funding acquisition—K.A.G. and A.-M.K. All authors have read and agreed to the published version of the manuscript.

Funding: Research was funded by the ERDF project “The Quest for Disclosing How Surface Characteristics Affects Slideability” (No.1.1.1.1/16/A/129), and a Natural Sciences and Engineering Research Council of Canada (NSERC) Discovery Grant, grant number: RGPIN-2016-04641.

Institutional Review Board Statement: Not applicable.

Informed Consent Statement: Not applicable.

Data Availability Statement: Data is contained within the article or Supplementary Material.

Acknowledgments: The authors are grateful for the assistance provided by D. Petrovics on the assembly of the enclosure, assistance in sliding experiments, and analysis of data to confirm a lower variability in air and ice conditions. Also thanks for the last reviewer, who provided valuable comments.

Conflicts of Interest: The authors declare no conflict of interest.

References

1. Kietzig, A.-M.; Hatzikiriakos, P.; Englezos, P. Physics of ice friction. *J. Appl. Phys.* **2010**, *107*, 081101. [[CrossRef](#)]
2. Makkonen, L.; Tikanmäki, M. Modeling the friction of ice. *Cold Reg. Sci. Technol.* **2014**, *102*, 84–93. [[CrossRef](#)]
3. Bowden, F.P.; Hughes, T.P. The mechanism of sliding on ice and snow. *Proc. R. Soc. Lond. Ser. A Math. Phys. Sci.* **1939**, *172*, 280–298. [[CrossRef](#)]
4. Bäurle, L.; Szabó, D.; Fauve, M.; Rhyner, H.; Spencer, N.D. Sliding friction of polyethylene on ice: Tribometer measurements. *Tribol. Lett.* **2006**, *24*, 77–84. [[CrossRef](#)]
5. Yun, C.; Choi, J.W.; Kim, H.; Kim, D.; Kim, H.-Y. Sliding on ice: Real contact area, melted film thickness, and friction force. *Int. J. Heat Mass Transf.* **2020**, *160*, 120166. [[CrossRef](#)]
6. Lungevics, J.; Jansons, E.; Gross, K.A. Skeleton runner roughness and surface contact area influence on sliding ability: Field experiments. *Key Eng. Mater.* **2019**, *800*, 303–307. [[CrossRef](#)]
7. Lozowski, E.P.; Szilder, K.; Maw, S.; Morris, A. A model of ice friction for skeleton sled runners. In Proceedings of the The Twenty-fourth International Ocean and Polar Engineering Conference; Busan, Korea, 15 June 2014.
8. Hertz, H. Über die berührung fester elastischer körper (On the contact of elastic solids). *J. Reine Angew. Math.* **1882**, *92*, 156–171. (In German)
9. Spagni, A.; Berardo, A.; Marchetto, D.; Gualtieri, E.; Pugno, N.M.; Valeri, S. Friction of rough surfaces on ice: Experiments and modeling. *Wear* **2016**, *368–369*, 258–266. [[CrossRef](#)]
10. Scherge, M.; Böttcher, R.; Spagni, A.; Marchetto, D. High-Speed measurements of steel–ice friction: Experiment vs. calculation. *Lubricants* **2018**, *6*, 26. [[CrossRef](#)]

11. Jansons, E.; Lungevičs, J.; Jerāne, I.; Gross, K.A. A Smaller bearing ratio, as a surface texture measure, promotes faster sliding on ice. *J. Biotribol.* **2021**, *143*, 111801. [CrossRef]
12. Abbott, E.J.; Firestone, F.A. Specifying surface quality: A method based on accurate measurement and comparison. *Mech. Eng.* **1933**, *55*, 569–572. [CrossRef]
13. Hanna, G.; Jon, W.; Barnes, W.P.J. Adhesion and Detachment of the toe pads of tree frogs. *J. Exp. Biol.* **1991**, *155*, 103–125. [CrossRef]
14. Brian, D.; Bharat, B. Shark-skin surfaces for fluid-drag reduction in turbulent flow: A review. *Philos. Trans. R. Soc. A Math. Phys. Eng. Sci.* **2010**, *368*, 4775–4806. [CrossRef]
15. Motta, P.; Habegger, M.L.; Lang, A.; Hueter, R.; Davis, J. Scale morphology and flexibility in the shortfin mako *Isurus oxyrinchus* and the blacktip shark *Carcharhinus limbatus*. *J. Morphol.* **2012**, *273*, 1096–1110. [CrossRef] [PubMed]
16. Bixler, G.D.; Bhushan, B. Bioinspired rice leaf and butterfly wing surface structures combining shark skin and lotus effects. *Soft Matter* **2012**, *8*, 11271–11284. [CrossRef]
17. De-yuan, Z.; Yue-hao, L.; Xiang, L.I.; Hua-wei, C. Numerical simulation and experimental study of drag-reducing surface of a real shark skin. *J. Hydrodyn.* **2011**, *23*, 204–211. [CrossRef]
18. Bhushan, B. Biomimetics inspired surfaces for drag reduction and oleophobicity/phillicity. *Beilstein J. Nanotechnol.* **2011**, *2*, 66–84. [CrossRef]
19. Zhao, D.-Y.; Huang, Z.-P.; Wang, M.-J.; Wang, T.; Jin, Y. Vacuum casting replication of micro-riblets on shark skin for drag-reducing applications. *J. Mater. Process. Technol.* **2012**, *212*, 198–202. [CrossRef]
20. Mielonen, K.; Jiang, Y.; Voyer, J.; Diem, A.; Hillman, L.; Suvanto, M.; Pakkanen, T.A. Sliding friction of hierarchically micro-micro textured polymer surfaces on ice. *Cold Reg. Sci. Technol.* **2019**, *163*, 8–18. [CrossRef]
21. Scherge, M.; Böttcher, R.; Richter, M.; Gurgel, U. High-speed ice friction experiments under lab conditions: On the influence of speed and normal force. *ISRN Tribol.* **2013**, *2013*, 703202. [CrossRef]
22. Rohm, S.; Hasler, M.; Knoflach, C.; Van Putten, J.; Unterberger, S.H.; Schindelwig, K.; Lackner, R.; Nachbauer, W. Friction between steel and snow in dependence of the steel roughness. *Tribol. Lett.* **2015**, *59*, 12552. [CrossRef]
23. Lungevics, J.; Jansons, E.; Gross, K.A. An Ice Track Equipped with Optical Sensors for Determining the Influence of Experimental Conditions on the Sliding Velocity. *Latv. J. Phys. Tech. Sci.* **2018**, *55*, 64–75. [CrossRef]
24. Gross, K.A.; Lungevics, J.; Zavickis, J.; Pluduma, L. A comparison of quality control methods for scratch detection on polished metal surfaces. *Measurement* **2018**, *117*, 397–402. [CrossRef]
25. ISO 25178-2:2012: Geometric Product Specifications (GPS)—Surface texture: Areal—Part 2: Terms, Definitions and Surface Texture Parameters. Available online: <https://www.google.com.hk/url?sa=t&rc=1&q=&esrc=s&source=web&cd=&cad=rja&uact=8&ved=2ahUKewjC9lO3sMTzAhUYad4KHSY7DPMQFnoECAgQAQ&url=https%3A%2F%2Fwww.iso.org%2Fstandard%2F42785.html&usq=A0vVaw3djfoVhu7A6Ftev2Xxtm7g> (accessed on 12 October 2021).
26. Jansons, E.; Irbe, M.; Gross, K.A. Influence of weather conditions on sliding over ice at a push-start training facility. *Biotribology* **2021**, *25*, 100152. [CrossRef]
27. Kim, S.; Kang, H.; Kim, D.; Lee, Y.-Z.; Lee, J. Measurement of sliding friction coefficient of micro-line patterned surfaces on ice. *Appl. Phys. Lett.* **2017**, *111*, 211601. [CrossRef]
28. Kietzig, A.-M.; Hatzikiriakos, S.G.; Englezos, P. Ice friction: The effects of surface roughness, structure, and hydrophobicity. *J. Appl. Phys.* **2009**, *106*, 024303. [CrossRef]
29. Hutchings, I.M. Leonardo da Vinci’s studies of friction. *Wear* **2016**, *360–361*, 51–66. [CrossRef]
30. Ahmed, K.M.T.; Grambow, C.; Kietzig, A.-M. Fabrication of micro/nano structures on metals by femtosecond laser micromachining. *Micromachines* **2014**, *5*, 1219–1253. [CrossRef]
31. Kietziga, A.-M.; Mirvakilia, M.N.; Kamalb, S.; Englezosa, P.; Hatzikiriakosa, S.G. Nanopatterned metallic surfaces: Their wettability and impact on ice friction. *J. Adhes. Sci. Technol.* **2011**, *25*, 1293–1303. [CrossRef]
32. Jendoubi, H.; Smerdova, O.; Brunetière, N. Unexpected frictional behavior of laser-textured hydrophobic surfaces. *Lubricants* **2021**, *9*, 31. [CrossRef]
33. Jaber, S.B.; Hamilton, A.; Xu, Y.; Kartal, M.E.; Gadegaard, N.; Mulvihill, D.M. Friction of flat and micropatterned interfaces with nanoscale roughness. *Tribol. Int.* **2021**, *153*, 106563. [CrossRef]
34. Huang, Y.; Zhang, X.; Ma, Z.; Zhou, Y.; Zheng, W.; Zhou, J.; Sun, C.Q. Hydrogen-bond relaxation dynamics: Resolving mysteries of water ice. *Coord. Chem. Rev.* **2015**, *285*, 109–165. [CrossRef]
35. Zhang, X.; Huang, Y.; Ma, Z.; Niu, L.; Sun, C.Q. From ice superlubricity to quantum friction: Electronic repulsivity and phononic elasticity. *Friction* **2015**, *3*, 294–319. [CrossRef]
36. Weber, B.; Nagata, Y.; Ketzetzi, S.; Tang, F.; Smit, W.J.; Bakker, H.J.; Backus, E.H.G.; Bonn, M.; Bonn, D. Molecular insight into the slipperiness of ice. *J. Phys. Chem. Lett.* **2018**, *9*, 2838–2842. [CrossRef] [PubMed]
37. Celano, U.; Hantschel, T.; Giammaria, G.; Chintala, R.C.; Conard, T.; Bender, H.; Vandervorst, W. Evaluation of the electrical contact area in contact-mode scanning probe microscopy. *J. Appl. Phys.* **2015**, *117*, 214305. [CrossRef]
38. Weber, B.; Suhina, T.; Junge, T.; Pastewka, L.; Brouwer, A.M.; Bonn, D. Molecular probes reveal deviations from Amontons’ law in multi-asperity frictional contacts. *Nat. Commun.* **2018**, *9*, 888. [CrossRef]
39. Petrova, D.; Weber, B.; Allain, C.; Audebert, P.; Bonn, D.; Brouwer, A.M. Fast 3D microscopy imaging of contacts between surfaces using a fluorescent liquid. *ACS Appl. Mater. Interfaces* **2018**, *10*, 40973–40977. [CrossRef]

40. Poirier, L.; Lozowski, E.P.; Thompson, R.I. Ice hardness in winter sports. *Cold Reg. Sci. Technol.* **2011**, *67*, 129–134. [[CrossRef](#)]
41. Liefferink, R.W.; Hsia, F.-C.; Weber, B.; Bonn, D. Friction on ice: How temperature, pressure, and speed control the slipperiness of ice. *Phys. Rev. X* **2021**, *11*, 011025. [[CrossRef](#)]
42. Seymour-Pierce, A.; Lishman, B.; Sammonds, P. Recrystallization and damage of ice in winter sports. *Philos. Trans. R. Soc. A Math. Phys. Eng. Sci.* **2017**, *375*, 20150353. [[CrossRef](#)]
43. Lungevics, J.; Jansons, E.; Boiko, I.; Velkavrh, I.; Voyer, J.; Wright, T. A holistic approach towards surface topography analyses for ice tribology applications. *Front. Mech. Eng.* **2021**, *9*, 691485. [[CrossRef](#)]
44. Irbe, M.; Gross, K.A.; Viba, J.; Cerpinska, M. Unveiling ice friction and aerodynamic drag at the initial stage of sliding on ice: Faster sliding in winter sports. *Tribol. Int.* **2021**, *160*, 106967. [[CrossRef](#)]
45. Link, J.M.; Salinas, E.Y.; Hu, J.C.; Athanasiou, K.A. The tribology of cartilage: Mechanisms, experimental techniques, and relevance to translational tissue engineering. *Clin. Biomech.* **2020**, *79*, 104880. [[CrossRef](#)] [[PubMed](#)]

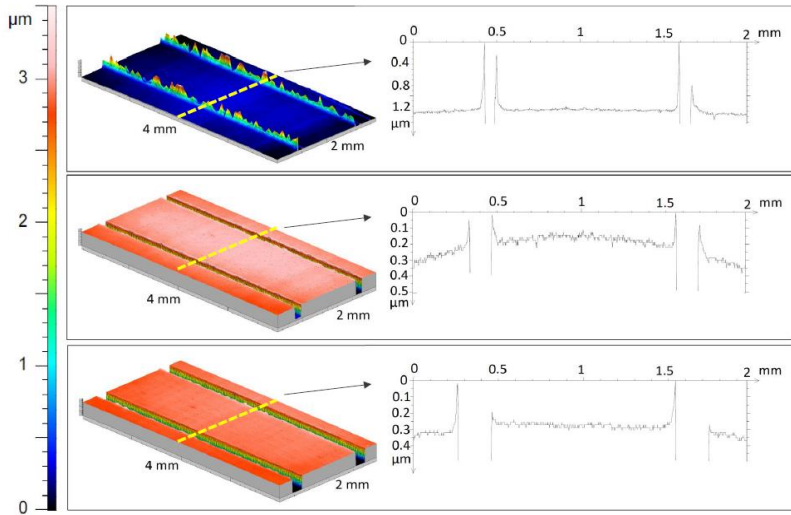


Figure S1. An enlarged view of the grooved blocks and the associated profile for the 50 μm grooved block (upper), 100 μm grooved block (middle) and 150 μm grooved block (lower). The pileup is seen at the edge of the grooves.

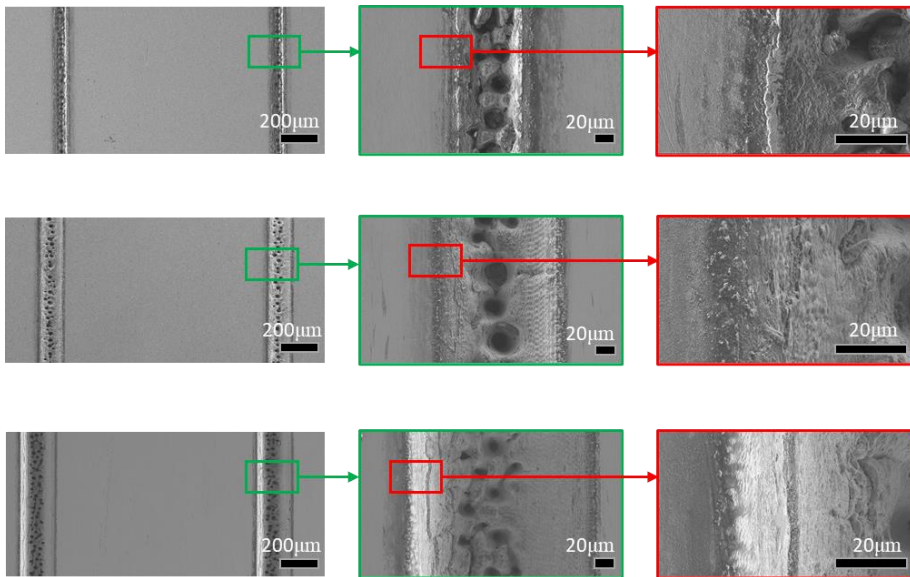


Figure S2. SEM micrographs showing the grooves seen at lower magnification, the holes in the grooves at the intermediate magnification, and the pileup at higher magnification.

APPENDIX 8

**LATVIAN LUGE FEDERATION CONFIRMATION ABOUT JANIS
LUNGEVICS DOCTORAL THESIS APPROBATION**

Confirmation about Jānis Lungevičs Doctoral Thesis "*Effect of stainless steel surface macrogeometry and microgeometry on the coefficient of sliding friction on ice*" approbation.

Herby, I, Mārtiņš Rubenis, the Latvian Luge Federation coach, and the mechanic confirm that I have received and read Janis Lungevics Doctoral Thesis, *Effect of stainless steel surface macrogeometry and microgeometry on the coefficient of sliding friction on ice*.

Latvian Luge Federation has collaborated with Jānis Lungevičs for several years, and results and observations collected in this Doctoral Thesis have been used to measure and improve Latvian National Luge team runner geometry and surface preparation methods. Jānis Lungevičs regularly discussed his research observations with the Latvian Luge Federation and planned his further research considering our feedback.

In my opinion, achieved research results have high practical importance; therefore, I recommend that Doctoral Thesis author Jānis Lungevičs continue his scientific research in sliding surface macrogeometry and microgeometry optimization to reduce friction coefficient on ice.

Latvian Luge Federation coach and mechanic,

Mārtiņš Rubenis

11.04.2023



APPENDIX 9

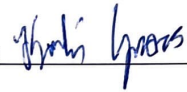
**CORRESPONDING AUTHOR CONFIRMATION OF JANIS LUNGEVICS'
CONTRIBUTION TO THE PUBLICATIONS SUMMARIZED IN THIS
DOCTORAL THESIS**

Jānis Lungevičs' contribution to the publications summarized in this Thesis.

The corresponding authors of these listed publications confirm that Jānis Lungevičs contributed to the research stages underlined below:

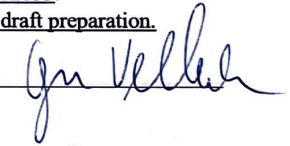
- 1) **Gross K.**, Lungevics J., Zavickis J., Pluduma L. A Comparison of Quality Control Methods for Scratch Detection on Polished Metal Surfaces. Measurement, 2018, Vol.117, pages 397-402. ISSN 0263-2241. Available: doi:10.1016/j.measurement.2017.12.022.
 - Conceptualization, investigation, analysis, visualization, writing-review and editing.
- 2) **Gross K.**, Lungevics J., Jansons E., Jerane I., Wood M., Kietzig A. Surface Hierarchy: Macroscopic and Microscopic Design Elements for Improved Sliding on Ice. Lubricants, 2021, Vol. 9, No. 103, Article 103. ISSN 2075-4442. Available: doi:10.3390/lubricants9100103.
 - Conceptualization: hierarchy, investigation, visualization, storyline development with visuals and text.

Kārlis Agris Gross



- 1) **Velkavrh I.**, Lungevics J., Jansons E., Klien S., Voyer J., Ausserer, F. The Influence of Isotropic Surface Roughness of Steel Sliders on Ice Friction Under Different Testing Conditions. Lubricants, 2019, Vol. 7, No. 12, pages 50-63. ISSN 2075-4442. Available: doi:10.3390/lubricants7120106.
 - Conceptualization, investigation, methodology, analysis and validation, writing-original draft preparation.
- 2) **Velkavrh I.**, Voyer J., Wright T., Lungevics J., Jansons E., Boiko, I. Variations of ice friction regimes in relation to surface topography and applied operating parameters, IOP Conf. Ser. Mater. Sci. Eng. 1140 (2021) 012033. Available: <https://doi.org/10.1088/1757-899X/1140/1/012033>.
 - Conceptualization, investigation, analysis, visualization, writing-original draft preparation.

Igor Velkavrh



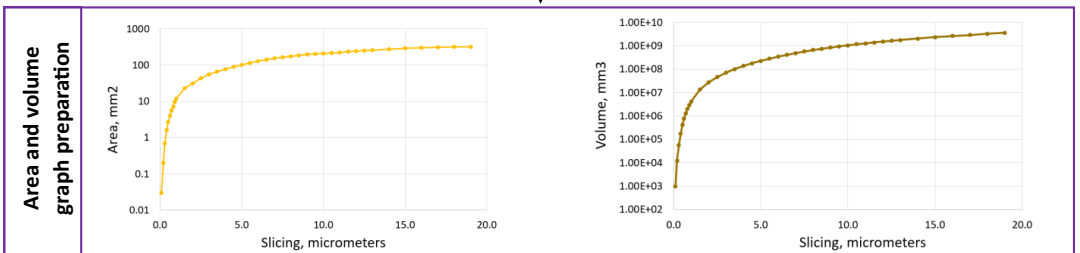
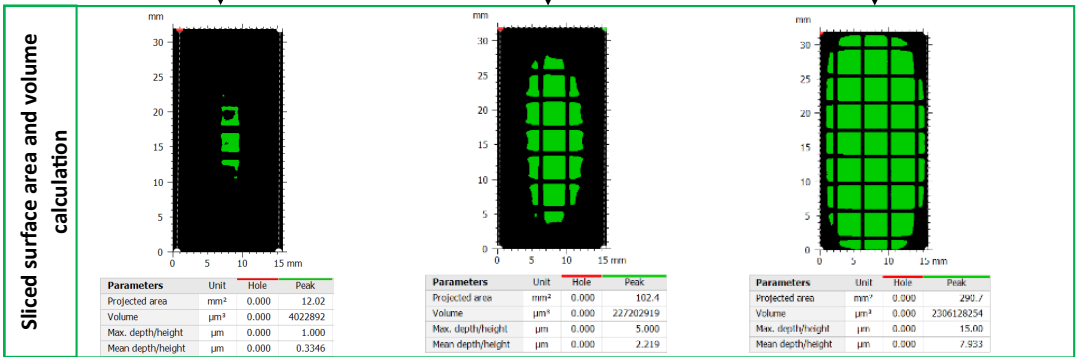
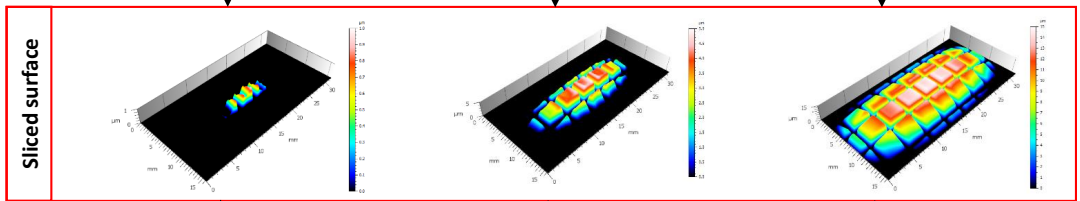
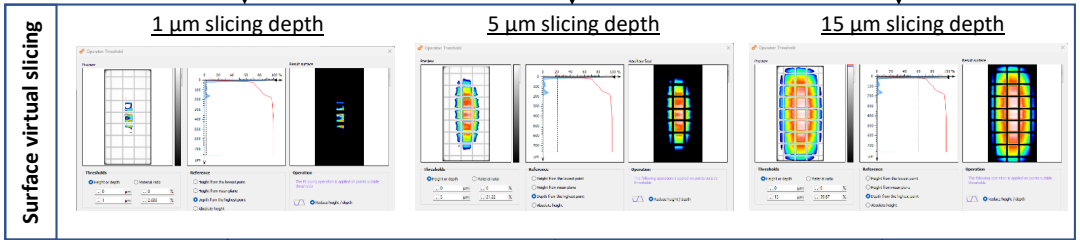
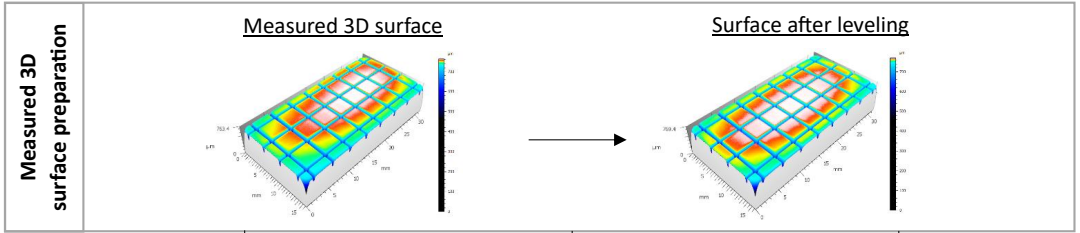
- 1) **Jansons E.**, Lungevics J., Jerane I., Gross K. A Smaller Bearing Ratio, as a Surface Texture Measure, Promotes Faster Sliding on Ice. Journal of Tribology, 2021, Vol. 143, No. 11, Article number 111801. ISSN 0742-4787. e-ISSN 1528-8897. Available: doi:10.1115/1.4049704.
 - Conceptualization, investigation, methodology, analysis and validation, writing-original draft preparation.
- 2) **Jansons E.**, Lungevics J., Gross K. Surface Roughness Measure that Best Correlates to Ease of Sliding. 15th International Scientific Conference Engineering for Rural Development: Proceedings. Vol.15, Jelgava, Latvia, May 25-27, 2016, pages 687- 695. ISSN 1691-5976. Available: <https://www.tf.llu.lv/conference/proceedings2016/Papers/N127.pdf>.
 - Conceptualization, investigation, methodology, analysis and validation, writing-original draft preparation.

Ernests Jansons



APPENDIX 10

**A VISUAL EXAMPLE OF SURFACE MEASUREMENT POST-PROCESSING
ACCORDING TO THE NEW METHODOLOGY**





Jānis Lungevičs dzimis 1990. gadā Madonā. Rīgas Tehniskajā universitātē (RTU) ieguvis profesionālo bakalaura grādu un inženiera kvalifikāciju mehatronikā (2014) un akadēmisko maģistra grādu ražošanas tehnoloģijā (2016). Kopš 2014. gada strādā RTU, ieņemot Mehānikas un mašīnbūves institūta zinātniskā asistenta amatu, patlaban ir pētnieks un lektors mašīnbūves un mehānikas (mēraparāti un metroloģija) nzarē. Piedalījies vairākos nacionālajos un Eiropas zinātniskajos projektos, kas saistīti ar virsmu triboloģiskajām īpašībām. Vada ģeometriskās metroloģijas laboratoriju un piedalās vairāku studiju kursu vadīšanā un satura pilnveidošanā. Aktīvi darbojas RTU un ražošanas industrijas sadarbības veicināšanā.

Jānis Lungevičs was born in 1990 in Madona. He holds a Bachelor's degree and an engineering qualification in mechatronics from Riga Technical University (RTU) (2014) and an Academic Master's degree in Manufacturing Technology (2016). Since 2014, he has been a research assistant at the Institute of Mechanics and Mechanical Engineering of RTU, where he is currently a researcher and lecturer in the field of mechanical engineering and mechanics (measuring instruments and metrology). He has participated in several national and European scientific projects related to the tribological properties of surfaces. He is the Head of the Geometric Metrology Laboratory and participates in the content development of several study course lectures. He actively promotes cooperation between RTU and the industry.